# SUPPORTING INFORMATION

# Meta-Analysis of Nanoparticle Delivery to Tumors Using a Physiologically Based Pharmacokinetic Modeling and Simulation Approach

Yi-Hsien Cheng,[†,‡] Chunla He,[†] Jim E. Riviere,[†,¶] Nancy A. Monteiro-Riviere,[‡] Zhoumeng Lin[*,†,‡]

† Institute of Computational Comparative Medicine (ICCM), Department of Anatomy and Physiology, College of Veterinary Medicine, Kansas State University, Manhattan, KS 66506, USA

‡ Nanotechnology Innovation Center of Kansas State (NICKS), Department of Anatomy and Physiology, College of Veterinary Medicine, Kansas State University, Manhattan, KS 66506, USA

¶ 1Data Consortium, Kansas State University, Manhattan, KS 66506, USA

Yi-Hsien Cheng: yhcheng1987@ksu.edu; Chunla He: chunla.he0321@gmail.com; Jim E. Riviere: jim.riviere@gmail.com; Nancy A. Monteiro-Riviere: nmonteiro@ksu.edu; Zhoumeng Lin: zhoumeng@ksu.edu

*Corresponding author: Institute of Computational Comparative Medicine (ICCM), Department of Anatomy and Physiology, College of Veterinary Medicine, Kansas State University, 1800 Denison Avenue, P200 Mosier Hall, Manhattan, KS 66506, USA. Email: zhoumeng@ksu.edu. Phone: +1-785-532-4087. Fax: +1-785-532-4953.

## Table of Contents

**Description for supplementary Excel files**

**E1.** Summarized information including physicochemical properties of administered inorganic nanomaterials (INMs), implanted tumor type, site, size, and body weight as well as the injected dose for tumor-bearing mice, estimated tumor delivery efficiencies, and adequacy in the model simulation of NM kinetics in the tumor.

**E2.** Summarized information including physicochemical properties of administered organic nanomaterials (ONMs), implanted tumor type, site, size, and body weight as well as the injected dose for tumor-bearing mice, estimated tumor delivery efficiencies, and adequacy in the model simulation of NM kinetics in the tumor.

**E3.** PBPK simulations of pharmacokinetics in healthy mice intravenously injected with 13 nm gold nanoparticles (AuNPs). In addition, PBPK simulations of tumor pharmacokinetics and associated tumor- and NM-specific parameters for INMs following systemic administration in tumor-bearing mice were included.

**E4.** PBPK simulations of tumor pharmacokinetics and associated tumor- and NM-specific parameters for ONMs following systemic administration in tumor-bearing mice.

## Supplementary figures

### Figure S1

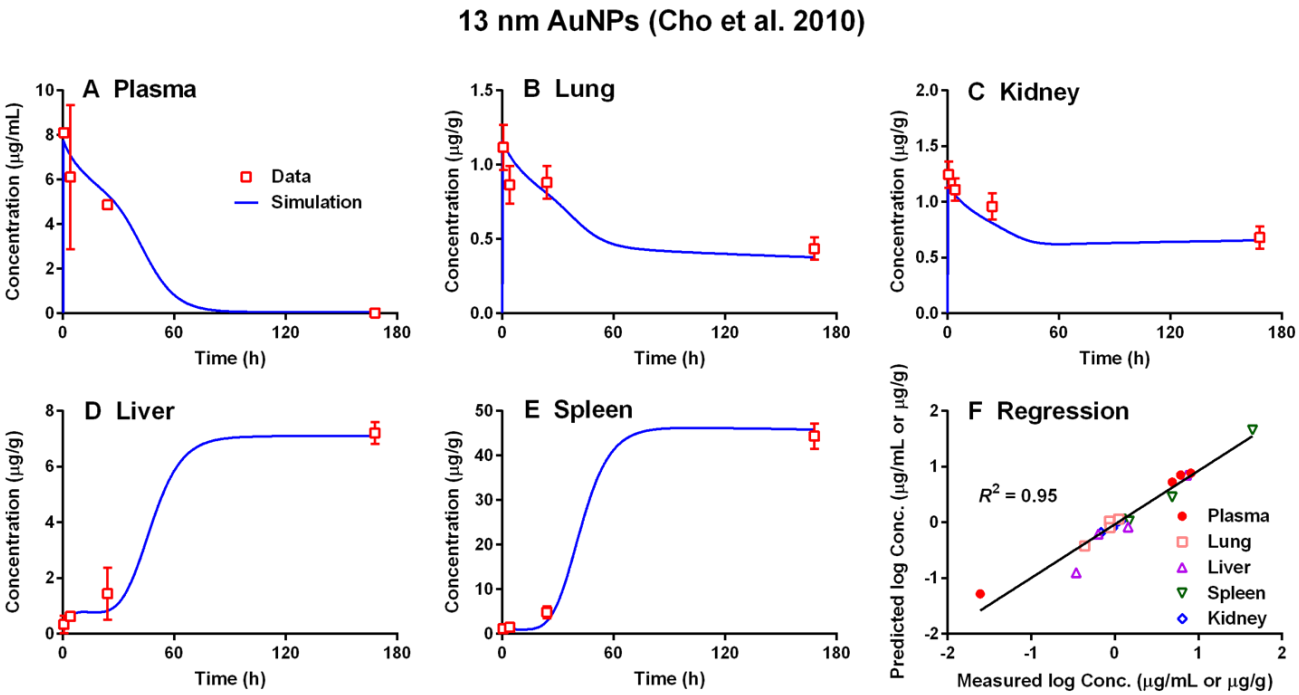


**Figure S1.** PBPK model calibration and simulation of the concentrations of gold nanoparticles (AuNPs) in the (A) plasma, (B) lung, (C) kidney, (D) liver, and (E) spleen from healthy mice by intravenous (IV) injection with 13 nm AuNPs. Panel (F) is the result of linear regression between log-transformed measured and simulated concentrations of 13 nm AuNPs. $R^2$ is the coefficient of determination.

**Figure S2**

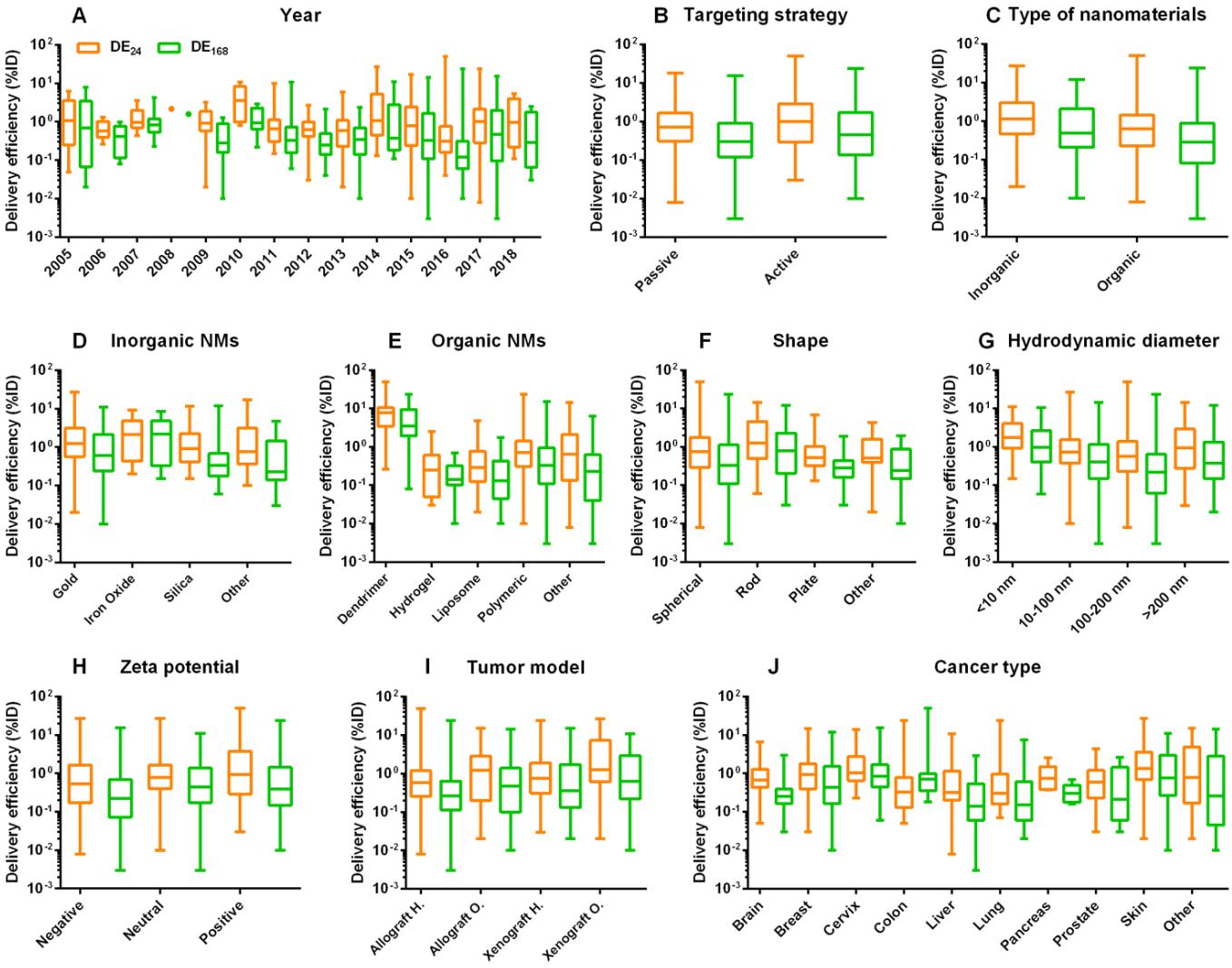


**Figure S2.** Subgroup analyses on tumor delivery efficiencies estimated at 24h ($DE_{24}$) (orange) and 168h ($DE_{168}$) (green) using our tumor-bearing PBPK model from 376 analyzed datasets in this study (2005–2018). Box-and-whisker plots of tumor delivery efficiency data (percent injected dose, %ID) for different subgroups: (A) year, (B) targeting strategy, (C) type of nanomaterials (NMs), (D) inorganic NMs, (E) organic NMs, (F) shape, (G) hydrodynamic diameter, (H) zeta potential, (I) tumor model, and (J) cancer type. The boxes represent the $25^{th}$ – $75^{th}$ percentiles and solid lines in the boxes indicate the median values.

**Supplementary tables**

**Table S1.** Estimated tumor delivery efficiencies, physicochemical properties of administered nanomaterials (NMs), tumor physiology, and dosing regimens for each of the included studies.

| Material | Surface chemistry | Shape | Hydro-dynamic diameter [nm] | Zeta potential [mV] | Animal, cancer type, and tumor model | Tumor size [a] | Dosing regimen [mg/kg] | $DE_{Tlast\_PK}$ [%ID] [b] | Ref. |
|---|---|---|---|---|---|---|---|---|---|
| Gold | PEG_5kDa [c]; Folic acid [active] | AR 3.8<br>Rod | 24<br>38×10 (TEM) | -18 [c] | Human cervical carcinoma (HeLa) s.c. inoculated to the flank of mice (20 g) [cervix/xenograft heterotopic] | 0.1 $cm^3$ [c]<br>~0.1 g | 20<br>(7 d) | 1.97 | 1 |
| Gold | PEG_5kDa [c] [passive] | AR 3.2<br>Rod | 29.5<br>45×14 (TEM) | 0 [c] | Murine colon carcinoma (CT26.wt) s.c. inoculated to the flank of mice (20 g) [colon/allograft heterotopic] | ~0.1 g | 12<br>(2 d) | 1.51 | 2 |
| Gold | PEG_5kDa; EGFR peptide [active] | Spherical | 42 | -5 [c] | Rat glioblastoma (9L.E29) s.c. inoculated to the flank of mice (20 g) [brain/xenograft heterotopic] | ~0.9 g | 1<br>(7 d) | 2.85 | 3 |
| | PEG_5kDa [passive] | | 38.3 | -5 [c] | | | | 3.61 | |
| Gold | PEG_2kDa; Aptamer AS1411 [active] | Star | 68.4 | -9.3 | Human breast adenocarcinoma (MDA-MB-231) s.c. inoculated to the flank of mice (20 g) [breast/xenograft heterotopic] | 0.2 $cm^3$<br>~0.2 g | 4.8<br>(3 d) | 0.64 | 4 |
| Gold | PEG_5k/10kDa; Alexa Fluor 750 [passive] | Spherical | 46.3 | -6.7 | Human melanoma (MDA-MB-435) s.c. inoculated to the hind flank of mice (21 g) [skin/xenograft orthotopic] | 1.1 $cm^3$<br>~1.3 g | 4.1 (2 d) | 18.64 | 5 |
| | | | 64.2 | -15 | | | 8.1 (2 d) | 14.28 | |
| | | | 104.2 | -10 | | | 16.2 (2 d) | 11.19 | |
| | | | 166 | -6 | | | 27.1 (2 d) | 4.94 | |
| | PEG_5k/10kDa; Transferrin Alexa Fluor 750 [active] | | 49.5 | -0.6 | | | 4.1 (2 d) | 25.07 | |
| | | | 60 | -11 | | | 8.1 (2 d) | 23.86 | |
| | | | 100.4 | -9 | | | 16.2 (2 d) | 21.37 | |
| | | | 175.6 | -5 | | | 27.1 (2 d) | 8.21 | |

| | | | | | | | | | |
|---|---|---|---|---|---|---|---|---|---|
| Gold | HSA [passive] | Spherical | 6.1 | NA | Human glioblastoma (U87MG) s.c. inoculated to the flank of mice (20 g) [brain/xenograft heterotopic] | 75 $mm^3$ ~0.1 g | 1.3 (1 d) | 1.12 | 6 |
| Gold | Choline and PEI [passive] | Spherical | 27.3 (TEM) | NA | Human prostate carcinoma (DU145) s.c. inoculated to the flank of mice (20 g) [prostate/xenograft heterotopic] | 0.3 $cm^3$ ~0.4 g | 7.2 (1 d) | 0.06 | 7 |
| Gold | Quaternary ammonium; Sulfonic groups [passive] | Spherical | 17.1 | -9.8 | Human cervix carcinoma (KB) s.c. inoculated to right rear flank of mice (16–18 g) [cervix/xenograft heterotopic] | 0.1 $cm^3$ ~0.1 g | 5.9 (3 d) | 1.13 | 8 |
| | PEG_2kDa [passive] | | 31 | -10.5 | | | | 0.54 | |
| Gold | PEG_2kDa [passive] | Tripod | 18.2 | 25.4 | Human glioblastoma (U87MG) s.c. inoculated to the right front or hind flank of mice (20 g) [brain/xenograft heterotopic] | ~0.2 $cm^3$ ~0.2 g | 2 (2 d) | 0.36 | 9 |
| | PEG_3.4kDa [passive] | | 20.8 | 24.6 | | | | 0.51 | |
| | PEG_6kDa [passive] | | 25.8 | 21.7 | | | | 0.59 | |
| | PEG; cRGDfC peptide [active] | | 24.1 | -21.3 | | | | 1.57 | |
| Gold | PEG_2kDa; Glutathione; Folic acid [active] | Spherical | 6.1 | -5 [c] | Human gastric carcinoma (MGC-803) s.c. inoculated to the right flank of mice (18–22 g) [stomach/xenograft heterotopic] | ~0.2 $cm^3$ ~0.2 g | 4 (7 d) | 9.5 | 10 |
| Gold | PEG_5kDa [passive] | Spherical | 69.8 | ~0 [c] | Murine mammary carcinoma (EMT-6) s.c. inoculated to the right flank of mice (15–20 g) | 0.1 $cm^3$ ~0.1 g | 0.3 (1 d) | 1.74 | 11 |
| | | Disk (Plate) | 130.5 92×7 (TEM) | | | | 1.6 (1 d) | 0.46 | |

| | | | | | | | | | |
|---|---|---|---|---|---|---|---|---|---|
| Gold | PEG_5kDa [passive] | AR 4.3 Rod | 77 39×9 (TEM) | ~0 [c] | [breast/allograft heterotopic] | 0.1 $cm^3$ ~0.1 g | 0.2 (1 d) | 0.15 | |
| | | Cage (Cubic) | 111.3 50×50 (TEM) | | | | 1 (1 d) | 0.62 | |
| Gold | PEG_1kDa [passive] | Spherical | 5.5 | ~0 | Human breast carcinoma (MCF-7) orthotopically inoculated to mammary fat pad of mice (20–25 g) [breast/xenograft orthotopic] | ~0.2 $cm^3$ ~0.2 g | 63 (2 d) | 1.24 | 12 |
| Gold | Plasma-polymerized allylamine; Cetuximab antibody [active] | Spherical | 31 | NA | Human epithelial carcinoma (A431) s.c. inoculated to both flanks of mice (32–37 g) [skin/xenograft orthotopic] | ~0.3 $cm^3$ ~0.7 g | 8 (7 d) | 2.23 | 13 |
| Gold | PEG_5kDa [passive] | Cage (Cubic) | 63.7 30×30 (TEM) | 10.2 | Murine mammary carcinoma (EMT-6) s.c. implanted to the hind flank of mice (15–20 g) [breast/allograft heterotopic] | 0.3–0.4 g | 1.4e-9 (1 d) | 2.45 | 14 |
| | | | 96 55×55 (TEM) | 18.7 | | | 6.4e-9 (1 d) | 0.44 | |
| Gold | PEG_5kDa [passive] | Spherical | 66.5 | -2.6 | Human prostate carcinoma (LNCaP) s.c. injected to hind limb of mice (20 g) [prostate/xenograft heterotopic] | ~0.3 $cm^3$ ~0.3 g | 11 (1 d) | 0.64 | 15 |
| | | | 62.8 | -27.1 | | | | 0.59 | |
| | | | 60.2 | -10.6 | | | | 0.03 | |
| | PEG_5kDa; TNF-$\alpha$ ligand [active] | | 71.7 | -2.9 | | | | 0.55 | |
| Gold | PEG_5kDa [passive] | Spherical | 63 | 0 [c] | Human lymphoblastoid carcinoma (LCL) s.c. inoculated to right flank of mice (20 g) [other cancer type/xenograft heterotopic] | ~0.1 g [c] | 3.8 (2 d) | 0.35 | 16 |

| | | | | | | | | | |
|---|---|---|---|---|---|---|---|---|---|
| Gold | PEG_5kDa [passive] | AR 4.0 Rod | 37.8 61×15 (TEM) | -10 | Human prostate carcinoma (DU145) s.c. inoculated bilaterally to flank of mice (20 g) [prostate/xenograft heterotopic] | ~0.1 $cm^3$ ~0.2 g | 9.6 (2 d) | 1.30 | [17] |
| | PEG_5kDa; cRGDfK peptide; [active] | | | -44.1 | | | | 0.25 | |
| Gold | PEG_5kDa [passive] | Spherical | 88.9 | -27.1 | Human ovarian carcinoma (A2780) orthotopically inoculated to left ovarian bursa of mice (25 g) [ovary/xenograft orthotopic] | 5 g | 2.4 (7 d) | 0.64 | [18] |
| | | AR 4.5 Rod | 27.5 45×10 (TEM) | 1.1 | | | 1.6 (7 d) | 6.47 | |
| Gold | PEG_2kDa [passive] | Spherical | 22.4 | ~0 [c] | Human melanoma (MDA-MB-435) orthotopically inoculated to dorsal skin of mice (20 g) [skin/xenograft orthotopic] | 1 $cm^3$ ~1.2 g | 4.5 (1 d) | 0.02 | [19] |
| | | | 39.6 | | | | 8 (1 d) | 0.80 | |
| | PEG_5kDa [passive] | | 61.3 | | | | 12.3 (1 d) | 0.70 | |
| | PEG_10kDa [passive] | | 82.6 | | | | 16.6 (1 d) | 0.94 | |
| | | | 99.4 | | | | 20 (1 d) | 0.59 | |
| Gold | PEG_2kDa; MSN coating [passive] | AR 4.0 Rod | 41.8 60×15 (TEM) | -0.1 | Murine mammary carcinoma (4T1) s.c. inoculated to right hind leg of mice (20 g) [breast/allograft heterotopic] | 0.5 $cm^3$ ~0.6 g | 1 (3 d) | 0.65 | [20] |
| | BSA coating; MSN coating [passive] | | 44.3 60×15 (TEM) | -14.1 | | | | 0.29 | |
| | BSA coating [passive] | | 20.2 60×15 (TEM) | -20.2 | | | | 0.21 | |
| | BSA coating [passive] | Spherical | 7.2 | -23.5 | | | | 0.42 | |
| Dendrimer entrapped AuNPs | PEG_2kDa; cRGDfK peptide [active] | Spherical | 71.7 | 6.1 | Human glioblastoma (U87MG) s.c. inoculated to the right oxter of mice (20–22 g) [brain/xenograft heterotopic] | ~0.04 $cm^3$ ~0.05 g | 188 (5 d) | 0.03 | [21] |

| | | | | | | | | | |
|---|---|---|---|---|---|---|---|---|---|
| Gold-dendrimer composite nanodevice | Amine-terminated PAMAM [passive] | Spherical | 5 | Positive | Murine melanoma (B16-F10) s.c. inoculated to the dorsal surface of mice (25 g) [skin/allograft orthotopic] | 0.5 $cm^3$ 0.6 g | 16 (4 d) | 3.08 | 22 |
| | Carboxy-terminated PAMAM [passive] | | 5 | Negative | | | | 1.85 | |
| | Acetylated PAMAM [passive] | | 5 | 2.5 (Neutral) | | | | 1.81 | |
| | Carboxy-terminated PAMAM [passive] | | 11 | Negative | | | | 0.24 | |
| | Amine-terminated PAMAM [passive] | | 22 | Positive | | | | 1.21 | |
| | Amine-terminated PAMAM [passive] | | 22 | Positive | Rat prostate carcinoma (MatLyLu) s.c. inoculated to the dorsal surface of mice (25 g) [prostate/xenograft heterotopic] | | | 0.63 | |
| Gold | Tiopronin [passive] | Spherical | 2.7 | -16.8 | Murine melanoma (B16-F10) s.c. inoculated to the right flank of mice (25 g) [skin/allograft orthotopic] | ~5 g | 3.4 (3 d) | 0.95 | 23 |
| | PEG_5kDa [passive] | | 2.7 | -42.3 | | | | 1.51 | |
| | Myxoma peptide [active] | | 2.7 | -22.1 | | | | 1.62 | |
| | PEG_5kDa; Myxoma peptide [active] | | 2.7 | -25.6 | | | | 1.36 | |
| | cRGD peptide [active] | | 2.7 | -16.6 | | | | 1.15 | |
| | PEG_5kDa; cRGD peptide [active] | | 2.7 | -18.4 | | | | 2.04 | |

| | | | | | | | | | |
|---|---|---|---|---|---|---|---|---|---|
| Gold | Polyprodrug shell coating (Biotin/PEG/LA) [active] | AR 3.5<br>Rod | 51.6<br>38×11 (TEM) | 3 | Murine epidermoid carcinoma (SCC-7) orthotopically inoculated to back of mice (20 g) [skin/allograft orthotopic] | 0.1 $cm^3$<br>~0.1 g | 1.5<br>(1 d) | 2.43 | [24] |
| Magnetic AuNPs | PEG_5kDa [passive] | Spherical | 22 | -25.9 | Murine Ehrlich ascites carcinoma (EAC) s.c. inoculated to right flank of mice (22–25 g) [breast/allograft heterotopic] | ~0.5 $cm^3$<br>~0.5 g | 10<br>(1 d) | 1.17 | [25] |
| Gold | PEG_5kDa [passive] | AR 4.1<br>Rod | 37.4<br>60×15 (TEM) | -11 | Human prostate carcinoma (DU145) s.c. inoculated to flank of mice (28 g) [prostate/xenograft heterotopic] | ~0.2 $cm^3$<br>~0.2 g | 8<br>(3 d) | 2.81 | [26] |
| | | Cage<br>(Cubic) | 50<br>50×50 (TEM) | -9.2 | | | 4.1<br>(3 d) | 3.83 | |
| Gold | PEG_3.3kDa [passive] | Spherical | 4.5<br>(TEM) | NA | Murine melanoma (B78H1) orthotopically transplanted to mice (18–20 g) [skin/allograft orthotopic] | 0.4 $cm^3$<br>~0.5 g | 1.7<br>(7 d) | 7.13 | [27] |
| Gold-iron oxide | PEG_2kDa; Affibody protein [active] | Spherical | 24.4 | -28.6 | Human epithelial carcinoma (A431) s.c. inoculated to shoulder of mice (20 g) [skin/xenograft orthotopic] | ~0.2 $cm^3$<br>~0.3 g | 10<br>(2 d) | 1.09 | [28] |
| Iron oxide | PEG_5kDa and silica coating; Trastuzumab antibody [active] | Spherical | 16<br>(TEM) | NA | Human breast carcinoma (SkBr3) s.c. inoculated to flank of mice (20–25 g) [breast/xenograft heterotopic] | ~0.1 $cm^3$<br>~0.1 g | 22.5<br>(2 d) | 0.70 | [29] |
| Iron oxide | Starch shell modified with PEG_1kDa and PSMA antigen [active] | Spherical | 139.1 | -11.6 | Human prostate carcinoma (PC-3 PIP & PC-3 flu) s.c. inoculated to opposite front flanks of mice (22 g) [prostate/xenograft heterotopic] | ~0.1 $cm^3$<br>~0.2 g | 11.4<br>(4 d) | 0.37 | [30] |

| | | | | | | | | | |
|---|---|---|---|---|---|---|---|---|---|
| Iron oxide | PEG_5kDa [passive] | Spherical | 68 (assumed) | NA | Human glioblastoma (U87MG) s.c. inoculated to flank of mice (26 g) [brain/xenograft heterotopic] | ~0.2 $cm^3$ ~0.2 g | 10 (2 d) | 0.56 | [31] |
| | PEG_5kDa; cRGD peptide [active] | | 68 | NA | | | | 1.17 | |
| Iron oxide | Dopamine; HSA [passive] | Spherical | 50.8 | NA | Murine breast carcinoma (4T1) s.c. inoculated to right flank of mice (24 g) [skin/allograft heterotopic] | 0.5 $cm^3$ 0.6 g | 5 (1 d) | 1.14 | [32] |
| Iron oxide | PEG; DOTA; ChL6 mAb; [active] | Spherical | 20 (TEM) | NA | Human breast adenocarcinoma (HBT3477) s.c. inoculated on both sides of abdomen of mice (26 g) [breast/xenograft heterotopic] | ~0.2 $cm^3$ ~0.6 g | 84.6 (4 d) | 5.11 | [33] |
| Iron oxide | Trastuzumab antibody [active] | Spherical | 39.4 | -4.5 | Human gastric carcinoma (N87) s.c. inoculated to the hind flank of mice (22 g) [stomach/xenograft heterotopic] | ~2 g (NA, estimated) | 21.4 (3 d) | 5.26 | [34] |
| | IgG antibody [active] | | 40.3 | -3.3 | | | | 4.97 | |
| | Anti-HER2 scFv antibody [active] | | 22.3 | -4.6 | | | | 9.36 | |
| | Anti-HER2 peptide [active] | | 28.1 | -0.6 | | | | 7.42 | |
| Silica (HMSN) | PEG_5kDa; cRGDyK peptide [active] | Spherical | 226.2 | -3.5 | Human glioblastoma (U87MG) s.c. inoculated to flank of mice (28 g) [brain/xenograft heterotopic] | ~0.2 $cm^3$ ~0.2 g | 9.5 (18 h) | 1.28 | [35] |
| | PEG_5kDa [passive] | | 219.4 | -3.6 | | | | 0.74 | |

| | | | | | | | | | |
|---|---|---|---|---|---|---|---|---|---|
| Silica | Polypyrrole [passive] | Spherical | 59 | -7.4 | Murine mammary carcinoma (4T1) s.c. inoculated to right rear flank of mice (20 g) [breast/allograft heterotopic] | ~0.1 $cm^3$ ~0.1 g | 10 (1 d) | 0.34 | [36] |
| Silica (MSN) | PEG_5kDa [passive] | Spherical | 125.2 | -10.9 | Human glioblastoma (U87MG) s.c. inoculated to front flank of mice (28 g) [brain/xenograft heterotopic] | ~0.1 $cm^3$ ~0.1 g | 9.5 (22 h) | 0.18 | [37] |
| | PEG_5kDa; VEGF ligand [active] | | 129 | -10.2 | | | | 0.50 | |
| Silica (HMSN) | PEG_5kDa [passive] | Spherical | 194.4 (assumed) | -5.1 (assumed) | Murine mammary carcinoma (4T1) s.c. inoculated to front flank of mice (28 g) [breast/allograft heterotopic] | ~0.2 $cm^3$ ~0.2 g | 9.5 (1 d) | 0.63 | [38] |
| | PEG_5kDa; TRC105 antibody [active] | | 194.4 | -5.1 | | | | 1.60 | |
| Silica (MSN) | PEG_5kDa [passive] | Spherical | 175.3 (assumed) | -3.3 (assumed) | Murine mammary carcinoma (4T1) s.c. inoculated to the front flank of mice (28 g) [breast/allograft heterotopic] | ~0.2 $cm^3$ ~0.2 g | 9.5 (2 d) | 0.41 | [39] |
| | PEG_5kDa; TRC105(Fab) antibody [active] | | 175.3 | -3.3 | | | | 0.84 | |
| Silica | PEG_0.5kDa [passive] | Spherical | 6.8 | 0 [c] | Human melanoma (M21) s.c. inoculated to hind leg of mice (27 g) [skin/xenograft orthotopic] | 0.2 $cm^3$ ~0.2 g | 0.5 (4 d) | 0.07 | [40] |
| | PEG_0.5kDa; cRGDY peptide [active] | | 7 | -3 [c] | | | 0.5 (7 d) | 0.17 | |
| Silica (MSN) | PEG_5kDa [passive] | Spherical | 150.2 | -2.3 | Murine mammary carcinoma (4T1) s.c. inoculated to the front flank of mice (20 g) [breast/allograft heterotopic] | ~0.2 $cm^3$ ~0.2 g | 9.5 (2 d) | 0.52 | [41] |
| | PEG_5kDa; TRC105 antibody [active] | | 168 | -2.7 | | | | 0.95 | |

| | | | | | | | | | |
|---|---|---|---|---|---|---|---|---|---|
| Enzyme & iron oxide entrapped dendritic MSN | PEG_5kDa; $Fe_3O_4$ NPs; Natural glucose oxidase [passive] | Spherical | 255.3 | -27.6 | Murine mammary carcinoma (4T1) s.c. implanted to mammary fat pad of mice (16 g) [breast/allograft orthotopic] | 30 $mm^3$ ~0.04 g | 10 (2 d) | 0.22 | [42] |
| Liposome coated HMSN | PEG_2kDa-liposome coating [passive] | Spherical | 210 | 27 | Human hepatocellular carcinoma (HepG2) s.c. inoculated to front armpit of mice (16–18 g) [liver/xenograft heterotopic] | 0.5 $cm^3$ 0.6 g | 8 (1 d) | 0.88 | [43] |
| Liposome coated HMSN | PEG_2kDa-liposome coating [passive] | Spherical | 243 | -11.7 | Murine melanoma (B16-F10) orthotopically inoculated to the right flank of mice (20 g) [skin/allograft orthotopic] | ~0.1 $cm^3$ ~0.1 g | 750 (2 d) | 6.06 | [44] |
| Silica (MSN) | RBC membrane vesicle coating [passive] | Spherical | 107.7 | -14 | Murine mammary carcinoma (4T1) injected to right mammary gland of mice (20 g) to establish spontaneous tumor model [breast/allograft orthotopic] | ~0.3 $cm^3$ ~0.4 g | 5 (1 d) | 2.12 | [45] |
| Hollow mesoporous silica | PEG_3.5kDa; PDA coating [passive] | AR 2.5 Rod | 210 200×80 (TEM) | 24.1 | Murine mammary carcinoma (4T1) orthotopically administered to right mammary fat pad of mice (20 g) [breast/allograft orthotopic] | 0.7 $cm^3$ ~0.8 g | 5 (2 d) | 6.35 | [46] |
| | PEG_3.5kDa; PDA coating; Folic acid [active] | | | | | | | 16.64 | |
| Magnetic silica (MSN) | $Fe_3O_4$ NPs [passive] | Spherical | 18.7 (TEM) | NA | Murine colon adenocarcinoma (C-26) s.c. inoculated to right flank of mice (20 g) [colon/allograft heterotopic] | ~0.1 $cm^3$ ~0.2 g | 12 (2 d) | 0.29 | [47] |
| Polymer and carbon coated silica | PGA & MHPCNs coating; Folic acid [active] | Spherical | ~210 | -31.6 | Human cervical carcinoma (HeLa) s.c. inoculated to flank of mice (20 g) [cervix/xenograft heterotopic] | ~0.1 $cm^3$ ~0.1 g | 10 (2 d) | 2.62 | [48] |

| | | | | | | | | | |
|---|---|---|---|---|---|---|---|---|---|
| Periodic mesoporous organosilica | Copper sulfide capped [passive] | Spherical | 222.6 | -17.9 | Murine sarcoma cell line (S180) s.c. inoculated to shoulder of mice (15–20 g) [other cancer type/ allograft orthotopic] | 0.1 $cm^3$ ~0.1 g | 5 (1 d) | 5.12 | [49] |
| Silica coated $Mn_3O_4$ | PEG_0.6kDa; Silica shell; Aptamer AS411 [active] | Spherical | 53.2 | -12.4 | Human cervical carcinoma (HeLa) s.c. inoculated to left flank of mice (31 g) [cervix/xenograft heterotopic] | ~1.1 $cm^3$ ~1.3 g | 16 (1 d) | 5.83 | [50] |
| $NaGdF_4$ | PEG_2kDa; $(cRGDyK)_2$ peptide [active] | Spherical | 32 | NA | Human glioblastoma (U87MG) s.c. inoculated to shoulder of mice (20–24 g) [brain/xenograft heterotopic] | ~1.8 $cm^3$ ~2.1 g | 90.9 (22 h) | 4.28 | [51] |
| $MoS_2/Fe_3O_4$ composite | PEG_0.4kDa [passive] | Flake | 190.1 | -21.9 | Human pancreatic adenocarcinoma (PANC-1) s.c. inoculated to backside of mice (18 g) [pancreas/xenograft heterotopic] | 0.1 $cm^3$ ~0.1 g | 20 (7 d) | 0.21 | [52] |
| CaP | PEG_12kDa [passive] | Spherical | 80 | -0.5 | Murine colon adenocarcinoma (C-26) s.c. inoculated in mice [colon/allograft heterotopic] | 0.1 $cm^3$ ~0.1 g | 11 (1 d) | 0.37 | [53] |
| MnO | PEG_1.9kDa; cRGD peptide [active] | Spherical | 100 | 3 [c] | Human lung adenocarcinoma (A549) s.c. inoculated to right flank of mice (18 g) [lung/xenograft heterotopic] | 65 $mm^3$ ~0.1 g | 0.5 (4 h) | 41.69 | [54] |
| $Mg_2Al$ layered double hydroxide | BSA coating [passive] | Sheet | 150 | -19 | Murine mammary carcinoma (4T1) s.c. inoculated to the flank of mice (20 g) [breast/allograft heterotopic] | ~0.2 $cm^3$ ~0.2 g | 1.2 (1 d) | 1.69 | [55] |
| Cobalt nanotube | Folate [active] | AR 38.2 Rod | 166.8 325×9 (TEM) | -14.6 | Human cervical carcinoma (HeLa) s.c. inoculated to flank of mice (20–22 g) [cervix/xenograft heterotopic] | ~0.2 $cm^3$ ~0.2 g | 5 (1 d) | 0.23 | [56] |

| | | | | | | | | | |
|---|---|---|---|---|---|---|---|---|---|
| AuNPs coated fullerene | PEG_5kDa [passive] | Spherical | 112.2 | -9.8 | Murine sarcoma cell line (S180) s.c. inoculated to shoulder of mice (18–20 g) [other cancer type/ allograft orthotopic] | ~0.1 $cm^3$ ~0.1 g | 5 (12 h) | 0.75 | [57] |
| | | | 143.4 | -12.7 | | | | 0.59 | |
| $Bi_2Se_3$ | HSA and PDA coating [passive] | Spherical | 112 | -14.4 | Human cervical carcinoma (HeLa) s.c. inoculated to flank of mice (20–22 g) [cervix/xenograft heterotopic] | ~0.4 $cm^3$ ~0.5 g | 25 (1 d) | 1.99 | [58] |
| Calcium phosphate | PEG_12kDa [passive] | Spherical | 60 | -0.5 | Murine colon adenocarcinoma (C-26) s.c. inoculated to right femoral of mice (18 g) [colon/allograft heterotopic] | 0.1 $cm^3$ ~0.1 g | 9.1 (3x) (1.25 d) | 0.89 | [59] |
| $Gd_3N$ | PEG_5kDa; $C_{80}$ encapsulated [passive] | Spherical | 49.2 | NA (assumed neutral) | Murine colon adenocarcinoma (C-26) s.c. inoculated to right femoral of mice (23 g) [colon/allograft heterotopic] | 0.1 $cm^3$ ~0.1 g | 0.7 (3.1 d) | 0.31 | [60] |
| Hollow mesoporous CuS | Transferrin [active] | Spherical | 205 | -25.5 | Human breast adenocarcinoma (MCF-7) s.c. inoculated to shoulder of mice (20 g) [breast/xenograft heterotopic] | 0.1 $cm^3$ ~0.1 g | 35 (4 d) | 0.04 | [61] |
| Polymeric | PLG160-*g*-PEG_5kDa [passive] | Spherical | 36.7 | -8.5 | Murine Lewis lung carcinoma (LLC) s.c. inoculated to right flank of mice (17 g) [lung/allograft heterotopic] | 0.2 g | CDDP: 5 (2 d) | 1.26 | [62] |
| Polymeric | PAMAM-PLA-*b*-PEG5kDa; TRC105 antibody [active] | Spherical | 37 | NA | Murine mammary carcinoma (4T1) s.c. inoculated to front flank of mice (20 g) [breast/allograft heterotopic] | 180 $mm^3$ ~0.2 g | 0.3 (2 d) | 0.91 | [63] |
| | PAMAM-PLA-*b*-PEG5kDa [passive] | | 37 | NA | | | | 0.50 | |

| | | | | | | | | | |
|---|---|---|---|---|---|---|---|---|---|
| Polymeric | Cy7-labeled PEG_5kDa-*b*-p(HPMAm-Bz) loaded with Cy5.5-based model drug [passive] | Spherical | 72 | -0.5 | Human epithelial carcinoma (A431) orthotopically inoculated to right flank of mice (22.5 g) [skin/xenograft orthotopic] | 100 $mm^3$ ~0.1 g | 14.2 (2 d) | 1.04 | [64] |
| | Cy7-labeled PEG_5kDa-*b*-p(HPMAm-Bz) [passive] | | 72 | -0.5 | | | | 1.16 | |
| Polymeric | Pluronic P105; F127 [passive] | Spherical | 22.3 | -1.5 | Human breast adenocarcinoma (MCF-7/ADR) s.c. inoculated to right hind leg of mice (20 g) [breast/xenograft heterotopic] | ~0.3 $cm^3$ ~0.3 g | DOX: 2 PTX: 3 (2 d) | 0.17 | [65] |
| Polymeric | PEG_2kDa [passive] | Mixed spherical/ cylindrical | 89 | -7 | Human epidermoid carcinoma (A431) s.c. inoculated in forelimb oxter of mice (21–23 g) [skin/xenograft orthotopic] | 30 $mm^3$ ~0.04 g | PTX: 5 (8 h) | 0.02 | [66] |
| | PEG_2kDa; C225 cetuximab antibody [active] | | 88 | -24.2 | | | | 0.06 | |
| Polymeric | PLGA [passive] | AR 4.0 Rod | 227 320×80 (TEM) | -3.2 | Human ovarian carcinoma (SKOV-3) s.c. inoculated to the right flank of mice (14–18 g) [ovary/xenograft heterotopic] | 150 $mm^3$ ~0.2 g | DTX: 10 (7 d) | 0.30 | [67] |
| | | Cylinder (Cubic) | 263 200×200 (TEM) | -3.4 | | | | 0.23 | |
| Polymeric | PLGA; 9% DTX [passive] | AR 4.0 Rod | 216 320×80 (TEM) | -3.1 | Human alveolar adenocarcinoma (A549) s.c. inoculated to the right flank of mice (20 g) [lung/xenograft heterotopic] | 150 $mm^3$ ~0.2 g | DTX: 10 (7 d) | 0.08 | [68] |
| | PLGA; 20% DTX [passive] | AR 4.0 Rod | 216 200×200 (TEM) | -3.4 | | | | 0.09 | |

| | | | | | | | | | |
|---|---|---|---|---|---|---|---|---|---|
| Polymeric | PEG_2kDa; Folic acid; PLGA [active] | Spherical | 274.1 | -12.1 | Human breast adenocarcinoma (MDA-MB-231) s.c. injected to the right flank of mice (20 g) [breast/xenograft heterotopic] | ~0.2 $cm^3$ ~0.2 g | 1.25 (12 h) | 1.26 | 69 |
| | PLGA [passive] | | 216.6 | -14.3 | | | | 0.42 | |
| Polymeric | DACHPt-loaded micelles; PEG-*b*-P(Glu) copolymer; P(Glu) homopolymer [passive] | Spherical | 30 | -2.3 | Murine colon adenocarcinoma (C-26) s.c. inoculated in mice (20 g) [colon/allograft heterotopic] | 100 $mm^3$ ~0.1 g | 5 (1 d) | 0.80 | 70 |
| | | | 54 | -1.6 | | | | 0.82 | |
| | | | 69 | -0.9 | | | | 0.91 | |
| | | | 110 | 0.2 | | | | 0.70 | |
| | | | 30 | -2.3 | Human pancreatic adenocarcinoma (BxPC3) s.c. inoculated in mice (20 g) [pancreas/xenograft heterotopic] | | | 0.98 | |
| | | | 54 | -1.6 | | | | 0.63 | |
| | | | 69 | -0.9 | | | | 0.39 | |
| | | | 110 | 0.2 | | | | 0.39 | |
| Polymeric | Hydrazine; PEG_2kDa; Folic acid [active] | Spherical | 70.9 | 4 [c] | Murine mammary carcinoma (4T1) s.c. inoculated to the right back of mice (20 g) [breast/allograft heterotopic] | 50 $mm^3$ 0.06 g | DOX: 5 (1 d) | 0.63 | 71 |
| | Carbamate; PEG_2kDa; Folic acid [active] | | 86.6 | 2 [c] | | | | 0.49 | |
| | PEG_2kDa-PCL [passive] | | 64 [c] | 3 [c] | | | | 0.36 | |
| Polymeric | Cross-linked PEG_9.5kDa; Carborane Tyrosine [passive] | Spherical | 88.9 | -0.5 | Murine colon adenocarcinoma (C-26) s.c. inoculated to the back of mice (22 g) [colon/allograft heterotopic] | 100 $mm^3$ ~0.1 g | 1.3 (1 d) | 0.33 | 72 |
| | Non-cross-linked PEG_9.5kDa; Tyrosine [passive] | | 87.1 | -1 | | | | 0.21 | |

| | | | | | | | | | |
|---|---|---|---|---|---|---|---|---|---|
| Polymeric | PEG [passive] | Spherical | 64.2 | -0.4 | Human cervix carcinoma (KB, HeLa derivative) transplanted to abdominal region of mice (20 g) [cervix/xenograft heterotopic] | 100 $mm^3$ ~0.1 g | ADR: 10 (1 d) | 0.67 | [73] |
| | PEG; 5% folate [active] | | 68.4 | -1.1 | | | | 0.59 | |
| | PEG; 10% folate [active] | | 69.2 | -2 | | | | 0.73 | |
| | PEG; 25% folate [active] | | 72.5 | -2.3 | | | | 0.68 | |
| | PEG; 50% [active] | | 77.5 | -7 | | | | 0.78 | |
| | PEG; 100% folate [active] | | 91.3 | -9.3 | | | | 0.74 | |
| Polymeric | DACHPt-loaded micelles; PEG_12kDa [passive] | Spherical | 40 | -2 [c] | Murine colon adenocarcinoma (C-26) s.c. inoculated in mice (20 g) [colon/allograft heterotopic] | 0.2 g | 5 (3 d) | 1.54 | [74] |
| Polymeric | PEG_0.4kDa; cRGD peptide [active] | Spherical | 22.5 | 0 [c] | Murine mammary adenocarcinoma (Cl-66) injected to mammary fat pad of mice (19 g) [breast/allograft orthotopic] | 625 $mm^3$ ~0.8 g | 13.2 (5 d) | 4.52 | [75] |
| Polymeric | PEG_12kDa [passive] | Spherical | 65 | -2 [c] | Murine colon adenocarcinoma (C-26) s.c. inoculated in mice (20 g) [colon/allograft heterotopic] | 100 $mm^3$ ~0.1 g | ADR: 10 (2 d) | 1.13 | [76] |
| Polymeric | Pyrene-ended poly($_{DL}$-lactic acid) [passive] | Spherical | 222 | NA | Murine sarcoma cell line (S180) s.c. inoculated to axillary of mice (30 g) [other cancer type/ allograft orthotopic] | 350 $mm^3$ [c] ~0.4 g | 20 (2 d) | 1.95 | [77] |

| | | | | | | | | | |
|---|---|---|---|---|---|---|---|---|---|
| Polymeric | PEG_1.6kDa; Folate [active] | Spherical | 20 (assumed) | NA | Human nasopharyngeal epidermal carcinoma (KB, HeLa derivative) s.c. inoculated to the nape of the neck of mice (20–25 g) [cervix/xenograft heterotopic] | ~55 mg | 4 (1 d) | 0.24 | [78] |
| | PAA-*b*-PMA [passive] | | 20 | NA | | | | 0.30 | |
| Polymeric | PLGA [passive] | Spherical | 133.5 | -15.8 | Murine Ehrlich ascites carcinoma (EAC) s.c. inoculated to right hind leg of mice (25–30 g) [breast/allograft heterotopic] | 1 $cm^3$ 1.2 g | LTZ: 11.1 (1 d) | 0.95 | [79] |
| Polymeric | Rhodamine B labeled carboxymethyl chitosan [passive] | Spherical | 149.2 | -13.2 | Murine hepatocellular carcinoma (H22) s.c. inoculated to axillary region of mice (18–22 g) [liver/allograft heterotopic] | 100 $mm^3$ ~0.1 g | 100 (1 d) | 10.53 | [80] |
| | | | 157.3 | -23.2 | | | | 8.84 | |
| | | | 156 | -38.4 | | | | 7.66 | |
| | | | 456.5 | -25.1 | | | | 3.59 | |
| | Rhodamine B labeled chitosan hydrochloride [passive] | | 150.1 | 14.8 | | | 15 (1 d) | 1.94 | |
| | | | 150.6 | 25.5 | | | | 2.96 | |
| | | | 152.7 | 34.6 | | | | 3.94 | |
| | | | 300.7 | 24.4 | | | | 1.77 | |
| Polymeric | DACHPt-loaded micelles; PEG_12kDa [passive] | Spherical | 40 | -4 | Murine colon adenocarcinoma (C-26) s.c. inoculated in mice (20 g) [colon/allograft heterotopic] | 100 $mm^3$ ~0.1 g | 5 (3 d) | 0.94 | [81] |
| Polymeric | PEI_25kDa [passive] | Spherical | 399 | 38.1 | Murine Ehrlich ascites carcinoma (EAC) s.c. inoculated to left hind flank of mice (25–30 g) [breast/allograft heterotopic] | ~1.8 $cm^3$ ~2.2 g | 0.05 (1 d) | 0.62 | [82] |
| | 3% chondroitin sulfate-PEI [passive] | | 276 | 16.4 | | | 0.36 (1 d) | 3.28 | |

| | | | | | | | | | |
|---|---|---|---|---|---|---|---|---|---|
| Graphene oxide | NOTA; PEG_5kDa [passive] | Flake | 26.2 | -16.4 | Murine mammary carcinoma (4T1) s.c. inoculated to the flank of mice (20 g) [breast/allograft heterotopic] | ~0.2 $cm^3$ ~0.2 g | 5 (2 d) | 0.46 | 83 |
| | NOTA; PEG_5kDa; TRC105 antibody [active] | | 37 | -2 | | | | 0.99 | |
| Graphene oxide | NOTA; PEG_10kDa [passive] | Flake | 21.9 | -9.5 | Murine mammary carcinoma (4T1) s.c. inoculated to front flank of mice (20 g) [breast/allograft heterotopic] | ~0.2 $cm^3$ ~0.2 g | 5 (2 d) | 0.46 | 84 |
| | NOTA; PEG_10kDa; TRC105 antibody [active] | | 27 | -0.1 | | | | 0.89 | |
| Graphene oxide | PEG_4kDa [passive] | Flake | 90 50×1.9 (AFM) | -30 [c] | Murine melanoma (B16-F10) s.c. inject to right arm of mice (18–20 g) [skin/allograft orthotopic] | 200 $mm^3$ ~0.2 g | PTX: 50 (1 d) | 9.72 | 85 |
| Graphene oxide | NOTA; PEG_5kDa [passive] | Flake | 27.7 | -9.5 | Human glioblastoma (U-87MG) s.c. inoculated to flank of mice (20 g) [brain/xenograft heterotopic] | 60 $mm^3$ ~0.07 g | 5 (2 d) | 0.21 | 86 |
| | NOTA; PEG_5kDa; VEGF121 ligand [active] | | 32.9 | -5 [c] | | | | 0.37 | |
| Graphene oxide | NOTA; PEG_5kDa [passive] | Flake | 21.9 | -9.5 | Murine mammary carcinoma (4T1) s.c. inoculated to front flank of mice (20 g) [breast/allograft heterotopic] | ~0.2 $cm^3$ ~0.2 g | 5 (1 d) | 0.68 | 87 |
| | NOTA; PEG_5kDa; TRC105 antibody [active] | | 27 | -0.1 | | | | 1.04 | |

| | | | | | | | | | |
|---|---|---|---|---|---|---|---|---|---|
| Single-walled carbon nanotubes (SWCNTs) | PEG_2kDa [passive] | AR 80 Rod | 2.5×200 (AFM) | NA | Human glioblastoma (U-87MG) s.c. inoculated to the front left leg of mice (25 g) [brain/xenograft heterotopic] | ~250 $mm^3$ ~0.3 g | 0.04 (1 d) | 0.79 | 88 |
| | PEG_2kDa; RGD peptide [active] | | | | | | | 1.25 | |
| | PEG_5.4kDa [passive] | | | | | | | 1.14 | |
| | PEG_5.4kDa; RGD peptide [active] | | | | | | | 3.56 | |
| Liposomes | DPPC; Cholesterol; DSPE-PEG_2kDa; Iohexol; GH680 [passive] | Spherical | 96.4 | -59.4 | Human cervical carcinoma (ME180) orthotopically inoculated in mice (21 g) [cervix/xenograft orthotopic] | ~500 $mm^3$ ~0.6 g | 1220 (5 d) | 1.91 | 89 |
| Liposomes | PEG_2kDa [passive] | Spherical | 79.1 | -36.1 | BALB/c TP53(-/-) mammary adenocarcinoma transplanted to mammary fat pad of mice (23 g) [breast/allograft orthotopic] | ~0.1 $cm^3$ ~0.1 g | DOX: 6 (4 d) | 0.15 | 90 |
| | | | | | Mice (23 g) carrying a transgene (C3-Tag) were bred in house until tumor size reaching >0.5 cm in any dimension [breast/other tumor model] | ~0.1 $cm^3$ ~0.1 g | | 0.43 | |
| Lipid nanocarrier (Liposomes) | Alendronate-hyaluronate grafted polymer [active] | Spherical | 386 [c] | 20 [c] | Murine Ehrlich ascites carcinoma (EAC) s.c. inoculated to right hind flank of mice (25–30 g) [breast/allograft heterotopic] | ~600 $mm^3$ ~0.7 g | 13.1 (1 d) | 1.66 | 91 |

| | | | | | | | | | |
|---|---|---|---|---|---|---|---|---|---|
| Liposomes | DSPE-PEG_2kDa [passive] | Spherical | 120 | 0 [c] | Syngeneic murine mammary carcinoma (MET1) transplanted to mammary fat pad of mice (15–25 g) [breast/allograft orthotopic] | ~0.2 g | 50 (2 d) | 0.93 | [92] |
| Lipid nanocapsule (Liposomes) | PEG_0.9kDa [passive] | Spherical | 25 | -3 | Human embryonic kidney cell line (HEK293($\beta_3$)) s.c. inoculated in mice (27 g) [kidney/xenograft heterotopic] | ~65 $mm^3$ ~0.08 g | 741 (1 d) | 0.10 | [93] |
| | | | 51 | -4 | | | | 0.06 | |
| | | | 93 | -6 | | | | 0.07 | |
| Liposomes | PEG-*nido*-carborane [passive] | Spherical | 168 [c] | NA | Murine colon adenocarcinoma (C-26) s.c. inoculated to back of mice (20–25 g) [colon/allograft heterotopic] | ~270 $mm^3$ ~0.3 g | 11.1 (3 d) | 0.52 | [94] |
| | PEG-*nido*-carborane; Transferrin [active] | | 225 [c] | NA | | | | 0.88 | |
| Lipid nanocapsule (Liposomes) | DSPE-PEG_2kDa [passive] | Spherical | 118 | 0 [c] | Murine colon adenocarcinoma (C-26) s.c. inoculated to back regions of mice (18–21 g) [colon/allograft heterotopic] | 20 $mm^3$×3 ~0.07 g | 15 (1 d) | 0.55 | [95] |
| Liposomes | PEG_2kDa [passive] | Spherical | 200 | -2 | Human anaplastic thyroid carcinoma (ARO) s.c. inoculated to the flank of mice (25–30 g) [other cancer type/ xenograft heterotopic] | ~400 $mm^3$ ~0.5 g | 145.5 (1 d) | 0.43 | [96] |
| Liposomes | PEG [passive] | Spherical | 100 | 0 [c] | Human melanoma (A375) s.c. inoculated to right flank of mice (21 g) [skin/xenograft orthotopic] | ~1.25 g | 1 (3 d) | 0.96 | [97] |

| | | | | | | | | | |
|---|---|---|---|---|---|---|---|---|---|
| Hyaluronic acid hydrogel | HA; HP-*β*-cyclodextrin (HPCD); Vitamin E succinate (VES) [active] | Spherical | 200.8 | -14 | Murine mammary carcinoma (4T1) s.c. inoculated to right flank of mice (18–20 g) [breast/allograft heterotopic] | ~125 $mm^3$ ~0.15 g | DOX: 10 (1 d) | 0.04 | 98 |
| | HA bearing 2 PEG_5kDa chains; HPCD; VES [active] | | 217.4 | -13.5 | | | | 0.05 | |
| | HA bearing 5 PEG_5kDa chains; HPCD; VES [active] | | 225.8 | -13.1 | | | | 0.09 | |
| | HA bearing 10 PEG_5kDa chains; HPCD; VES [active] | | 241.7 | -10.8 | | | | 0.07 | |
| Hyaluronic acid hydrogel | HA modified with methacrylic anhydride [active] | Spherical | 50 | -45 | Murine hepatocellular carcinoma (H22) s.c. inoculated to left flank of mice (20–25 g) [liver/allograft heterotopic] | 50 $mm^3$ 0.06 g | DOX: 4.5 (3 d) | 0.12 | 99 |
| Heparin-based hydrogel | Heparin copolymerized with cystamine bisacrylamide [passive] | Spherical | 87.5 | -30 | Murine hepatocellular carcinoma (H22) s.c. inoculated to left flank of mice (20–25 g) [liver/allograft heterotopic] | ~50 $mm^3$ 0.06 g | DOX: 4 (1 d) | 0.44 | 100 |
| Chitosan hydrogel | Chitosan [passive] | Spherical | 146 | 9 [c] | Murine hepatocellular carcinoma (H22) s.c. inoculated to right limb armpit of mice (20–25 g) [liver/allograft heterotopic] | ~70 $mm^3$ ~0.08 g | 4 (1 d) | 0.22 | 101 |
| | Chitosan; Bradykinin-potentiating peptide [active] | | 138.5 | 9 [c] | | | | 0.25 | |

| | | | | | | | | | |
|---|---|---|---|---|---|---|---|---|---|
| Hyaluronic acid hydrogel | HA-PEI_10kDa; HA-PEG_2kDa; Indocyanine green [active] | Spherical | 200 | -14.6 | Human alveolar adenocarcinoma ($A549^{DDP}$) s.c. inoculated to right shoulder of mice (20 g) [lung/xenograft heterotopic] | 200 mm3<br>~0.2 g | 0.5×3<br>(3 d) | 0.37 | [102] |
| Gelatin hydrogel | Thiolated gelatin [passive] | Spherical | 132.6 | -24.6 | Human pancreatic adenocarcinoma (PANC-1) s.c. inoculated to left flank of mice (20 g)<br>[pancreas/xenograft heterotopic] | 150 $mm^3$<br>~0.2 g | 0.75<br>(1 d) | 0.84 | [103] |
| | Thiolated gelatin; PEG_2kDa [passive] | | 179 | -22.3 | | | | 1.39 | |
| | Thiolated gelatin; PEG_2kDa; EGFR peptide [active] | | 230.8 | -18.1 | | | | 2.40 | |
| Alginic acid hydrogel | Alginic acid [passive] | Spherical | 132 | -34.2 | Murine hepatocellular carcinoma (H22) s.c. inoculated to right armpit of mice (25 g) [liver/allograft heterotopic] | 150 $mm^3$<br>~0.2 g | DOX: 4<br>(3 d) | 0.68 | [104] |
| Cellulose hydrogel | Methacrylated carboxymethyl cellulose; Cystamine Bisacrylamide [passive] | Spherical | 193 | -25.7 | Murine hepatocellular carcinoma (H22) s.c. inoculated to left flank of mice (20–25 g) [liver/allograft heterotopic] | 100 $mm^3$<br>~0.1 g | DOX: 5<br>(3 d) | 0.18 | [105] |
| Dendrimers *vs.* copolymers | PAMAM G7.0 dendrimers [passive] | Spherical | 8 | -1.3 | Human ovarian carcinoma (A2780) orthotopically inoculated to left ovarian bursa of mice (30 g) [ovary/xenograft heterotopic] | ~1.8 $cm^3$<br>~2.1 g | 20<br>(7 d) | 9.87 | [106] |
| | HPMA copolymers (52 kDa) [passive] | | 6.6 | -1.5 | | | 40<br>(1 d) | 3.23 | |
| Dendrimers | Lysine G6.0 [passive] | Spherical | 5.9 | 19.8 | Murine colon adenocarcinoma (C-26) s.c. inoculated to back of mice (25–27 g) [colon/allograft heterotopic] | 100 $mm^3$<br>~0.1 g | 1<br>(1 d) | 0.27 | [107] |
| | Lysine G6.0; 76 PEG_5kDa chains [passive] | | 16.9 | -6.5 | | | | 1.37 | |

| | | | | | | | | | |
|---|---|---|---|---|---|---|---|---|---|
| Dendrimers | PAMAM G5.0 [passive] | Spherical | 5 (reported as <5 nm) | NA | Human carcinoma (KB, HeLa derivative) s.c. inoculated to flank of mice (21 g) [cervix/xenograft heterotopic] | ~0.9 $cm^3$ ~1.1 g | 8.3 (7 d) | 2.09 | 108 |
| | PAMAM G5.0; Folic acid [active] | | | | | | 9.5 (7 d) | 7.97 | |
| Dendrimers *vs.* copolymers | HPMA copolymers (131 kDa) [passive] | Spherical | 16.4 | -19.2 | Human ovarian carcinoma (A2780) orthotopically inoculated to left ovarian bursa of mice (30 g) [ovary/xenograft heterotopic] | ~1.8 $cm^3$ ~2.1 g | 20 (7 d) | 3.34 | 109 |
| Tabacco mosaic virus | PEG_8kDa [passive] | AR 16.7 Rod | 95 [c] 300×18 (TEM) | -36 [c] | Human glioblastoma (U-87MG) s.c. inoculated to flank of mice (20 g) [brain/xenograft heterotopic] | ~0.2 $cm^3$ [c] ~0.2 g | 0.05 (3 d) | 0.05 | 110 |
| Anticancer drug (HCPT) | HCPT PEGylated with C18-PMH-PEG [passive] | AR 1.3 Rod | 163 | -4.3 | Murine mammary carcinoma (4T1) s.c. inoculated to right shoulder of mice (20 g) [breast/allograft heterotopic] | ~100 $mm^3$ ~0.1 g | HCPT: 10 (1 d) | 3.41 | 111 |
| | | AR 2.0 Rod | 221 | | | | | 2.81 | |
| | | AR 3.2 Rod | 324 | | | | | 2.33 | |
| | | AR 4.0 Rod | 402 | | | | | 2.04 | |
| Solid lipid NPs | DOPE; Cholesterol; DC-cholesterol [passive] | Spherical | 85.8 | 71.3 | Human lung adenocarcinoma (H1975) s.c. inoculated to flank region of mice (20 g) [lung/xenograft heterotopic] | ~75 $mm^3$ ~0.09 g | 50 (1 d) | 0.15 | 112 |
| | DOPE; Cholesterol; DC-cholesterol; PEG_5kDa [passive] | | 134.7 | 0.6 | | | | 0.36 | |

| | | | | | | | | | |
|---|---|---|---|---|---|---|---|---|---|
| | DOPE; Cholesterol; DC-cholesterol; PEG_5kDa; Cetuximab antibody [active] | | 168.2 | -0.8 | | | | 0.38 | |
| Solid lipid NPs | Tripalmitin [passive] | Spherical | 387 (SEM) | -46.6 | Dalton's lymphoma cells s.c. inoculated to right hind leg of mice (25–30 g) [other cancer type/ allograft heterotopic] | ~0.9 $cm^3$ ~1.1 g | 3.6 (1 d) | 0.04 | [113] |
| Polymer-lipid hybrid | PTX loaded [passive] | Spherical | 164.7 | -30.5 | Human glioblastoma (T98G) orthotopically injected into the right striatum of mice (20 g) [brain/xenograft orthotopic] | 100 $mm^3$ ~0.1 g | PTX: 10 (1 d) | 0.43 | [114] |
| | PTX loaded; DSPE-PEG_2kDa; Folic acid [active] | | 175.3 | -27.2 | | | | 0.61 | |
| | PTX-cRGDfK peptide conjugate (PTXR) loaded [passive] | | 171.7 | -32.8 | | 100 $mm^3$ ~0.1 g | PTX: 10 (1 d) | 0.54 | |
| | PTXR loaded; DSPE-PEG_2kDa; Folic acid [active] | | 186.9 | -29.5 | | | | 0.90 | |
| Polymeric | PEG_3.5kDa-*b*-PLGA polymer [passive] | Spherical | 134 | NA | Murine mammary carcinoma (4T1) s.c. inoculated to right flank of mice (18–20 g) [breast/allograft heterotopic] | 100 $mm^3$ ~0.1 g | DOX: 5 (1 d) | 0.03 | [115] |
| Polymeric | Poly(styrene-*co*-maleic anhydride) copolymer [passive] | Spherical | 174 | -22.9 | Murine Ehrlich ascites carcinoma (EAC) s.c. inoculated to right hind leg of mice (18–22 g) [breast/allograft heterotopic] | 50 $mm^3$ 0.06 g | PTX: 20 (1 d) | 0.03 | [116] |

| | | | | | | | | | |
|---|---|---|---|---|---|---|---|---|---|
| Polymeric | $PEG_{3.4k}$-$PCL_{8.3k}$ copolymer [passive] | Spherical | 98 | -3.4 | Human breast adenocarcinoma (MDA-MB-231) orthotopically inoculated to mammary fat pad of mice (20 g) [breast/xenograft orthotopic] | 60 $mm^3$ ~0.07 g | 0.36 (1 d) | 0.14 | 117 |
| | $PEG_{3.4k}$-$PCL_{5.7k}$ copolymer [passive] | | 94 | | | | | 0.85 | |
| | $PEG_{3.4k}$-$PCL_{5.3k}$ copolymer [passive] | | 104 | | | | | 1.39 | |
| | $PEG_{3.4k}$-$PCL_{4.5k}$ copolymer [passive] | | 96 | | | | | 2.76 | |
| | $PEG_{3.4k}$-$PCL_{3.7k}$ copolymer [passive] | | 103 | | | | | 6.94 | |
| Polymeric | PEG_2kDa-PLGA [passive] | Spherical | 176.6 | -23.1 | Murine lung carcinoma (M109) s.c. transplanted to right flank of mice (20 g) [lung/allograft heterotopic] | 60 $mm^3$ ~0.07 g | CDDP: 5 PTX: 12 (1 d) | 0.07 | 118 |
| | Folate; PEG_2kDa-PLGA [active] | | 185.9 | -24.7 | | | | 0.16 | |
| Polymeric | Cholesterol; DOPA; DSPC; DSPE-PEG_2kDa; Pyrolipid coating [passive] | Spherical | 108 | -2.3 | Murine colon adenocarcinoma (C-26) s.c. inoculated to the right flank of mice (20 g) [colon/allograft heterotopic] | 100 $mm^3$ ~0.1 g | CDDP: 3 (2 d) | 1.56 | 119 |
| Polymeric | Cy3 dye labeled; PEG_12kDa [passive] | Spherical | 49.9 | 0.1 | Murine colon adenocarcinoma (C-26) s.c. inoculated in mice (20 g) [colon/allograft heterotopic] | 100 $mm^3$ ~0.1 g | 16 (2 d) | 0.37 | 120 |
| Polymeric | Dextran (polysaccharide) [passive] | Spherical | 50 (STEM) | -20 | Murine mammary carcinoma (4T1) s.c. inoculated to mammary fat pad of mice (20 g) [breast/allograft orthotopic] | 400 $mm^3$ ~0.5 g | CDDP: 5 (1 d) | 0.94 | 121 |
| | Dextran; LHRH peptide [active] | | 55 (STEM) | -17 | | | | 1.43 | |

| | | | | | | | | | |
|---|---|---|---|---|---|---|---|---|---|
| Polymeric | Chimeric polypeptide [passive] | Spherical | 40 (AFM) | NA | Murine mammary carcinoma (4T1) orthotopically inoculated in the 4$^{th}$ mammary fat pad of mice (18–22 g) [breast/allograft orthotopic] | 100 $mm^3$ ~0.1 g | DOX: 20 (3 d) | 0.44 | [122] |
| Polymeric | Cholesterol; DOPA; DOPC; DSPE-PEG_2kDa; [passive] | Spherical | 49.5 | -1.3 | Murine colon adenocarcinoma (C-26) s.c. inoculated in mice (20 g) [colon/allograft heterotopic] | 100 $mm^3$ ~0.1 g | OP: 3 (2 d) | 0.83 | [123] |
| Polymeric | PEGylated PVP-PASP [passive] | Spherical | 115 | -20 | Murine hepatocellular carcinoma (H22) s.c. inoculated on left flank of mice (32–36 g) [liver/allograft heterotopic] | 20 $mm^3$ ~0.02 g | CDDP: 6 (1 d) | 0.02 | [124] |
| Polymeric | $PEG_{5k}$-P(HEMA-$SN38_{3.5k}$) [passive] | Spherical | 35 | -4 | Human cervix adenocarcinoma (Bcap37, HeLa derivative) s.c. inoculated in mice (20 g) [cervix/xenograft heterotopic] | 100 $mm^3$ ~0.1 g | SN38: 5 (1 d) | 0.30 | [125] |
| | $PEG_{5k}$-P(HEMA-$SN38_{3.5k}$) [passive] | | 100 | | | | | 0.81 | |
| | $PEG_{5k}$-P(HEMA-$SN38_{7k}$) [passive] | | 110 | | | | | 1.00 | |
| | $PEG_{20k}$-P(HEMA-$SN38_{25k}$) [passive] | | 100 | | | | | 1.01 | |
| | $PEG_{5k}$-P(HEMA-$SN38_{3.5k}$) [passive] | | 150 | | | | | 0.98 | |
| Polymeric | PEG_2kDa-PLMB [passive] | Spherical | 107.8 | NA | Murine cervical carcinoma (U14) s.c. implanted to right leg of mice (18–20 g) [cervix/allograft heterotopic] | ~75 $mm^3$ 0.09 g | DOX: 2 (3 d) | 0.30 | [126] |

| | | | | | | | | | |
|---|---|---|---|---|---|---|---|---|---|
| Polymeric | $PBD_{1.8k}$-*b*-$PEO_{4k}$; $PBD_{1k}$-*b*-$PAA_{2.2k}$ [passive] | Star | 25 | NA | Human colon carcinoma (LS174T) s.c. injected to hind limb of mice (20 g) [colon/xenograft heterotopic] | ~250 $mm^3$ ~0.3 g | ~0.01 g (5 d) | 1.39 | 127 |
| Polymeric | mPEG_1kDa-s-s-vitamin E succinate; Polymer-based liposome coating [passive] | Spherical | 113.3 | <10 | Murine mammary carcinoma (4T1) orthotopically transplanted to the 4$^{th}$ mammary fat pad of mice (18–20 g) [breast/allograft orthotopic] | ~175 $mm^3$ ~0.2 g | DTX: 10 (1 d) | 0.25 | 128 |
| Polymeric | PLGA [passive] | Spherical | 152 | -10.3 | Murine hepatocellular carcinoma (H22) s.c. inoculated to armpit of mice (20–25 g) [liver/allograft heterotopic] | 50 $mm^3$ 0.06 g | EPI: 5 (1 d) | 0.12 | 129 |
| | Tat peptide-conjugated PLGA [active] | | 157 | -8.8 | | | | 0.22 | |
| Polymeric | PLA [passive] | Spherical | 135 | NA | Murine sarcoma cell line (S180) s.c. inoculated to armpit of mice (25 g) [other cancer type/ allograft orthotopic] | ~125 $mm^3$ 0.15 g | OP: 3 (12 h) | 0.08 | 130 |
| | PEG-PLA [passive] | | 154.6 | NA | | | | 0.13 | |
| Polymeric | PEG_2kDa; Stearic acid; Glycerol carbonate [passive] | Spherical | 20.4 | 3.9 | Murine hepatocellular carcinoma (H22) s.c. injected to right flank of mice (22–25 g) [liver/allograft heterotopic] | ~150 $mm^3$ ~0.2 g | DOX: 5 (2 d) | 0.01 | 131 |
| Polymeric | PLGA-lecithin-PEG_2kDa [passive] | Spherical | 110 | -5.1 | Human hepatocellular carcinoma (HepG2) s.c. inoculated to dorsum of mice (25 g) [liver/xenograft heterotopic] | ~250 $mm^3$ 0.3 g | DOX: 2 (1 d) | 0.15 | 132 |
| | PLGA-lecithin-PEG_2kDa; Biotin [active] | | 111.3 | -6.2 | | | | 0.21 | |

| | | | | | | | | | |
|---|---|---|---|---|---|---|---|---|---|
| Polymeric | Cholesterol; DOPA; DOPC; DSPE-PEG_2kDa; DSPE-siRNA [passive] | Spherical | 105.3 | -4.8 | Murine colon adenocarcinoma (C-26) s.c. injected in mice (20–25 g) [colon/allograft heterotopic] | 100 $mm^3$ ~0.1 g | CDDP: 3 (2 d) | 0.46 | [133] |
| Polymeric | PCB-PCL [passive] | Spherical | 143 | ~0 | Human hepatocellular carcinoma (HepG2) s.c. inoculated in mice (20 g) [liver/xenograft heterotopic] | 100 $mm^3$ ~0.1 g | DOX: 10 (1 d) | 0.32 | [134] |
| | PCB-s-s-PCL [passive] | | 145 | ~0 | | | | 0.31 | |
| | PCB-s-s-PCL; cRGDfK peptide [active] | | 148 | ~0 | | | | 0.43 | |
| Polymeric | Chitosan [passive] | Spherical | 106.8 | 35.6 | Human alveolar adenocarcinoma (A549-WT) s.c. injected to right flank of mice (20 g) [lung/xenograft heterotopic] | 200 $mm^3$ ~0.2 g | 3 (5 d) | 0.15 | [135] |
| | Chitosan; EGFR peptide [active] | | 227.3 | 28.3 | | | | 0.20 | |
| | Chitosan [passive] | | 106.8 | 35.6 | Human alveolar adenocarcinoma ($A549^{DDP}$) s.c. injected to right flank of mice (20 g) [lung/xenograft heterotopic] | | | 0.16 | |
| | Chitosan; EGFR peptide [active] | | 227.3 | 28.3 | | | | 0.31 | |
| Polymeric | PEG_2kDa-Fmoc-NLG [passive] | Spherical | 96.6 | NA (assumed neutral) | Murine mammary carcinoma (4T1) s.c. inoculated in mice (16–18 g) [breast/allograft heterotopic] | ~500 $mm^3$ ~0.6 g | PTX: 10 (2 d) | 0.52 | [136] |

| | | | | | | | | | |
|---|---|---|---|---|---|---|---|---|---|
| Polymeric | PCL-s-s-$PEG_{2k}$ [passive] | Spherical | 125.5 | -7.4 | Murine hepatocellular carcinoma (H22) s.c. inoculated at right backside of mice (20 g) [liver/allograft heterotopic] | 50 $mm^3$ 0.06 g | DOX: 5 (1 d) | 0.19 | 137 |
| | PCL-s-s-$PEG_{2k}$; PBA ligand [active] | | 130.4 | -2.3 | | | | 0.32 | |
| Polymeric | PLGA-TPGS [passive] | Spherical | 182.6 | -22.6 | Murine hepatocellular carcinoma (Hca-F) s.c. inoculated to right armpit of mice (20–22 g) [liver/allograft heterotopic] | ~1.5 $cm^3$ 1.8 g | EMO: 10 (1 d) | 5.40 | 138 |
| Polymeric | PEG-s-s-PCL; PBA ligand [active] | Spherical | 163 | NA (assumed neutral) | Murine hepatocellular carcinoma (H22) s.c. inoculated to backside of mice (20 g) [liver/allograft heterotopic] | 50 $mm^3$ 0.06 g | DOX: 2 (1 d) | 0.56 | 139 |
| | 6-arm PEG_6kDa cross linked with PEG-s-s-PCL [passive] | | 152 | | | | | 0.67 | |
| | 6-arm PEG_6kDa cross linked with PEG-s-s-PCL; PBA ligand [active] | | 152 | | | | | 1.14 | |
| Polymeric | Linear HPMA_27kDa [passive] | Spherical | 8.6 | NA | Murine lymphoma cells (EL4) s.c. transplanted into right flank of mice (20 g) [other cancer type/ allograft heterotopic] | ~150 $mm^3$ ~0.2 g | DOX: 85 (4 d) | 0.56 | 140 |
| | Star-like HPMA_250kDa [passive] | | 25.6 | NA | | | DOX: 22.5 (4 d) | 1.79 | |
| Polymeric | $PEG_{2k}$-PLGA; LHRH peptide [active] | Spherical | 150 (TEM) | -22.1 | Human breast adenocarcinoma (MCF-7) i.m. injected in thigh of left hind leg of mice (20 g) [breast/xenograft heterotopic] | ~75 $mm^3$ ~0.1 g | PTX: 5 (1 d) | 0.17 | 141 |

| | | | | | | | | | |
|---|---|---|---|---|---|---|---|---|---|
| Polymeric | Inulin-ibuprofen [passive] | Spherical | 143 | NA | Murine hepatocellular carcinoma (H22) s.c. inoculated to armpit of mice (18–22 g) [liver/allograft heterotopic] | 50 $mm^3$ 0.06 g | EPI: 5 (1 d) | 0.21 | 142 |
| | Inulin-ibuprofen; cRGDfK peptide [passive] | | 149 | NA | | | | 0.30 | |
| Polymeric | Heparin-deoxycholate [passive] | Spherical | 166.1 | -36.7 | Murine melanoma (B16-F10) s.c. inoculated to mice (17–21 g) [skin/allograft orthotopic] | 100 $mm^3$ ~0.1 g | DOX: 5 (1 d) | 0.15 | 143 |
| Polymeric | $PEG_{2k}$-PLGA-s-s-siRNA [passive] | Spherical | 76.3 | -13 | Human colorectal adenocarcinoma (HT-29) s.c. implanted above the mammary fat pad of mice (20 g) [colon/xenograft heterotopic] | 85 $mm^3$ ~0.1 g | 3 (7 d) | 0.23 | 144 |
| Polymeric | $PEG_{5k}$-*b*-PDTC [passive] | Spherical | 150 | ~0 | Murine melanoma (B16-F10) s.c. inoculated to hind flank of mice (20 g) [skin/allograft orthotopic] | ~125 $mm^3$ 0.15 g | DOX: 10 (1 d) | 0.38 | 145 |
| | $PEG_{5k}$-*b*-PDTC; cRGDfK peptide [active] | | 152.5 | ~0 | | | | 0.69 | |
| Polymeric | Trimethyl chitosan [passive] | Spherical | 166.4 | 12.3 | Murine hepatocellular carcinoma (H22) s.c. inoculated to axillary region of mice (23.5 g) [liver/allograft heterotopic] | 100 $mm^3$ ~0.1 g | PTX: 10 (1 d) | 0.17 | 146 |
| | Trimethyl chitosan; Folic acid [active] | | 175.1 | 8.7 | | | | 0.24 | |
| Polymeric | PEG_2kDa; Acetylated carboxymethyl cellulose [passive] | Spherical | 20.3 | -2 | Murine mammary carcinoma (EMT6/AR1) s.c. inoculated to right flank of mice (18–20 g) [breast/allograft heterotopic] | ~150 $mm^3$ ~0.2 g | PPT: 180 (4 d) | 0.75 | 147 |

| | | | | | | | | | |
|---|---|---|---|---|---|---|---|---|---|
| Polymeric | POEAd-*g*-LacA20 [active] | Spherical | 197.4 | -20.4 | Murine hepatocellular carcinoma (H22) s.c. inoculated to right flank of mice (18–22 g) [liver/allograft heterotopic] | 300 $mm^3$ ~0.4 g | DOX: 6 (2 d) | 2.63 | 148 |
| | POEAd-*g*-LacA50 [active] | | 276.8 | -23.5 | | | | 2.29 | |
| | POEAd-*g*-LacA80 [active] | | 350 | -27.2 | | | | 0.94 | |
| Polymeric | Poly(ortho ester malonamides) [passive] | Spherical | 258.3 | -23.7 (assumed according to above study) | Murine hepatocellular carcinoma (H22) s.c. inoculated to right flank of mice (18–22 g) [liver/allograft heterotopic] | 300 $mm^3$ ~0.4 g | DOX: 6 (2 d) | 2.60 | 149 |
| | Poly(ortho ester adipamides) [passive] | | 156.6 | | | | | 4.01 | |
| Polymeric | PEG-Chitosan [passive] | Spherical | 165.3 | 25.1 | Human alveolar adenocarcinoma (A549) i.v. injected *via* tail vein to induce tumor in lung region of mice (25 g) [lung/xenograft heterotopic] | ~300 $mm^3$ ~0.4 g | GEM: 15 (1 d) | 10.14 | 150 |
| | PEG-Chitosan; Folic acid [active] | | 184.3 | 21.1 | | | | 23.81 | |
| Polymeric | $mPEG_{2k}$-P(CL-co-(DMMA-CL)) [passive] | Spherical | 122.6 | -15 | Murine mammary carcinoma (4T1) orthotopically inoculated to mammary gland of mice (20 g) [breast/allograft orthotopic] | 100 $mm^3$ ~0.1 g | DOX: 5 (1 d) | 1.46 | 151 |
| Polymeric | Trimethyl chitosan [passive] | Spherical | 107.3 | 23.3 | Murine hepatocellular carcinoma (H22) s.c. injected to right axillary of mice (22 g) [liver/allograft heterotopic] | 200 $mm^3$ ~0.2 g | DOX: 2 (1 d) | 0.82 | 152 |
| | Trimethyl chitosan; Folate [active] | | 190 | 26.1 | | | | 0.65 | |

| | | | | | | | | | |
|---|---|---|---|---|---|---|---|---|---|
| Polymeric | 30% cross-linked PGlu-*g*-mPEG [passive] | Spherical | 137 | -15.6 | Murine hepatocellular carcinoma (H22) s.c. injected to right axillary of mice (22 g) [liver/allograft heterotopic] | 200 $mm^3$ ~0.2 g | CTX: 10 (8 h) | 0.31 | 153 |
| | 70% cross-linked PGlu-*g*-mPEG [passive] | | 129 | -9.1 | | | | 0.24 | |
| Polymeric | P(LA-co-TMCC)-*g*-PEG; Taxane-binding peptide; Anti-HER2 antibody, Fab 73J [active] | Spherical | 121 | -2.4 | Human breast adenocarcinoma (MDA-MB-231) transplanted to mammary fat pad of mice (24 g) [breast/xenograft orthotopic] | 150 $mm^3$ ~0.2 g | DTX: 5 (1 d) | 0.16 | 154 |
| Polymeric | Acetylated carboxymethyl-cellulose; PEG_2kDa [passive] | Spherical | 96 | NA (assumed neutral) | Resistant human prostate carcinoma (PC3-RES) s.c. injected to right flank of mice (20 g) [prostate/xenograft heterotopic] | ~80 $mm^3$ ~0.1 g | CTX: 20 (6 d) | 2.89 | 155 |
| Polymeric | Heparin [passive] | Spherical | 20 | ~5 | Human KB epidermoid carcinoma (KB-3-1, HeLa derivative) s.c. injected to right flank of mice (20 g) [cervix/xenograft heterotopic] | ~100 $mm^3$ ~0.1 g | CDDP: 2.5 (1 d) | 1.67 | 156 |
| | Heparin; Folate [active] | | | | | | | 3.21 | |
| Polymeric | PLGA-$PEG_{5k}$; Perfluorooctyl bromide [passive] | Spherical | 120 | -18 | Murine colon adenocarcinoma (C-26) s.c. injected on left flank of mice (22 g) [colon/allograft heterotopic] | ~320 $mm^3$ ~0.4 g | PTX: 5 (1 d) | 0.15 | 157 |
| Polymeric | PLGA loaded with AuNRs and DTX; $MnO_2$ nanosheets coating [passive] | Spherical | 282.1 | -9.7 | Murine sarcoma cell line (S180) s.c. inoculated to armpit of mice (18–20 g) [other cancer type/ allograft orthotopic] | ~90 $mm^3$ ~0.1 g | DTX: 15 (8 h) | 0.17 | 158 |

| | | | | | | | | | |
|---|---|---|---|---|---|---|---|---|---|
| Lipid-polymer hybrid | Lipid-PLGA; DSPE-PEG [passive] | Spherical | 163.4 | -19.6 | Human cervical carcinoma (HeLa) s.c. injected at right armpit of mice (18–22 g) [cervix/xenograft heterotopic] | 100 $mm^3$ ~0.1 g | CDDP: 1 CUR: 5 (2 d) | 17.34 | 159 |
| | PLGA [passive] | | 118.5 | -13.7 | | | | 14.59 | |
| Lipid-polymer hybrid | DOX and MMC added into fatty acid-block copolymer nanoemulsion [passive] | Spherical | 146 | -22.7 | Murine mammary carcinoma (EMT6/WT) orthotopically injected into the right mammary fat pad of mice (21 g) [breast/allograft orthotopic] | ~175 $mm^3$ ~0.2 g | DOX: 9.2 MMC: 2.9 (1 d) | 0.14 | 160 |
| Polymeric | $PLA_{16k}$-$PEG_{5k}$; Cholic acid [passive] | Spherical | 102.8 | NA (assumed neutral) | Human breast carcinoma (MX-1) s.c. inoculated in the right flank of mice (22 g) [breast/xenograft heterotopic] | 399 $mm^3$ ~0.5 g | 30 (2 d) | 1.67 | 161 |
| | | | | | | | 70 (2 d) | 1.70 | |
| | | | | | | | 140 (2 d) | 1.70 | |
| | $PLA_{30k}$-$PEG_{5k}$; Pamoic acid [passive] | | 108 | | | 572 $mm^3$ ~0.7 g | 30 (2 d) | 2.22 | |
| | | | | | | | 70 (2 d) | 2.78 | |
| | | | | | | | 140 (2 d) | 2.31 | |
| | $PLA_{50k}$-$PEG_{5k}$; Pamoic acid [passive] | | 118 | | | 432 $mm^3$ ~0.5 g | 30 (2 d) | 1.37 | |
| | | | | | | | 70 (2 d) | 1.18 | |
| | | | | | | | 140 (2 d) | 1.52 | |
| | $PLA_{16k}$-$PEG_{5k}$; Decanoic acid [passive] | | 92 | | | 525 $mm^3$ ~0.6 g | 30 (2 d) | 1.78 | |
| | | | | | | | 70 (2 d) | 2.40 | |
| | | | | | | | 140 (2 d) | 2.32 | |
| Liposomes | Phospholipid [passive] | Spherical | 157.7 | -17.4 | Murine sarcoma cell line (S180) s.c. inoculated in right armpit of mice (20 g) [other cancer type/ allograft orthotopic] | 100 $mm^3$ ~0.1 g | SN38: 8 (2 h) | 0.02 | 162 |

| | | | | | | | | | |
|---|---|---|---|---|---|---|---|---|---|
| Liposomes | HSPC; $mPEG_{2k}$-DSPE; Cholesterol [passive] | Spherical | 103.9 | -15 | Murine colon adenocarcinoma (C-26) s.c. injected to right flank of mice (20 g) [colon/allograft heterotopic] | 70 $mm^3$ ~0.08 g | 159.6 (2 d) | 0.20 | 163 |
| | HSPC; DSPG; Cholesterol [passive] | | 102.5 | -39.5 | | | 70.9 (2 d) | 0.19 | |
| Lipid nanocarrier (Liposomes) | Nanostructured lipid carrier (NLC) [passive] | Spherical | 89 | -40 | Murine mammary carcinoma (4T1) s.c. injected to left flank region of mice (20 g) [breast/allograft heterotopic] | ~125 $mm^3$ ~0.15 g | DOX: 5 (4 h) | 0.09 | 164 |
| | Layer-by-layer attachment of polyelectrolytes (PEs) on NLCs [passive] | | 138 | -14 | | | | 0.13 | |
| | Layer-by-layer PEs attachment on NLCs; mPEG_5kDa coating [passive] | | 128 | 5 | | | | 0.14 | |
| Liposomes | DSPC; Cholesterol; $mPEG_{2k}$-DSPE [passive] | Spherical | 93 | -32.2 | Human prostate carcinoma (PC3) s.c. inoculated in mice (20 g) [prostate/xenograft heterotopic] | ~250 $mm^3$ 0.3 g | DOX: 2 (2 d) | 0.15 | 165 |
| | DSPC; Cholesterol; $mPEG_{2k}$-DSPE; SP204-$PEG_{3.4k}$-DSPE [active] | | 102 | -12.2 | | | | 0.40 | |

| | | | | | | | | | |
|---|---|---|---|---|---|---|---|---|---|
| Dendrosome (Liposomes) | $Fe_3O_4$; FA-PAMAM G4.0 dendrimers entrapped [active] | Spherical | 12.4 | 27.2 | Human cervical carcinoma (HeLa) s.c. inoculated in mice (21 g) [cervix/xenograft heterotopic] | ~1 $cm^3$ 1.2 g | 4 (1 d) | 3.98 | 166 |
| Liposomes | CFL; DHPC; DSPE-PEG_2kDa; Silica-coated bicelles [passive] | Disc (Plate) | 56.2 | NA (assumed neutral) | Human breast adenocarcinoma (MDA-MB-231) s.c. inoculated to back of mice (20 g) [breast/xenograft heterotopic] | 100 $mm^3$ ~0.1 g | DOX: 5 (1 d) | 0.38 | 167 |
| Liposomes | Cholesterol; Stearic acid; DSPE-PEG_2kDa; PLGA [passive] | Spherical | 115.7 | -36.4 | Human Burkitt's lymphoma cell line s.c. inoculated to flank of mice (18–22 g) [other cancer type/ xenograft heterotopic] | 50 $mm^3$ 0.06 g | VCR: 10 QU: 10 (2 d) | 0.25 | 168 |
| Lipid nanocarrier (Liposomes) | Organic solvent mixed with VCR and DOX-GEM prodrug added into polyvinyl acetate [passive] | Spherical | 112.6 | -39.7 | Human Burkitt's lymphoma cell line s.c. inoculated to flank of mice (18–22 g) [other cancer type/ xenograft heterotopic] | 100 $mm^3$ ~0.1 g | DOX: 5 GEM: 5 VCR: 5 (12 h) | 4.39 | 169 |
| Solid emulsion (Liposomes) | Nanoemulsion [passive] | Spherical | 57.3 | 34.5 | Human ovarian carcinoma (SKOV-3) s.c. inoculated to flank of mice (18–22 g) [ovary/xenograft heterotopic] | 200 $mm^3$ ~0.2 g | PTX: 10 (1 d) | 0.39 | 170 |
| | Nanoemulsion; HA_0.5kDa [active] | | 80.3 | -36.9 | | | | 0.59 | |
| Lipid emulsion (Liposomes) | PEG_0.4kDa; Blank lipid emulsion [passive] | Spherical | 113.2 | -53.2 | Human breast adenocarcinoma (MCF-7) s.c. inoculated in mice (18–20 g) [breast/xenograft heterotopic] | 100 $mm^3$ ~0.1 g | PTX: 15 (12 h) | 0.10 | 171 |
| | | | 226.6 | -52.4 | | | | 0.07 | |
| | | | 383.1 | -53.9 | | | | 0.05 | |

| | | | | | | | | | |
|---|---|---|---|---|---|---|---|---|---|
| Dendrimers | Folate-PPI G3.0 [active] | Spherical | 7.7 | NA | Human breast adenocarcinoma (MCF-7) s.c. inoculated in mice (25 g) [breast/xenograft heterotopic] | 50 $mm^3$ 0.06 g | MP: 1 (1 d) | 5.89 | 172 |
| | Folate-PPI G4.0 [active] | | | | | | | 8.19 | |
| | Folate-PPI G5.0 [active] | | | | | | | 10.42 | |
| Dendrimers | PAMAM G4.0 [passive] | Spherical | 6.7 | 16.3 | Murine sarcoma cell line (S180) s.c. inoculated to armpit of mice (18–22 g) [other cancer type/ allograft orthotopic] | 100 $mm^3$ ~0.1 g | 1 (2 d) | 4.57 | 173 |
| | PAMAM G4.0; Tat peptide [active] | | 69.1 | 36.7 | | | | 16.23 | |
| Dendrimers | PAMAM G4.0 [passive] | Spherical | 227 | 30.3 | Murine colon adenocarcinoma (C-26) s.c. inoculated in mice (20 g) [colon/allograft heterotopic] | ~0.6 g | 2.5 (5 h) | 6.88 | 174 |
| | PAMAM G4.0; $\alpha$-cyclodextrin; Folate-PEG [active] | | 148 | 18.4 | | | | 31.15 | |
| Dendrimers | PAMAM G4.0; PEG_7.5kDa; Folic acid [active] | Spherical | 69.9 | -2.1 | Murine mammary carcinoma (4T1) s.c. injected to right post neck region of mice (16 g) [breast/allograft heterotopic] | 619 $mm^3$ ~0.7 g | 46.9 (1 d) | 8.51 | 175 |
| Albumin | BSA [active] | Spherical | 158.2 | -18.1 | Murine melanoma (B16-F10) s.c. inoculated to back of mice (20–25 g) [skin/allograft orthotopic] | 100 $mm^3$ ~0.1 g | PTX: 10 (8 h) | 1.11 | 176 |
| | Cholesterol-BSA [active] | | 147.6 | -20.5 | | | | 2.00 | |
| Albumin | HSA loaded with lapatinib [active] | Spherical | 140 (TEM) | 21.7 | Murine mammary carcinoma (4T1) injected to the mammary fat pad of mice (20 g) [breast/allograft orthotopic] | 100 $mm^3$ ~0.1 g | 10 (12 h) | 0.03 | 177 |

| | | | | | | | | | |
|---|---|---|---|---|---|---|---|---|---|
| Albumin | BSA [active] | Spherical | 100.5 (assumed) | -23.1 (assumed) | Murine hepatocellular carcinoma (H22) s.c. inoculated to dorsa of mice (25–30 g) [liver/allograft heterotopic] | 100 $mm^3$ ~0.1 g | DOX: 5 (2 d) | 0.04 | 178 |
| | BSA crosslinked with vanillin [active] | | 100.5 | -23.1 | | | | 0.04 | |
| Albumin | HSA [active] | Spherical | 125 (SEM) | NA | Human prostate carcinoma (PC3) s.c. injected in right flank of mice (20 g) [prostate/xenograft heterotopic] | 100 $mm^3$ ~0.1 g | CTX: 8 (12 h) | 0.24 | 179 |
| Albumin | HSA [active] | Spherical | 134.7 | -35.1 | Murine sarcoma cell line (S180) s.c. inoculated to armpit of mice (18–22 g) [other cancer type/ allograft orthotopic] | 300 $mm^3$ ~0.4 g | PTX: 15 (12 h) | 2.83 | 180 |
| | HSA; PEG_6kDa [active] | | 142.2 | -31 | | | | 4.15 | |
| Zinc-crosslinked polymeric hydrogel | Zinc-crosslinked PMAA hydrogel; PEG_1kDa [passive] | Spherical | 122.5 | -30.1 | Murine hepatocellular carcinoma (H22) s.c. inoculated to flank region of mice (20–25 g) [liver/allograft heterotopic] | 100 $mm^3$ ~0.1 g | DOX: 5 (1 d) | 0.04 | 181 |
| | Zinc-crosslinked PMAA hydrogel; PEG_1kDa; Folate [active] | | 218.6 | -30.1 (assumed) | | | | 0.05 | |
| Hyaluronic acid hydrogel | Redox-responsive HA hydrodel [active] | Spherical | 79.1 | -40 | Murine hepatocellular carcinoma (H22) s.c. inoculated to left flank of mice (20–25 g) [liver/allograft heterotopic] | 100 $mm^3$ ~0.1 g | DOX: 4.5 (3 d) | 0.43 | 182 |
| | Non-redox-responsive HA hydrogel [active] | | 66.3 | -40 | | | | 0.20 | |

| | | | | | | | | | |
|---|---|---|---|---|---|---|---|---|---|
| Chitosan hydrogel | Methacrylated succinyl chitosan dispersed in OEAM [passive] | Spherical | 161 | -30.9 | Murine hepatocellular carcinoma (H22) s.c. inoculated to left flank of mice (20–25 g) [liver/allograft heterotopic] | 50 $mm^3$<br>0.06 g | DOX: 6<br>(2 d) | 0.31 | [183] |
| Multiwalled carbon nanotubes<br>(MWCNTs) | MWCNTs [passive] | Rod | 230.4 | NA | Human breast adenocarcinoma (MCF-7) s.c. inoculated in right hind leg of mice (20–25 g)<br>[breast/xenograft heterotopic] | 100 $mm^3$<br>~0.1 g | DOX: 5<br>(1 d) | 6.42 | [184] |
| | Oxidized MWCNTs [passive] | | 230.1 | -10 | | | | 6.56 | |
| | PEGylated MWCNTs [passive] | | 241 | NA (assumed neutral) | | | | 5.88 | |
| | PEG-MWCNTs; Folic acid [active] | | 242.3 | 3.8 | | | | 13.92 | |
| | PEG-MWCNTs; Estrone [active] | | 240.3 | -10 (assumed) | | | | 14.10 | |
| Hyaluronic acid | HA-based NPs [active] | Spherical | 206.4 | -20 | Human colorectal carcinoma (HT-29) s.c. inoculated in mice (20 g) [colon/xenograft heterotopic] | 300 $mm^3$<br>~0.4 g | DOX: 7<br>(2 d) | 0.71 | [185] |
| HCPT suspension | 10-HCPT crystal nanosuspension; Cholesterol; PEG_0.6kDa [passive] | Spherical | 115 | -31.8 | Murine hepatocellular carcinoma (H22) s.c. inoculated to right armpit of mice (20 g) [liver/allograft heterotopic] | 100 $mm^3$<br>~0.1 g | HCPT: 8<br>(1 d) | 0.08 | [186] |
| Mesoporous carbon nanosphere | Glucose-based mesoporous carbon; phospholipid [passive] | Spherical | 180 | 34.4 | Murine mammary carcinoma (4T1) s.c. inoculated in mice (20 g) [breast/allograft heterotopic] | ~275 $mm^3$<br>~0.3 g | SNX-2112: 9<br>(12 h) | 0.25 | [187] |

| | | | | | | | | | |
|---|---|---|---|---|---|---|---|---|---|
| Hyaluronic acid | HA-based NPs [active] | Spherical | 180.2 | -20.3 | Murine hepatocellular carcinoma (H22) s.c. injected to right flank of mice (29 g) [liver/allograft heterotopic] | ~100 $mm^3$ ~0.1 g | DOX: 5 (2 h) | 0.08 | 188 |
| | HA-based NPs encapsulated in liposomes [active] | | 130.5 | -8.2 | | | | 0.10 | |
| CPDG assembly | CPDG; CHS-PEG_1.5kDa [passive] | Spherical | 54.4 | -22.3 | Murine hepatocellular carcinoma (H22) s.c. injected under left forelimb armpit of mice (20–24 g) [liver/allograft heterotopic] | ~100 $mm^3$ ~0.1 g | CPDG: 10 (2.5 h) | 1.18 | 189 |
| Docetaxel | DTX NPs; LPLTPLP peptide [active] | Spherical | 161.1 | -31.1 | Human alveolar adenocarcinoma (A549) s.c. inoculated to right axilla of mice (20 g) [lung/xenograft heterotopic] | 150 $mm^3$ ~0.2 g | DTX: 30 (4 h) | 0.09 | 190 |
| HCPT nanocrystal | Anticancer drug HCPT nanocrystal [passive] | Spherical | 133.5 | -27.1 | Murine mammary carcinoma (4T1) s.c. injected into right underarm of mice (18–22 g) [breast/allograft heterotopic] | 100 $mm^3$ ~0.1 g | HCPT: 8 (1 d) | 0.05 | 191 |
| Graphene oxide | Gd decorated; PEG_2kDa [passive] | Sheet (Plate) | 32.5 (TEM) | -6 | Murine sarcoma cell line (S180) s.c. inoculated to right shoulder of mice (18–20 g) [other cancer type/ allograft orthotopic] | 20 $mm^3$ ~0.02 g | DOX: 5 (12 h) | 0.13 | 192 |
| | Gd decorated; PEG_2kDa; Folic acid [active] | | | | | | | 0.17 | |
| Soy protein | Soy protein NPs [passive] | Spherical | 204.7 | -26.9 | Murine hepatocellular carcinoma (H22) s.c. inoculated into left limb armpit of mice (18–22 g) [liver/allograft heterotopic] | 200 $mm^3$ ~0.2 g | DOX: 4 (2 d) | 0.34 | 193 |
| | Soy protein NPs; Folic acid [active] | | 220.3 | -38 | | | | 0.44 | |

| | | | | | | | | | |
|---|---|---|---|---|---|---|---|---|---|
| Curcumin suspension | CUR suspension; $mPEG_{2k}$-DSPE; Soybean lecithin [passive] | Spherical | 186.3 | -19 | Murine hepatocellular carcinoma (H22) s.c. inoculated into right armpit of mice (26–28 g) [liver/allograft heterotopic] | 100 $mm^3$ ~0.1 g | CUR: 8 (1 d) | 0.008 | [194] |
| Curcumin | DOX loaded with CUR NPs; PEG_3.4kDa; Transferrin [active] | Spherical | 89 | -15.6 | Human breast adenocarcinoma (MCF-7) s.c. inoculated to posterolateral region of mice (25 g) [breast/xenograft heterotopic] | 200 $mm^3$ ~0.2 g | CUR: 50 DOX: 50 (2 d) | 1.28 | [195] |
| HCPT-loaded nanorod | PAMAM-*b*-oligoethylene glycols codendrimer [passive] | AR 6.0 Rod | 168.6 120×20 (TEM) | 24.2 | Murine hepatocellular carcinoma (H22) s.c. inoculated into right armpit of mice (18–22 g) [liver/allograft heterotopic] | 400 $mm^3$ ~0.5 g | HCPT: 5 (1 d) | 0.80 | [196] |
| BSA-based polymeric | BSA surrounded by cross-linked PMPC and benzaldehyde [passive] | Spherical | 18.6 | -1.8 | Human hepatocellular carcinoma (HepG2) s.c. injected into right flank of mice (20 g) [liver/xenograft heterotopic] | 100 $mm^3$ ~0.1 g | DOX: 5 (1 d) | 1.01 | [197] |
| CDDP-SAHA conjugate | CDDP-SAHA NPs [passive] | Spherical | 54 | 0 | Human alveolar adenocarcinoma ($A549^{DDP}$) s.c. inoculated in mice (18–20 g) [lung/xenograft heterotopic] | 100 $mm^3$ ~0.1 g | CDDP-SAHA: 5 (16 h) | 0.21 | [198] |
| Ginseng | Ginsenoside Rb1/ PPD-type extracts [passive] | Spherical | 122.5 | -13.2 | Murine Lewis lung carcinoma (LLC) s.c. inoculated in mice (18 g) [lung/allograft heterotopic] | 300 $mm^3$ ~0.4 g | Rb1/PPD: 10 (2 d) | 0.85 | [199] |
| Paclitaxel nanocrystal | PTX nanocrystal with albumin coating [passive] | AR 6.2 Rod | 190.5 260×42 (TEM) | -10.1 | Murine melanoma (B16-F10) s.c. inject to right arm of mice (23 g) [skin/allograft orthotopic] | 100 $mm^3$ ~0.1 g | PTX: 30 (1 d) | 0.12 | [200] |

**Abbreviations:** ADR, adriamycin; AFM, atomic force microscopy; AuNPs, gold nanoparticles; AuNRs, gold nanorods; BSA, bovine serum albumin; CDDP/DDP, cisplatin or *cis*-diamminedichloroplatinum(II); ChL6 mAb, chimeric L6 monoclonal antibody; CPDG, cyclic phosphoryl *N*-dodecanoyl gemcitabine; cRGD, cyclo(Arg-Gly-Asp) peptide; cRGDY, cyclo(Arg-Gly-Asp-Tyr) peptide; cRGDfC, cyclo(Arg-Gly-Asp-D-Phe-Cys); cRGDfK, cyclo(Arg-Gly-Asp-D-Phe-Lys) peptide; cRGDyK, cyclo(Arg-Gly-Asp-D-Tyr-Lys) peptide; CTX/CBZ: cabazitaxel; CUR, curcumin; DOX, doxorubicin; DTX/DOC, docetaxel; EGFR, epidermal growth factor receptor; EMO, emodin; EPB/EPI, epirubicin; GEM, gemcitabine; HCPT, 10-hydroxycamptothecin; HER2, human epidermal growth factor receptor 2; HMSN, hollow mesoporous silica NPs; HSA, human serum albumin; IgG, immunoglobulin G; i.m., intramuscular injection; LA, lipoic acid; LacA, lactobionic acid; LHRH, luteinizing hormone-releasing hormone (or gonadotropin-releasing hormone); LPLTPLP, a targeting peptide specifically bound to non-small cell lung cancer (NSCLC); MHPCNs, magnetic hollow porous carbon nanoparticles; MMC, mitomycin C; MP, melphalan; mPEG, methoxypolyethylene glycol; MSN, mesoporous silica NPs; NA, not available from original literature; NPs, nanoparticles; OP, oxaliplatin; PAMAM, polyamidoamine dendrimer; PBA, phenylboronic acid; PDA, polydopamine; PEG, polyethylene glycol; PEI, polyethylenimine; PPD, protopanaxadiols; PPI, poly(propyleneimine); PPT: podophyllotoxin; PSMA, prostate-specific membrane antigen; PTX, paclitaxel; QU, quercetin; RGD, Arg-Gly-Asp peptide; SAHA, vorinostat; s.c., subcutaneous injection; SEM, scanning electron microscopy; SN38, 7-ethyl-10-hydroxylcamptothecin; STEM, scanning/transmission electron microscopy; Tat, twin-arginine translocation peptide; TEM, transmission electron microscopy; TRC105, human/murine chimeric IgG1 mAb; VCR, vincristine; VEGF, vascular endothelial growth factor.

[a] If only the tumor volume was reported, the tumor weight was approximated using an average tumor density of 1.2 g/cm$^3$ according to Sykes *et al*.[201]
[b] $DE_{Tlast\_PK}$: Tumor delivery efficiency (percent injected dose, %ID) was calculated by dividing the area under the tumor-concentration curve (AUC) (%ID*h) with the biodistribution time period (h) reported by the original study. AUC was estimated using non-compartmental linear trapezoidal method.[202,203]
[c] Value was not reported in the original study, adopted from Wilhelm *et al*.[203]

**Table S2.** Summary of tumor microenvironment-associated nanomaterial (NM) parameters, including distribution coefficient, permeability coefficient, maximum uptake rate constant, and releasing rate constant in the tumor compartment calibrated based upon 376 NM datasets.

| Material | NM ID [a] | Targeting strategy | Distribution coefficient (PT) [unitless] | Permeability coefficient (PATC) [unitless] | Maximum uptake rate constant ($K_{max, T}$) [per h] | Releasing rate constant ($K_{re, T}$) [per h] | Delivery efficiency ($DE_{Tlast}$) [%ID] [b] | Ref. |
|---|---|---|---|---|---|---|---|---|
| Gold | INM-1 | Active | 0.265 | 0.01 | 0.055 | 0.001 | 2.06 | [1] |
| Gold | INM-2 | Passive | 0.1 | 0.1 | 0.4 | 0.055 | 1.62 | [2] |
| Gold | INM-3A | Active | 0.07 | 0.07 | 0.045 | 0.007 | 2.83 | [3] |
| | INM-3B | Passive | 0.2 | 0.1 | 0.006 | 0.0001 | 2.99 | |
| Gold | INM-4 | Active | 0.055 | 0.005 | 24 | 0.001 | 0.74 | [4] |
| Gold | INM-5A | Passive | 0.048 | 0.09 | 1.75 | 0.115 | 19.38 | [5] |
| | INM-5B | | 0.046 | 0.09 | 1.4 | 0.14 | 14.63 | |
| | INM-5C | | 0.041 | 0.09 | 1.3 | 0.14 | 12.17 | |
| | INM-5D | | 0.132 | 0.017 | 0.2 | 0.001 | 5.18 | |
| | INM-5E | Active | 0.076 | 0.09 | 2.5 | 0.105 | 25.20 | |
| | INM-5F | | 0.12 | 0.2 | 2.3 | 0.19 | 25.83 | |
| | INM-5G | | 0.175 | 0.1 | 5 | 1.2 | 24.40 | |
| | INM-5H | | 0.05 | 0.1 | 5 | 1.05 | 8.79 | |
| Gold | INM-6 | Passive | 0.145 | 0.015 | 0.85 | 0.3 | 1.13 | [6] |
| Gold | INM-7 | Passive | 0.0085 | 0.0025 | 0.05 | 3 | 0.11 | [7] |
| Gold | INM-8A | Passive | 0.086 | 0.01 | 0.185 | 0.023 | 1.24 | [8] |
| | INM-8B | | 0.07 | 0.01 | 0.18 | 0.047 | 0.64 | |

| | | | | | | | | |
|---|---|---|---|---|---|---|---|---|
| Gold | INM-9A | Passive | 0.0355 | 0.03 | 0.12 | 0.05 | 0.38 | 9 |
| | INM-9B | | 0.045 | 0.03 | 0.15 | 0.048 | 0.55 | |
| | INM-9C | | 0.041 | 0.03 | 0.2 | 0.041 | 0.61 | |
| | INM-9D | Active | 0.115 | 0.03 | 0.22 | 0.055 | 1.63 | |
| Gold | INM-10 | Active | 1.55 | 0.095 | 2.7 | 0.0195 | 9.10 | 10 |
| Gold | INM-11A | Passive | 0.023 | 0.03 | 1.98 | 0.06 | 1.85 | 11 |
| | INM-11B | | 0.023 | 0.035 | 1 | 0.248 | 0.48 | |
| | INM-11C | | 0.0252 | 0.03 | 0.6 | 0.38 | 0.16 | |
| | INM-11D | | 0.0169 | 0.01 | 3.6 | 0.264 | 0.68 | |
| Gold | INM-12 | Passive | 0.195 | 0.03 | 0.1 | 0.65 | 1.26 | 12 |
| Gold | INM-13 | Active | 0.065 | 0.03 | 0.065 | 0.0009 | 2.25 | 13 |
| Gold | INM-14A | Passive | 0.04 | 0.012 | 2.5 | 0.375 | 2.67 | 14 |
| | INM-14B | | 0.028 | 0.01 | 1.25 | 0.95 | 0.48 | |
| Gold | INM-15A | Passive | 0.018 | 0.02 | 0.86 | 0.21 | 0.67 | 15 |
| | INM-15B | | 0.016 | 0.02 | 6.3 | 1.65 | 0.60 | |
| | INM-15C | | 0.0011 | 0.003 | 0.25 | 0.01 | 0.03 | |
| | INM-15D | Active | 0.016 | 0.02 | 4.7 | 0.8 | 0.61 | |

| | | | | | | | | |
|---|---|---|---|---|---|---|---|---|
| Gold | INM-16 | Passive | 0.03 | 0.02 | 1.25 | 0.245 | 0.37 | 16 |
| Gold | INM-17A | Passive | 0.115 | 0.03 | 0.05 | 0.001 | 1.41 | 17 |
| | INM-17B | Active | 0.0415 | 0.03 | 0.032 | 0.001 | 0.26 | |
| Gold | INM-18A | Passive | 0.016 | 0.01 | 0.1 | 0.1 | 0.47 | 18 |
| | INM-18B | | 0.11 | 0.025 | 0.01 | 0.01 | 3.98 | |
| Gold | INM-19A | Passive | 0.0003 | 0.0005 | 1.3 | 1.05 | 0.02 | 19 |
| | INM-19B | | 0.0165 | 0.01 | 6 | 3.5 | 1.86 | |
| | INM-19C | | 0.0011 | 0.0005 | 2.55 | 0.01 | 0.70 | |
| | INM-19D | | 0.011 | 0.001 | 1.5 | 1.15 | 0.92 | |
| | INM-19E | | 0.022 | 0.1 | 0.05 | 0.1 | 0.97 | |
| Gold | INM-20A | Passive | 0.004 | 0.0007 | 0.6 | 0.028 | 0.76 | 20 |
| | INM-20B | | 0.003 | 0.0007 | 0.5 | 0.055 | 0.34 | |
| | INM-20C | | 0.002 | 0.0005 | 0.33 | 0.026 | 0.24 | |
| | INM-20D | | 0.0105 | 0.005 | 0.115 | 0.038 | 0.47 | |
| Dendrimer entrapped AuNPs | INM-21 | Active | 0.027 | 0.001 | 3 | 0.03 | 0.03 | 21 |
| Gold-dendrimer composite nanodevice | INM-22A | Passive | 0.173 | 0.016 | 0.044 | 0.006 | 2.93 | 22 |
| | INM-22B | | 0.093 | 0.011 | 0.05 | 0.007 | 1.75 | |
| | INM-22C | | 0.09 | 0.011 | 0.05 | 0.007 | 1.69 | |
| | INM-22D | | 0.025 | 0.05 | 0.15 | 0.005 | 0.28 | |
| | INM-22E | | 0.097 | 0.015 | 0.125 | 0.0045 | 1.03 | |
| | INM-22F | | 0.055 | 0.0065 | 0.155 | 0.004 | 0.62 | |

| | | | | | | | | |
|---|---|---|---|---|---|---|---|---|
| Gold | INM-23A | Passive | 0.0085 | 0.0035 | 1.2 | 0.03 | 0.68 | 23 |
| | INM-23B | | 0.0195 | 0.00085 | 1 | 0.33 | 1.15 | |
| | INM-23C | Active | 0.02 | 0.0008 | 1 | 0.185 | 1.20 | |
| | INM-23D | | 0.017 | 0.0035 | 0.9 | 0.2 | 1.02 | |
| | INM-23E | | 0.0157 | 0.00063 | 1 | 0.45 | 0.87 | |
| | INM-23F | | 0.028 | 0.005 | 0.16 | 0.001 | 1.55 | |
| Gold | INM-24 | Active | 0.15 | 0.0017 | 0.68 | 0.004 | 2.51 | 24 |
| Magnetic AuNPs | INM-25 | Passive | 0.065 | 0.00123 | 0.4 | 0.225 | 1.20 | 25 |
| Gold | INM-26A | Passive | 0.35 | 0.03 | 0.075 | 0.023 | 3.18 | 26 |
| | INM-26B | | 0.51 | 0.00197 | 0.157 | 0.095 | 4.12 | |
| Gold | INM-27 | Passive | 0.065 | 0.015 | 0.43 | 0.001 | 7.84 | 27 |
| Gold-iron oxide | INM-28 | Active | 0.12 | 0.00043 | 0.56 | 0.024 | 1.07 | 28 |
| Iron oxide | INM-29 | Active | 0.18 | 0.008 | 0.34 | 0.0155 | 0.78 | 29 |
| Iron oxide | INM-30 | Active | 0.0325 | 0.0005 | 0.28 | 0.0165 | 0.40 | 30 |
| Iron oxide | INM-31A | Passive | 0.077 | 0.0022 | 0.043 | 0.001 | 0.56 | 31 |
| | INM-31B | Active | 0.167 | 0.0045 | 0.043 | 0.003 | 1.20 | |
| Iron oxide | INM-32 | Passive | 0.06 | 0.01 | 0.1 | 0.1 | 1.10 | 32 |
| Iron oxide | INM-33 | Active | 0.076 | 0.0055 | 0.34 | 0.0155 | 5.25 | 33 |

| | | | | | | | | |
|---|---|---|---|---|---|---|---|---|
| Iron oxide | INM-34A | Active | 0.071 | 0.006 | 0.11 | 0.002 | 5.20 | 34 |
| | INM-34B | | 0.071 | 0.0072 | 0.143 | 0.002 | 5.00 | |
| | INM-34C | | 0.133 | 0.0085 | 0.042 | 0.0001 | 9.46 | |
| | INM-34D | | 0.135 | 0.0115 | 2 | 0.063 | 7.20 | |
| Silica (HMSN) | INM-35A | Active | 0.225 | 0.02 | 0.15 | 3 | 1.31 | 35 |
| | INM-35B | Passive | 0.125 | 0.0035 | 0.5 | 5 | 0.74 | |
| Silica | INM-36 | Passive | 0.108 | 0.002 | 0.8 | 0.07 | 0.32 | 36 |
| Silica (MSN) | INM-37A | Passive | 0.078 | 0.00078 | 0.45 | 2.1 | 0.18 | 37 |
| | INM-37B | Active | 0.225 | 0.0037 | 0.45 | 2.1 | 0.53 | |
| Silica (HMSN) | INM-38A | Passive | 0.106 | 0.0035 | 0.8 | 2 | 0.63 | 38 |
| | INM-38B | Active | 0.245 | 0.03 | 0.8 | 1.8 | 1.63 | |
| Silica (MSN) | INM-39A | Passive | 0.057 | 0.0023 | 0.15 | 0.04 | 0.41 | 39 |
| | INM-39B | Active | 0.125 | 0.012 | 0.11 | 0.025 | 0.86 | |
| Silica | INM-40A | Passive | 0.023 | 0.0004 | 0.125 | 0.01 | 0.08 | 40 |
| | INM-40B | Active | 0.044 | 0.0004 | 0.14 | 0.0125 | 0.17 | |
| Silica (MSN) | INM-41A | Passive | 0.069 | 0.003 | 0.11 | 0.012 | 0.50 | 41 |
| | INM-41B | Active | 0.137 | 0.007 | 0.105 | 0.03 | 0.93 | |
| Enzyme & iron oxide entrapped dendritic MSN | INM-42 | Passive | 0.082 | 0.00043 | 0.098 | 0.0062 | 0.23 | 42 |

| | | | | | | | | |
|---|---|---|---|---|---|---|---|---|
| Liposome coated HMSN | INM-43 | Passive | 0.0315 | 0.007 | 1 | 8 | 0.90 | [43] |
| Liposome coated HMSN | INM-44 | Passive | 0.76 | 0.05 | 0.31 | 0.0195 | 6.29 | [44] |
| Silica (MSN) | INM-45 | Passive | 0.15 | 0.004 | 0.6 | 3 | 2.08 | [45] |
| Hollow mesoporous silica | INM-46A | Passive | 0.175 | 0.005 | 0.1 | 0.005 | 6.69 | [46] |
| | INM-46B | Active | 0.152 | 0.016 | 0.85 | 0.03 | 16.54 | |
| Magnetic silica (MSN) | INM-47 | Passive | 0.056 | 0.00027 | 0.09 | 0.21 | 0.29 | [47] |
| Polymer and carbon coated silica | INM-48 | Active | 0.41 | 0.0018 | 0.19 | 0.082 | 2.76 | [48] |
| Periodic mesoporous organosilica | INM-49 | Passive | 0.35 | 0.0036 | 1.13 | 0.2 | 5.32 | [49] |
| Silica coated $Mn_3O_4$ | INM-50 | Active | 0.165 | 0.0063 | 0.6 | 1 | 5.96 | [50] |
| $NaGdF_4$ | INM-51 | Active | 0.06 | 0.009 | 0.5 | 5 | 4.27 | [51] |
| $MoS_2/Fe_3O_4$ composite | INM-52 | Passive | 0.065 | 0.0004 | 0.052 | 0.025 | 0.19 | [52] |
| CaP | INM-53 | Passive | 0.08 | 0.00016 | 0.55 | 1.1 | 0.39 | [53] |
| MnO | INM-54 | Active | 8 | 0.8 | 8 | 14 | 18.96 | [54] |
| $Mg_2Al$ layered double hydroxide | INM-55 | Passive | 0.16 | 0.0028 | 0.6 | 1.8 | 1.74 | [55] |

| | | | | | | | | |
|---|---|---|---|---|---|---|---|---|
| Cobalt nanotube | INM-56 | Active | 0.035 | 0.005 | 0.5 | 10 | 0.23 | [56] |
| AuNPs coated fullerene | INM-57A | Passive | 0.22 | 0.00055 | 0.05 | 2 | 0.74 | [57] |
| | INM-57B | | 0.155 | 0.00071 | 0.05 | 1 | 0.58 | |
| $Bi_2Se_3$ | INM-58 | Passive | 0.148 | 0.00058 | 4 | 6 | 1.99 | [58] |
| CaP | INM-59 | Passive | 0.14 | 0.000128 | 1.9 | 0.04 | 0.96 | [59] |
| $Gd_3N$ | INM-60 | Passive | 0.093 | 0.00065 | 2.2 | 0.045 | 0.30 | [60] |
| Hollow mesoporous CuS | INM-61 | Active | 0.0225 | 0.02 | 0.05 | 0.035 | 0.05 | [61] |
| Polymeric | ONM-1 | Passive | 0.058 | 0.017 | 0.175 | 0.04 | 1.30 | [62] |
| Polymeric | ONM-2A | Active | 0.131 | 0.0044 | 0.1 | 0.06 | 0.89 | [63] |
| | ONM-2B | Passive | 0.0685 | 0.0032 | 0.12 | 0.012 | 0.50 | |
| Polymeric | ONM-3A | Passive | 0.248 | 0.0011 | 0.15 | 0.029 | 1.05 | [64] |
| | ONM-3B | Passive | 0.124 | 0.0059 | 0.165 | 0.005 | 1.15 | |
| Polymeric | ONM-4 [c] | Passive | 0.052 | 0.01 | 0.1 | 2 | 0.44 | [65] |
| | | | 0.04 | 0.003 | 2 | 5 | | |
| Polymeric | ONM-5A | Passive | 0.018 | 0.0004 | 0.4 | 0.2 | 0.02 | [66] |
| | ONM-5B | Active | 0.0435 | 0.00058 | 0.2 | 0.2 | 0.06 | |
| Polymeric | ONM-6A | Passive | 0.049 | 0.0105 | 0.238 | 0.005 | 0.29 | [67] |
| | ONM-6B | Passive | 0.048 | 0.0075 | 0.25 | 0.0065 | 0.22 | |
| Polymeric | ONM-7A | Passive | 0.12 | 0.3 | 0.06 | 0.015 | 0.20 | [68] |

| | | | | | | | | |
|---|---|---|---|---|---|---|---|---|
| Polymeric | ONM-7B | Passive | 0.12 | 0.3 | 0.07 | 0.011 | 0.21 | |
| Polymeric | ONM-8A | Active | 0.07 | 0.023 | 0.25 | 0.01 | 1.15 | 69 |
| | ONM-8B | Passive | 0.05 | 0.0145 | 0.1 | 3 | 0.43 | |
| Polymeric | ONM-9A | Passive | 0.12 | 0.00035 | 0.26 | 0.005 | 0.78 | 70 |
| | ONM-9B | | 0.136 | 0.00042 | 0.25 | 0.06 | 0.81 | |
| | ONM-9C | | 0.126 | 0.00078 | 0.25 | 0.08 | 0.91 | |
| | ONM-9D | | 0.09 | 0.00045 | 0.22 | 0.085 | 0.70 | |
| | ONM-9E | | 0.155 | 0.00035 | 0.255 | 0.08 | 0.91 | |
| | ONM-9F | | 0.08 | 0.00052 | 0.265 | 0.06 | 0.60 | |
| | ONM-9G | | 0.05 | 0.00055 | 0.265 | 0.07 | 0.39 | |
| | ONM-9H | | 0.05 | 0.00032 | 0.23 | 0.065 | 0.37 | |
| Polymeric | ONM-10A | Active | 0.285 | 0.001 | 0.4 | 0.005 | 0.60 | 71 |
| | ONM-10B | Active | 0.238 | 0.00078 | 0.4 | 0.005 | 0.50 | |
| | ONM-10C | Passive | 0.0925 | 0.005 | 0.2 | 0.065 | 0.36 | |
| Polymeric | ONM-11A | Passive | 0.059 | 0.0055 | 0.135 | 0.05 | 0.31 | 72 |
| | ONM-11B | | 0.039 | 0.0058 | 0.11 | 0.05 | 0.19 | |
| Polymeric | ONM-12A | Passive | 0.151 | 0.0009 | 0.4 | 0.01 | 0.63 | 73 |
| | ONM-12B | Active | 0.138 | 0.00095 | 0.4 | 0.005 | 0.58 | |
| | ONM-12C | | 0.165 | 0.00125 | 0.4 | 0.005 | 0.70 | |
| | ONM-12D | | 0.157 | 0.00115 | 0.4 | 0.005 | 0.66 | |

| | | | | | | | | |
|---|---|---|---|---|---|---|---|---|
| | ONM-12E | Active | 0.18 | 0.00115 | 0.4 | 0.005 | 0.76 | |
| | ONM-12F | | 0.175 | 0.00155 | 0.4 | 0.005 | 0.74 | |
| Polymeric | ONM-13 | Passive | 0.135 | 0.00042 | 0.24 | 0.07 | 1.50 | [74] |
| Polymeric | ONM-14 | Active | 0.095 | 0.007 | 0.091 | 0.0089 | 4.51 | [75] |
| Polymeric | ONM-15 | Passive | 0.143 | 0.00255 | 0.19 | 0.035 | 1.17 | [76] |
| Polymeric | ONM-16 | Passive | 0.245 | 0.0016 | 0.5 | 0.01 | 1.96 | [77] |
| Polymeric | ONM-17A | Active | 0.053 | 0.01 | 1.5 | 0.8 | 0.23 | [78] |
| | ONM-17B | Passive | 0.057 | 0.0021 | 0.91 | 0.37 | 0.31 | |
| Polymeric | ONM-18 | Passive | 0.015 | 0.005 | 1 | 1 | 0.80 | [79] |
| Polymeric | ONM-19A | Passive | 0.6 | 0.15 | 25 | 7 | 10.67 | [80] |
| | ONM-19B | | 0.53 | 0.11 | 25 | 7.6 | 9.01 | |
| | ONM-19C | | 0.5 | 0.15 | 25 | 7.8 | 8.40 | |
| | ONM-19D | | 1.02 | 0.006 | 0.1 | 0.005 | 4.13 | |
| | ONM-19E | | 0.115 | 0.025 | 12 | 3 | 2.43 | |
| | ONM-19F | | 0.18 | 0.035 | 17 | 4.6 | 3.54 | |
| | ONM-19G | | 0.2 | 0.025 | 16.5 | 3.85 | 4.36 | |
| | ONM-19H | | 0.15 | 0.008 | 18 | 6.5 | 2.38 | |
| Polymeric | ONM-20 | Passive | 0.125 | 0.00036 | 0.24 | 0.075 | 1.35 | [81] |
| Polymeric | ONM-21A | Passive | 0.009 | 0.00115 | 0.7 | 2.5 | 0.58 | [82] |
| | ONM-21B | Passive | 0.052 | 0.0043 | 0.65 | 2.5 | 3.20 | |

| | | | | | | | | |
|---|---|---|---|---|---|---|---|---|
| Graphene oxide | ONM-22A | Passive | 0.069 | 0.009 | 0.5 | 0.05 | 0.46 | 83 |
| | ONM-22B | Active | 0.138 | 0.0053 | 0.55 | 0.09 | 0.97 | |
| Graphene oxide | ONM-23A | Passive | 0.05 | 0.003 | 0.059 | 0.001 | 0.46 | 84 |
| | ONM-23B | Active | 0.128 | 0.016 | 0.55 | 0.075 | 0.89 | |
| Graphene oxide | ONM-24 | Passive | 0.23 | 0.045 | 9.5 | 3.7 | 6.93 | 85 |
| Graphene oxide | ONM-25A | Passive | 0.093 | 0.005 | 0.45 | 0.015 | 0.21 | 86 |
| | ONM-25B | Active | 0.18 | 0.0023 | 0.29 | 0.035 | 0.39 | |
| Graphene oxide | ONM-26A | Passive | 0.083 | 0.0029 | 0.055 | 0.005 | 0.64 | 87 |
| | ONM-26B | Active | 0.095 | 0.0044 | 0.37 | 0.46 | 0.99 | |
| Single-walled carbon nanotubes (SWCNTs) | ONM-27A | Passive | 0.051 | 0.0013 | 1.1 | 0.46 | 0.77 | 88 |
| | ONM-27B | Active | 0.095 | 0.0016 | 0.39 | 0.23 | 1.26 | |
| | ONM-27C | Passive | 0.085 | 0.00127 | 0.47 | 0.24 | 1.14 | |
| | ONM-27D | Active | 0.264 | 0.0053 | 0.49 | 0.24 | 3.59 | |
| Liposomes | ONM-28 | Passive | 0.029 | 0.018 | 0.205 | 0.004 | 1.85 | 89 |
| Liposomes | ONM-29A | Passive | 0.031 | 0.00056 | 0.035 | 0.001 | 0.15 | 90 |
| | ONM-29B | | 0.115 | 0.00045 | 0.055 | 0.0005 | 0.40 | |
| Lipid nanocarrier (Liposomes) | ONM-30 | Active | 0.078 | 0.0035 | 0.1 | 0.09 | 1.68 | 91 |
| Liposomes | ONM-31 | Passive | 0.205 | 0.0002 | 0.2 | 0.08 | 0.97 | 92 |

| | | | | | | | | |
|---|---|---|---|---|---|---|---|---|
| Lipid nanocapsule (Liposomes) | ONM-32A | Passive | 0.045 | 0.01 | 0.3 | 0.55 | 0.10 | 93 |
| | ONM-32B | | 0.0205 | 0.004 | 0.185 | 0.14 | 0.06 | |
| | ONM-32C | | 0.0195 | 0.004 | 0.28 | 0.12 | 0.07 | |
| Liposomes | ONM-33A | Passive | 0.056 | 0.00074 | 0.19 | 0.005 | 0.52 | 94 |
| | ONM-33B | Active | 0.076 | 0.0005 | 0.62 | 0.005 | 0.92 | |
| Lipid nanocapsule (Liposomes) | ONM-34 | Passive | 0.215 | 0.0004 | 0.1 | 0.2 | 0.53 | 95 |
| Liposomes | ONM-35 | Passive | 0.065 | 0.003 | 0.01 | 0.005 | 0.82 | 96 |
| Liposomes | ONM-36 | Passive | 0.034 | 0.0005 | 0.4 | 0.015 | 0.94 | 97 |
| Hyaluronic acid hydrogel | ONM-37A | Active | 0.3 | 0.000005 | 1 | 0.005 | 0.03 | 98 |
| | ONM-37B | | 0.3 | 0.000005 | 1 | 0.005 | 0.03 | |
| | ONM-37C | | 5 | 0.00001 | 3 | 0.005 | 0.07 | |
| | ONM-37D | | 0.1 | 0.000008 | 3 | 0.005 | 0.05 | |
| Hyaluronic acid hydrogel | ONM-38 | Active | 0.092 | 0.00084 | 0.07 | 0.001 | 0.13 | 99 |
| Heparin-based hydrogel | ONM-39 | Passive | 0.145 | 0.00067 | 0.13 | 0.072 | 0.44 | 100 |
| Chitosan hydrogel | ONM-40A | Passive | 0.09 | 0.000125 | 0.105 | 0.005 | 0.22 | 101 |
| | ONM-40B | Active | 0.105 | 0.00022 | 0.09 | 0.04 | 0.24 | |
| Hyaluronic acid hydrogel | ONM-41 | Active | 0.03 | 0.0001 | 3 | 0.006 | 0.48 | 102 |

| | | | | | | | | |
|---|---|---|---|---|---|---|---|---|
| Gelatin hydrogel | ONM-42A | Passive | 0.165 | 0.04 | 0.4 | 0.4 | 1.08 | [103] |
| | ONM-42B | Passive | 0.255 | 0.05 | 0.4 | 1 | 1.65 | |
| | ONM-42C | Active | 0.4 | 0.022 | 0.4 | 1 | 2.56 | |
| Alginic acid hydrogel | ONM-43 | Passive | 0.146 | 0.00315 | 0.09 | 0.002 | 0.67 | [104] |
| Cellulose hydrogel | ONM-44 | Passive | 0.065 | 0.00072 | 0.074 | 0.001 | 0.17 | [105] |
| Dendrimers *vs.* copolymers | ONM-45A | Passive | 0.165 | 0.022 | 0.038 | 0.0005 | 10.77 | [106] |
| | ONM-45B | | 0.08 | 0.052 | 0.01 | 0.0005 | 4.09 | |
| Dendrimers | ONM-46A | Passive | 0.066 | 0.0027 | 0.1 | 0.085 | 0.26 | [107] |
| | ONM-46B | | 0.179 | 0.001 | 0.242 | 0.09 | 1.30 | |
| Dendrimers | ONM-47A | Passive | 0.076 | 0.027 | 0.157 | 0.005 | 1.94 | [108] |
| | ONM-47B | Active | 0.153 | 0.018 | 0.32 | 0.0039 | 7.96 | |
| Dendrimers *vs.* copolymers | ONM-48 | Passive | 0.12 | 0.049 | 0.012 | 0.0005 | 2.34 | [109] |
| Tabacco mosaic virus | ONM-49 | Passive | 0.011 | 0.00001 | 0.01 | 0.005 | 0.05 | [110] |
| Anticancer drug (HCPT) | ONM-50A | Passive | 0.39 | 0.05 | 0.3 | 0.092 | 3.52 | [111] |
| | ONM-50B | | 0.34 | 0.03 | 0.22 | 0.143 | 2.81 | |
| | ONM-50C | | 0.295 | 0.01 | 0.215 | 0.15 | 2.43 | |
| | ONM-50D | | 0.26 | 0.006 | 0.24 | 0.15 | 2.16 | |

| | | | | | | | | |
|---|---|---|---|---|---|---|---|---|
| Solid lipid NPs | ONM-51A | Passive | 0.044 | 0.00052 | 0.24 | 0.16 | 0.14 | [112] |
| | ONM-51B | Passive | 0.065 | 0.0007 | 0.23 | 0.185 | 0.39 | |
| | ONM-51C | Active | 0.07 | 0.00045 | 0.23 | 0.187 | 0.41 | |
| Solid lipid NPs | ONM-52 | Passive | 0.0013 | 0.000049 | 0.4 | 0.275 | 0.05 | [113] |
| Polymer-lipid hybrid | ONM-53A | Passive | 0.057 | 0.00061 | 0.35 | 0.1 | 0.43 | [114] |
| | ONM-53B | Active | 0.107 | 0.00103 | 0.35 | 0.185 | 0.61 | |
| | ONM-53C | Passive | 0.088 | 0.00102 | 0.36 | 0.121 | 0.54 | |
| | ONM-53D | Active | 0.155 | 0.0025 | 0.33 | 0.2 | 0.89 | |
| Polymeric | ONM-54 | Passive | 0.0065 | 0.000046 | 0.1 | 1 | 0.03 | [115] |
| Polymeric | ONM-55 | Passive | 0.013 | 0.0015 | 2 | 10 | 0.03 | [116] |
| Polymeric | ONM-56A | Passive | 0.046 | 0.0003 | 1 | 2 | 0.17 | [117] |
| | ONM-56B | | 0.106 | 0.003 | 2 | 1 | 0.78 | |
| | ONM-56C | | 0.142 | 0.005 | 2.5 | 1 | 1.20 | |
| | ONM-56D | | 0.205 | 0.03 | 4 | 0.95 | 2.65 | |
| | ONM-56E | | 0.35 | 0.05 | 6 | 0.75 | 7.30 | |
| Polymeric | ONM-57A [c] | Passive | 0.028 | 0.00014 | 0.005 | 0.4 | 0.07 | [118] |
| | | | 0.0295 | 0.00015 | 0.005 | 0.4 | | |
| | ONM-57B [c] | Active | 0.058 | 0.00023 | 0.005 | 0.5 | 0.16 | |
| | | | 0.069 | 0.00033 | 0.005 | 0.5 | | |

| | | | | | | | | |
|---|---|---|---|---|---|---|---|---|
| Polymeric | ONM-58 | Passive | 0.08 | 0.0025 | 0.7 | 0.095 | 1.60 | [119] |
| Polymeric | ONM-59 | Passive | 0.095 | 0.00032 | 0.04 | 0.6 | 0.35 | [120] |
| Polymeric | ONM-60A | Passive | 0.0465 | 0.00125 | 0.365 | 0.55 | 0.95 | [121] |
| | ONM-60B | Active | 0.07 | 0.00143 | 0.36 | 0.45 | 1.46 | |
| Polymeric | ONM-61 | Passive | 0.111 | 0.000183 | 0.06 | 0.023 | 0.47 | [122] |
| Polymeric | ONM-62 | Passive | 0.2 | 0.0013 | 0.05 | 0.1 | 0.84 | [123] |
| Polymeric | ONM-63 | Passive | 0.026 | 0.00025 | 0.005 | 0.5 | 0.01 | [124] |
| Polymeric | ONM-64A | Passive | 0.065 | 0.005 | 0.2 | 0.05 | 0.28 | [125] |
| | ONM-64B | | 0.092 | 0.00059 | 0.32 | 0.01 | 0.78 | |
| | ONM-64C | | 0.094 | 0.00135 | 0.26 | 0.08 | 1.06 | |
| | ONM-64D | | 0.097 | 0.00141 | 0.25 | 0.082 | 1.07 | |
| | ONM-64E | | 0.09 | 0.0007 | 0.23 | 0.038 | 1.03 | |
| Polymeric | ONM-65 | Passive | 0.075 | 0.00043 | 0.09 | 0.066 | 0.31 | [126] |
| Polymeric | ONM-66 | Passive | 0.133 | 0.00085 | 0.095 | 0.014 | 1.36 | [127] |
| Polymeric | ONM-67 | Passive | 0.03 | 0.00057 | 0.25 | 3.5 | 0.24 | [128] |
| Polymeric | ONM-68A | Passive | 0.062 | 0.00054 | 0.1 | 2.5 | 0.12 | [129] |
| | ONM-68B | Active | 0.115 | 0.00078 | 0.13 | 2.5 | 0.23 | |
| Polymeric | ONM-69A | Passive | 0.0145 | 0.002 | 0.4 | 4 | 0.07 | [130] |
| | ONM-69B | Passive | 0.0192 | 0.0016 | 0.65 | 1.5 | 0.12 | |

| | | | | | | | | |
|---|---|---|---|---|---|---|---|---|
| Polymeric | ONM-70 | Passive | 0.00193 | 0.000025 | 0.62 | 0.3 | 0.01 | 131 |
| Polymeric | ONM-71A | Passive | 0.00335 | 0.001 | 1.6 | 0.106 | 0.16 | 132 |
| | ONM-71B | Active | 0.0036 | 0.0002 | 2.2 | 0.101 | 0.22 | |
| Polymeric | ONM-72 | Passive | 0.03 | 0.01 | 0.42 | 0.07 | 0.45 | 133 |
| Polymeric | ONM-73A | Passive | 0.068 | 0.00084 | 0.5 | 3.5 | 0.31 | 134 |
| | ONM-73B | Passive | 0.0678 | 0.00091 | 0.5 | 3.5 | 0.31 | |
| | ONM-73C | Active | 0.0925 | 0.00085 | 0.7 | 3 | 0.43 | |
| Polymeric | ONM-74A | Passive | 0.028 | 0.000055 | 0.1 | 0.058 | 0.15 | 135 |
| | ONM-74B | Active | 0.0305 | 0.000057 | 0.15 | 0.048 | 0.20 | |
| | ONM-74C | Passive | 0.04 | 0.000025 | 0.2 | 0.3 | 0.16 | |
| | ONM-74D | Active | 0.101 | 0.000046 | 0.1 | 3 | 0.31 | |
| Polymeric | ONM-75 | Passive | 0.036 | 0.008 | 0.6 | 1.2 | 0.75 | 136 |
| Polymeric | ONM-76A | Passive | 0.0444 | 0.002 | 0.11 | 0.001 | 0.20 | 137 |
| | ONM-76B | Active | 0.0835 | 0.0015 | 0.107 | 0.062 | 0.31 | |
| Polymeric | ONM-77 | Passive | 0.095 | 0.06 | 1 | 6 | 6.26 | 138 |
| Polymeric | ONM-78A | Active | 0.09 | 0.004 | 0.4 | 0.075 | 0.58 | 139 |
| | ONM-78B | Passive | 0.0745 | 0.004 | 0.65 | 0.087 | 0.69 | |
| | ONM-78C | Active | 0.255 | 0.004 | 0.35 | 0.069 | 1.15 | |
| Polymeric | ONM-79A | Passive | 0.08 | 0.000178 | 0.185 | 0.0025 | 0.56 | 140 |
| | ONM-79B | Passive | 0.265 | 0.00047 | 0.25 | 0.002 | 1.77 | |

| | | | | | | | | |
|---|---|---|---|---|---|---|---|---|
| Polymeric | ONM-80 | Active | 0.0495 | 0.000125 | 0.08 | 0.105 | 0.17 | 141 |
| Polymeric | ONM-81A | Passive | 0.086 | 0.00067 | 0.105 | 0.42 | 0.21 | 142 |
| | ONM-81B | Passive | 0.1155 | 0.00102 | 0.095 | 0.225 | 0.30 | |
| Polymeric | ONM-82 | Passive | 0.0186 | 0.00021 | 0.132 | 0.087 | 0.15 | 143 |
| Polymeric | ONM-83 | Passive | 0.128 | 0.0007 | 0.08 | 0.022 | 0.19 | 144 |
| Polymeric | ONM-84A | Passive | 0.024 | 0.01 | 0.988 | 0.435 | 0.40 | 145 |
| | ONM-84B | Active | 0.043 | 0.05 | 1.1 | 0.48 | 0.73 | |
| Polymeric | ONM-85A | Passive | 0.0115 | 0.0005 | 2.3 | 0.5 | 0.15 | 146 |
| | ONM-85B | Active | 0.0185 | 0.00043 | 2.3 | 0.75 | 0.22 | |
| Polymeric | ONM-86 | Passive | 0.083 | 0.0005 | 0.115 | 0.0005 | 0.77 | 147 |
| Polymeric | ONM-87A | Active | 0.227 | 0.004 | 2 | 0.42 | 2.62 | 148 |
| | ONM-87B | | 0.19 | 0.0022 | 3 | 0.66 | 2.25 | |
| | ONM-87C | | 0.08 | 0.0015 | 3 | 0.62 | 0.96 | |
| Polymeric | ONM-88A | Passive | 0.235 | 0.0019 | 3 | 0.6 | 2.65 | 149 |
| | ONM-88B | Passive | 0.36 | 0.0024 | 3 | 0.55 | 3.99 | |
| Polymeric | ONM-89A | Passive | 0.29 | 0.3 | 3.61 | 1.21 | 10.72 | 150 |
| | ONM-89B | Active | 0.8 | 0.038 | 3.61 | 1.21 | 23.83 | |
| Polymeric | ONM-90 | Passive | 0.165 | 0.0005 | 3.5 | 2.5 | 1.36 | 151 |

| | | | | | | | | |
|---|---|---|---|---|---|---|---|---|
| Polymeric | ONM-91A | Passive | 0.064 | 0.0018 | 1 | 1.2 | 0.89 | [152] |
| | ONM-91B | Active | 0.056 | 0.0016 | 1 | 2 | 0.65 | |
| Polymeric | ONM-92A | Passive | 0.0275 | 0.0035 | 1 | 3.4 | 0.32 | [153] |
| | ONM-92B | Passive | 0.0226 | 0.008 | 0.99 | 4 | 0.26 | |
| Polymeric | ONM-93 | Active | 0.031 | 0.0007 | 0.6 | 5 | 0.17 | [154] |
| Polymeric | ONM-94 | Passive | 1.14 | 0.011 | 0.8 | 0.023 | 2.79 | [155] |
| Polymeric | ONM-95A | Passive | 0.255 | 0.05 | 0.4 | 0.31 | 1.71 | [156] |
| | ONM-95B | Active | 0.257 | 0.05 | 0.85 | 0.36 | 3.35 | |
| Polymeric | ONM-96 | Passive | 0.014 | 0.008 | 0.1 | 6 | 0.18 | [157] |
| Polymeric | ONM-97 | Passive | 0.0245 | 0.00035 | 2 | 8 | 0.13 | [158] |
| Lipid-polymer hybrid | ONM-98A [c] | Passive | 2.65 | 0.022 | 0.27 | 0.019 | 17.16 | [159] |
| | | | 0.8 | 0.009 | 0.19 | 0.0055 | | |
| | ONM-98B [c] | Passive | 2.13 | 0.01 | 0.26 | 0.006 | 14.68 | |
| | | | 0.9 | 0.0031 | 0.128 | 0.005 | | |
| Lipid-polymer hybrid | ONM-99 [c] | Passive | 0.0235 | 0.05 | 0.4 | 1 | 0.18 | [160] |
| | | | 0.024 | 0.1 | 1 | 10 | | |
| Polymeric | ONM-100A | Passive | 0.084 | 0.00053 | 0.07 | 0.002 | 1.71 | [161] |
| | ONM-100B | | 0.101 | 0.00031 | 0.07 | 0.002 | 1.71 | |
| | ONM-100C | | 0.101 | 0.00031 | 0.07 | 0.002 | 1.71 | |

| | | | | | | | | |
|---|---|---|---|---|---|---|---|---|
| Polymeric | ONM-100D | Passive | 0.045 | 0.0009 | 0.084 | 0.004 | 2.19 | |
| | ONM-100E | | 0.06 | 0.0009 | 0.089 | 0.004 | 2.84 | |
| | ONM-100F | | 0.07 | 0.00066 | 0.097 | 0.004 | 2.44 | |
| | ONM-100G | Passive | 0.052 | 0.0008 | 0.21 | 0.132 | 1.47 | |
| | ONM-100H | | 0.0293 | 0.001 | 0.098 | 0.008 | 1.17 | |
| | ONM-100I | | 0.071 | 0.00082 | 0.083 | 0.002 | 1.53 | |
| | ONM-100J | Passive | 0.086 | 0.0006 | 0.04 | 0.064 | 1.88 | |
| | ONM-100K | | 0.083 | 0.00067 | 0.067 | 0.004 | 2.42 | |
| | ONM-100L | | 0.059 | 0.00075 | 0.102 | 0.001 | 2.37 | |
| Liposomes | ONM-101 | Passive | 0.0047 | 0.009 | 0.001 | 0.1 | 0.02 | [162] |
| Liposomes | ONM-102A | Passive | 0.092 | 0.00028 | 0.065 | 0.6 | 0.25 | [163] |
| | ONM-102B | Passive | 0.079 | 0.00025 | 0.04 | 0.6 | 0.21 | |
| Lipid nanocarrier (Liposomes) | ONM-103A | Passive | 0.0102 | 0.004 | 0.84 | 0.125 | 0.10 | [164] |
| | ONM-103B | | 0.0094 | 0.0007 | 1.6 | 0.1 | 0.13 | |
| | ONM-103C | | 0.0092 | 0.005 | 1.65 | 0.1 | 0.14 | |
| Liposomes | ONM-104A | Passive | 0.0041 | 0.0001 | 0.405 | 0.095 | 0.15 | [165] |
| | ONM-104B | Active | 0.011 | 0.00025 | 0.405 | 0.099 | 0.40 | |
| Dendrosome (Liposomes) | ONM-105 | Active | 0.105 | 0.0017 | 0.05 | 4 | 3.67 | [166] |
| Liposomes | ONM-106 | Passive | 0.095 | 0.000195 | 0.0165 | 0.001 | 0.40 | [167] |

| | | | | | | | | |
|---|---|---|---|---|---|---|---|---|
| Liposomes | ONM-107 [c] | Passive | 0.12 | 0.05 | 0.39 | 0.13 | 0.24 | 168 |
| | | | 0.114 | 0.04 | 0.44 | 0.1 | | |
| Lipid nanocarrier (Liposomes) | ONM-108 [c] | Passive | 0.88 | 0.1 | 0.28 | 0.095 | 4.42 | 169 |
| | | | 0.452 | 0.05 | 0.24 | 0.095 | | |
| | | | 0.688 | 0.08 | 0.16 | 0.08 | | |
| Solid emulsion (Liposomes) | ONM-109A | Passive | 0.0105 | 0.0005 | 3.5 | 3 | 0.19 | 170 |
| | ONM-109B | Active | 0.0165 | 0.001 | 3.5 | 3.25 | 0.29 | |
| Lipid emulsion (Liposomes) | ONM-110A | Passive | 0.0205 | 0.0045 | 1.1 | 6 | 0.12 | 171 |
| | ONM-110B | | 0.014 | 0.0022 | 1.25 | 7 | 0.08 | |
| | ONM-110C | | 0.0111 | 0.0008 | 1.3 | 7 | 0.07 | |
| Dendrimers | ONM-111A | Active | 0.5 | 0.008 | 3.5 | 0.435 | 6.05 | 172 |
| | ONM-111B | | 1.35 | 0.03 | 1.1 | 0.105 | 8.78 | |
| | ONM-111C | | 1.95 | 0.05 | 0.85 | 0.088 | 11.04 | |
| Dendrimers | ONM-112A | Passive | 0.69 | 0.025 | 0.139 | 0.008 | 4.71 | 173 |
| | ONM-112B | Active | 2.998 | 0.12 | 0.115 | 0.005 | 16.70 | |
| Dendrimers | ONM-113A | Passive | 0.35 | 0.012 | 0.1 | 0.4 | 7.06 | 174 |
| | ONM-113B | Active | 1 | 0.031 | 2.3 | 0.4 | 29.80 | |
| Dendrimers | ONM-114 | Active | 0.253 | 0.0056 | 0.06 | 0.06 | 9.01 | 175 |
| Albumin | ONM-115A | Active | 0.3 | 0.01 | 1 | 6 | 1.46 | 176 |
| | ONM-115B | Active | 0.305 | 0.06 | 3 | 4 | 2.24 | |

| | | | | | | | | |
|---|---|---|---|---|---|---|---|---|
| Albumin | ONM-116 | Active | 0.0067 | 0.0005 | 0.1 | 3.5 | 0.03 | [177] |
| Albumin | ONM-117A | Active | 0.013 | 0.000085 | 0.1 | 0.02 | 0.04 | [178] |
| | ONM-117B | Active | 0.015 | 0.00007 | 0.102 | 0.005 | 0.04 | |
| Albumin | ONM-118 | Active | 0.039 | 0.005 | 0.9 | 1.44 | 0.25 | [179] |
| Albumin | ONM-119A | Active | 0.222 | 0.1 | 0.4 | 2 | 3.09 | [180] |
| | ONM-119B | Active | 0.25 | 0.014 | 1.5 | 8 | 4.00 | |
| Zinc-crosslinked polymeric hydrogel | ONM-120A | Passive | 0.00885 | 0.0003 | 0.1 | 0.167 | 0.04 | [181] |
| | ONM-120B | Active | 0.012 | 0.0003 | 0.107 | 0.167 | 0.05 | |
| Hyaluronic acid hydrogel | ONM-121A | Active | 0.16 | 0.0022 | 0.8 | 0.02 | 0.45 | [182] |
| | ONM-121B | Active | 0.083 | 0.005 | 0.8 | 0.025 | 0.22 | |
| Chitosan hydrogel | ONM-122 | Passive | 0.073 | 0.01 | 0.29 | 0.058 | 0.34 | [183] |
| Multiwalled carbon nanotubes (MWCNTs) | ONM-123A | Passive | 0.815 | 0.05 | 0.22 | 0.103 | 6.58 | [184] |
| | ONM-123B | Passive | 0.865 | 0.05 | 0.196 | 0.102 | 6.67 | |
| | ONM-123C | Passive | 0.83 | 0.05 | 0.205 | 0.107 | 6.04 | |
| | ONM-123D | Active | 2.27 | 0.05 | 0.22 | 0.093 | 14.53 | |
| | ONM-123E | Active | 2.35 | 0.05 | 0.22 | 0.092 | 14.59 | |
| Hyaluronic acid | ONM-124 | Active | 0.06 | 0.000245 | 0.065 | 0.1 | 0.73 | [185] |
| HCPT suspension | ONM-125 | Passive | 0.0162 | 0.00012 | 0.1 | 0.1 | 0.08 | [186] |

| | | | | | | | | |
|---|---|---|---|---|---|---|---|---|
| Mesoporous carbon nanosphere | ONM-126 | Passive | 0.0193 | 0.00072 | 0.24 | 3.5 | 0.25 | [187] |
| Hyaluronic acid | ONM-127A | Active | 0.0222 | 0.00065 | 0.4 | 6 | 0.08 | [188] |
| | ONM-127B | Active | 0.0265 | 0.00065 | 0.4 | 5 | 0.09 | |
| CPDG assembly | ONM-128 | Passive | 0.3 | 0.05 | 0.1 | 6 | 1.41 | [189] |
| Docetaxel | ONM-129 | Active | 0.0152 | 0.000165 | 0.02 | 0.03 | 0.09 | [190] |
| HCPT nanocrystal | ONM-130 | Passive | 0.012 | 0.000122 | 0.01 | 0.3 | 0.05 | [191] |
| Graphene oxide | ONM-131A | Passive | 0.06 | 0.025 | 0.74 | 0.55 | 0.13 | [192] |
| | ONM-131B | Active | 0.065 | 0.0012 | 0.8 | 0.375 | 0.18 | |
| Soy protein | ONM-132A | Passive | 0.017 | 0.003 | 3.7 | 1.8 | 0.37 | [193] |
| | ONM-132B | Active | 0.023 | 0.003 | 3.8 | 1.1 | 0.46 | |
| Curcumin suspension | ONM-133 | Passive | 0.00174 | 0.0001 | 0.056 | 0.069 | 0.008 | [194] |
| Curcumin | ONM-134 [c] | Active | 0.102 | 0.00265 | 0.032 | 0.0005 | 1.31 | [195] |
| | | | 0.155 | 0.004 | 0.038 | 0.0005 | | |
| HCPT-loaded nanorod | ONM-135 | Passive | 0.045 | 0.1 | 0.2 | 2.5 | 0.83 | [196] |
| BSA-based polymeric | ONM-136 | Passive | 0.225 | 0.00053 | 0.027 | 0.07 | 1.01 | [197] |
| CDDP-SAHA conjugate | ONM-137 | Passive | 0.044 | 0.000135 | 1.1 | 3.2 | 0.21 | [198] |

| | | | | | | | | |
|---|---|---|---|---|---|---|---|---|
| Ginseng | ONM-138 | Passive | 0.052 | 0.0009 | 0.26 | 0.25 | 0.87 | [199] |
| Paclitaxel nanocrystal | ONM-139 | Passive | 0.023 | 0.004 | 3 | 12 | 0.11 | [200] |

**Abbreviations:** AuNPs, gold nanoparticles; BSA, bovine serum albumin; CDDP, cisplatin or *cis*-diamminedichloroplatinum(II); CPDG, cyclic phosphoryl *N*-dodecanoyl gemcitabine; HCPT, 10-hydroxycamptothecin; HMSN, hollow mesoporous silica nanoparticles; INM, inorganic nanomaterial; MSN, mesoporous silica nanoparticles; ONM, organic nanomaterial; SAHA, vorinostat.

[a] Each nanomaterial has been provided with an identification number (NM ID) throughout this summary table. Please refer to Table S1 to look up specific NM characteristics for each study.

[b] $DE_{Tlast}$: Tumor delivery efficiency (%ID) was calculated by dividing AUC (%ID*h) estimated using the constructed NM-specific PBPK model with the biodistribution time period (h) reported by the original study.

[c] For those NM types that have only one tumor delivery efficiency but with different sets of parameter values represent a specific NM loaded with 2–3 anticancer drugs and delivery efficiency was estimated based upon the averaged value of each drug.

**Table S3.** Normalized sensitivity coefficients (NSCs) for highly influential parameters on tissue delivery of gold nanoparticles (AuNPs) in tumor-bearing mice.[13]

| | 24 h | | | | | 168 h | | | | |
|---|---|---|---|---|---|---|---|---|---|---|
| | AUCCP | AUCCL | AUCCS | AUCCK | AUCCT | AUCCP | AUCCL | AUCCS | AUCCK | AUCCT |
| **Physiological parameters** | | | | | | | | | | |
| QCC | -0.13 | 0.06 | -0.14 | -0.13 | -0.12 | -0.20 | **-0.34** | **-0.28** | **-0.30** | -0.21 |
| QSC | -0.08 | **0.27** | -0.08 | -0.08 | -0.08 | -0.09 | 0.21 | -0.09 | -0.12 | -0.09 |
| VLC | -0.21 | **0.62** | -0.20 | -0.21 | -0.21 | -0.24 | **0.63** | **-0.31** | **-0.32** | -0.23 |
| VSC | -0.01 | -0.01 | **0.99** | -0.01 | -0.01 | -0.09 | **-0.30** | **0.73** | -0.23 | -0.09 |
| VKC | -0.04 | -0.04 | -0.04 | **0.96** | -0.04 | -0.03 | 0.00 | 0.00 | **0.99** | -0.03 |
| VPlasmaC | **0.74** | **-0.26** | -0.25 | **-0.25** | **-0.25** | **0.85** | 0.09 | 0.02 | 0.01 | -0.15 |
| VTC | -0.01 | -0.01 | -0.01 | -0.01 | **0.98** | -0.01 | -0.02 | -0.02 | -0.02 | **0.98** |
| BVL | -0.19 | **-0.52** | -0.18 | -0.19 | -0.19 | -0.23 | **0.55** | **-0.31** | **-0.33** | -0.21 |
| BVK | -0.03 | -0.03 | -0.03 | **-0.34** | -0.03 | -0.01 | 0.01 | 0.00 | **-0.31** | -0.02 |
| **Nanomaterial-specific parameters** | | | | | | | | | | |
| PL | -0.03 | **0.76** | -0.03 | -0.03 | -0.03 | -0.02 | 0.04 | -0.01 | 0.00 | -0.02 |
| PS | -0.01 | -0.01 | **0.99** | -0.01 | -0.01 | -0.09 | **-0.30** | **0.73** | -0.23 | -0.08 |
| PK | -0.01 | -0.01 | -0.01 | **0.98** | -0.01 | -0.01 | -0.01 | -0.01 | **0.99** | -0.01 |
| PT | -0.02 | -0.01 | -0.02 | -0.02 | **0.98** | -0.02 | -0.03 | -0.03 | -0.02 | **0.97** |
| $K_{max,L}$ | 0.00 | 0.03 | 0.00 | 0.00 | 0.00 | -0.12 | **0.51** | **-0.32** | **-0.34** | -0.10 |
| $t_{50,L}$ | 0.01 | -0.15 | 0.01 | 0.01 | 0.00 | **0.30** | **-1.35** | **0.85** | **0.81** | **0.29** |
| $n_L$ | 0.01 | -0.15 | 0.01 | 0.01 | 0.00 | 0.07 | **-0.28** | 0.16 | 0.12 | 0.07 |
| $K_{max,S}$ | 0.00 | 0.00 | 0.25 | 0.00 | 0.00 | -0.09 | **-0.31** | **0.72** | -0.23 | -0.08 |
| $t_{50,S}$ | 0.01 | 0.00 | **-1.15** | 0.01 | 0.01 | 0.18 | **0.52** | **-1.35** | **0.41** | 0.18 |
| $n_S$ | 0.01 | 0.00 | **-0.85** | 0.01 | 0.00 | 0.02 | 0.02 | -0.12 | 0.02 | 0.03 |
| $K_{max,K}$ | 0.00 | 0.00 | 0.00 | 0.00 | 0.00 | 0.00 | -0.01 | -0.01 | **0.64** | 0.00 |
| $t_{50,K}$ | 0.00 | 0.00 | 0.00 | -0.01 | 0.00 | 0.01 | 0.03 | 0.03 | **-1.59** | 0.01 |
| $n_K$ | 0.00 | 0.00 | 0.00 | -0.01 | 0.00 | 0.00 | 0.00 | 0.00 | **-0.29** | 0.00 |
| $K_{max,T}$ | -0.01 | 0.00 | -0.01 | -0.01 | **0.33** | -0.01 | -0.03 | -0.03 | -0.02 | **0.86** |

AUCCP, AUCCL, AUCCS, AUCCK, and AUCCT represent the area-under-the-concentration curve of AuNPs in venous plasma, liver, spleen, kidneys, and tumor, respectively. QCC, cardiac output; QSC, fractional cardiac output to spleen; VLC, VSC, VKC, VPlasmaC, and VTC are volume fractions of liver, spleen, kidneys, plasma, and tumor tissue, respectively, in the body; BVL and BVK represent the blood volume fractions of liver and kidneys, respectively; PL, PS, PK, and PT are plasma:tissue distribution coefficients for liver, spleen, kidneys, and tumor tissue, respectively; $K_{max,L}$, $K_{max,S}$, $K_{max,K}$, and $K_{max,T}$ represent maximum uptake rate by endocytic/phagocytic or tumor cells in liver, spleen, kidney, and tumor tissues, respectively; $t_{50,L}$, $t_{50,S}$, and $t_{50,K}$ are time reaching half maximum uptake rate for endocytic/phagocytic cells in liver, spleen, and kidney tissues, respectively; $n_L$, $n_S$, and $n_K$ are the Hill coefficients for endocytic/phagocytic uptake in liver, spleen, and kidney tissues, respectively.

**Table S4.** Summary of statistical analysis and multivariable linear regression results to identify critical tumor microenvironment-related factors affecting tumor delivery efficiency for gold nanomaterials (66 datasets) based upon the tumor delivery efficiency estimated at the last sampling time point ($DE_{Tlast}$) according to the original pharmacokinetic study.

| **Statistical analysis** | | | |
|---|---|---|---|
| **Mann-Whitney test for 2 groups of tumor delivery efficiency (high *vs.* low)** | | | |
| Distribution coefficient (PT) | Permeability coefficient (PATC) | Maximum uptake rate constant ($K_{max, T}$) | Releasing rate constant ($K_{re, T}$) |
| <0.001*** | 0.004** | 0.438 | 0.133 |
| **Multivariable linear regression analysis** | | | |
| $Y = -0.25 + 0.60*PT + 9.25*$**PATC(***)** $+ 0.01*K_{max, T} - 0.06*K_{re, T}$; $R^2 = 0.40$; $P<0.001$ | | | |

**$P$<0.01; ***$P$<0.001.

**Table S5.** Summary of statistical analysis results for comparing different groups of tumor delivery efficiencies estimated from 376 datasets of various types of nanomaterials (NMs).

| **Group of comparison** | |
|---|---|
| **Modeling approach (non-physiologically *vs.* physiologically based)** | |
| Welch's *t*-test | 0.998 |
| Mann-Whitney rank-sum test | 0.745 |
| **Non-physiologically-based (2005–2015 *vs.* 2015–2018)** | |
| Welch's *t*-test | 0.811 |
| Mann-Whitney rank-sum test | 0.245 |
| **Physiologically-based (2005–2015 *vs.* 2015–2018)** | |
| Welch's *t*-test | 0.647 |
| Mann-Whitney rank-sum test | 0.155 |
| **Type of nanomaterials (inorganic *vs.* organic)** | |
| Welch's *t*-test | 0.021* |
| Mann-Whitney rank-sum test | <0.001*** |
| **Targeting strategy (passive *vs.* active)** | |
| Welch's *t*-test | 0.004** |
| Mann-Whitney rank-sum test | 0.075 |

*$P$<0.05; **$P$<0.01; ***$P$<0.001. *,**, and *** indicate that there are significant differences between two groups of mean (*t*-test) and median (rank-sum test) tumor delivery efficiency.

**Table S6.** Statistical analysis results of simple linear regression analyses (continuous variable) and one-way analysis of variance (ANOVA) (categorical variable) tests for identifying variables with significant effects on log-transformed tumor delivery efficiency estimated from all the 376 datasets of various types of nanomaterials (NMs).

| Variable | $DE_{Tlast}$ | $DE_{Tlast\_PK}$ | $DE_{24}$ | $DE_{168}$ | $DE_{max}$ |
|---|---|---|---|---|---|
| **Gold NMs** | | | | | |
| Targeting strategy | 0.099 | 0.047* | 0.114 | 0.021* | 0.080 |
| Cancer type | 0.174 | 0.069 | 0.105 | 0.032* | 0.102 |
| Tumor model | 0.011* | 0.005** | 0.004** | 0.014* | 0.005** |
| Shape | 0.902 | 0.706 | 0.728 | 0.812 | 0.724 |
| Hydrodynamic diameter (log(HD)) | 0.597 | 0.790 | 0.646 | 0.892 | 0.306 |
| Zeta potential | 0.861 | 0.547 | 0.773 | 0.562 | 0.584 |
| **Inorganic NMs** | | | | | |
| Core materials | 0.530 | 0.474 | 0.654 | 0.090 | 0.568 |
| Targeting strategy | 0.009** | 0.005** | 0.011* | 0.002** | 0.009** |
| Cancer type | 0.013* | 0.003** | 0.004** | <0.001*** | 0.009** |
| Tumor model | 0.053 | 0.018* | 0.012* | 0.009** | 0.017* |
| Shape | 0.915 | 0.754 | 0.881 | 0.692 | 0.911 |
| Hydrodynamic diameter (log(HD)) | 0.799 | 0.869 | 0.963 | 0.404 | 0.676 |
| Zeta potential | 0.357 | 0.531 | 0.476 | 0.503 | 0.540 |
| **Organic NMs** | | | | | |
| Core materials | <0.001*** | <0.001*** | <0.001*** | <0.001*** | <0.001*** |
| Targeting strategy | 0.502 | 0.419 | 0.546 | 0.366 | 0.462 |
| Cancer type | 0.105 | 0.053 | 0.121 | <0.001*** | 0.033* |
| Tumor model | 0.361 | 0.359 | 0.329 | 0.077 | 0.184 |
| Shape | 0.004** | 0.039* | 0.003** | 0.029* | 0.016* |
| Hydrodynamic diameter (log(HD)) | 0.018* | 0.008** | 0.020* | 0.006** | 0.022* |
| Zeta potential | 0.001** | <0.001*** | 0.001** | 0.002** | <0.001*** |
| **Inorganic and organic NMs (INMs and ONMs)** | | | | | |
| INMs or ONMs | <0.001*** | <0.001*** | <0.001*** | <0.001*** | <0.001*** |
| Core materials | <0.001*** | <0.001*** | <0.001*** | <0.001*** | <0.001*** |
| Targeting strategy | 0.037* | 0.020* | 0.048* | 0.013* | 0.034* |
| Cancer type | <0.001*** | <0.001*** | <0.001*** | <0.001*** | <0.001*** |
| Tumor model | 0.011* | 0.007** | 0.005** | 0.004** | 0.004** |
| Shape | 0.068 | 0.147 | 0.056 | 0.063 | 0.083 |
| Hydrodynamic diameter (log(HD)) | 0.005** | 0.002** | 0.003** | <0.001*** | 0.007** |
| Zeta potential | <0.001*** | 0.001** | 0.001** | 0.001** | <0.001*** |

*$P$<0.05; **$P$<0.01; ***$P$<0.001. *,**, and *** indicate that the variable has significant contribution to the tumor delivery efficiency. $DE_{Tlast}$ and $DE_{Tlast\_PK}$ are tumor delivery efficiencies estimated at the last sampling time point according to the original literature using the PBPK modeling approach and non-compartmental trapezoidal integration method, respectively; $DE_{24}$ and $DE_{168}$ represent tumor delivery efficiency estimated at 24 h and 168 h using the PBPK modeling approach, respectively; $DE_{max}$ is the maximum tumor delivery efficiency obtained by implementing the PBPK model.

**Table S7.** Statistical analysis results of simple linear regression analyses (continuous variable) and one-way analysis of variance (ANOVA) (categorical variable) tests for identifying variables with significant effects on log-transformed tumor delivery efficiency estimated from 313 confidently predicted datasets of various types of nanomaterials (NMs).

| Variable | $DE_{Tlast}$ | $DE_{Tlast\_PK}$ | $DE_{24}$ | $DE_{168}$ | $DE_{max}$ |
|---|---|---|---|---|---|
| **Gold NMs** | | | | | |
| Targeting strategy | 0.188 | 0.095 | 0.176 | 0.042* | 0.127 |
| Cancer type | 0.017* | 0.002** | 0.010* | <0.001*** | 0.012* |
| Tumor model | <0.001*** | <0.001*** | <0.001*** | <0.001*** | <0.001*** |
| Shape | 0.499 | 0.215 | 0.232 | 0.435 | 0.443 |
| Hydrodynamic diameter (log(HD)) | 0.410 | 0.985 | 0.473 | 0.869 | 0.314 |
| Zeta potential | 0.897 | 0.605 | 0.888 | 0.633 | 0.926 |
| **Inorganic NMs** | | | | | |
| Core materials | 0.266 | 0.217 | 0.375 | 0.042* | 0.328 |
| Targeting strategy | 0.038* | 0.026* | 0.035* | <0.01** | 0.030* |
| Cancer type | 0.005** | 0.001** | 0.001** | <0.001*** | 0.004** |
| Tumor model | 0.001** | <0.001*** | <0.001*** | <0.001*** | <0.001*** |
| Shape | 0.841 | 0.577 | 0.677 | 0.710 | 0.854 |
| Hydrodynamic diameter (log(HD)) | 0.173 | 0.422 | 0.170 | 0.269 | 0.109 |
| Zeta potential | 0.418 | 0.600 | 0.487 | 0.530 | 0.398 |
| **Organic NMs** | | | | | |
| Core materials | <0.001*** | <0.001*** | <0.001*** | <0.001*** | <0.001*** |
| Targeting strategy | 0.107 | 0.126 | 0.085 | 0.184 | 0.139 |
| Cancer type | <0.001*** | <0.001*** | <0.001*** | <0.001*** | <0.001*** |
| Tumor model | 0.200 | 0.145 | 0.247 | 0.075 | 0.110 |
| Shape | <0.001*** | 0.004** | <0.001*** | 0.018* | 0.009** |
| Hydrodynamic diameter (log(HD)) | 0.030* | 0.017* | 0.030* | 0.029* | 0.033* |
| Zeta potential | <0.001*** | <0.001*** | 0.002** | <0.01** | 0.001** |
| **Inorganic and organic NMs (INMs and ONMs)** | | | | | |
| INMs or ONMs | <0.001*** | <0.001*** | <0.001*** | <0.001*** | <0.001*** |
| Core materials | <0.001*** | <0.001*** | <0.001*** | <0.001*** | <0.001*** |
| Targeting strategy | 0.007** | 0.006** | 0.005** | 0.006** | 0.008** |
| Cancer type | <0.001*** | <0.001*** | <0.001*** | <0.001*** | <0.001*** |
| Tumor model | 0.001** | <0.001*** | 0.001** | <0.001*** | <0.001*** |
| Shape | 0.040* | 0.072 | 0.078 | 0.103 | 0.084 |
| Hydrodynamic diameter (log(HD)) | 0.005** | 0.033* | 0.004** | 0.006** | 0.002** |
| Zeta potential | 0.002** | 0.002** | 0.004** | 0.016* | 0.002** |

*$P$<0.05; **$P$<0.01; ***$P$<0.001. *,**, and *** indicate that the variable has significant contribution to the tumor delivery efficiency. $DE_{Tlast}$ and $DE_{Tlast\_PK}$ are tumor delivery efficiencies estimated at the last sampling time point according to the original literature using the PBPK modeling approach and non-compartmental trapezoidal integration method, respectively; $DE_{24}$ and $DE_{168}$ represent tumor delivery efficiency estimated at 24 h and 168 h using the PBPK modeling approach, respectively; $DE_{max}$ is the maximum tumor delivery efficiency obtained by implementing the PBPK model.

**Table S8.** Multivariable linear regression results of selected models for the log-transformed tumor delivery efficiencies based on all the 376 datasets.

| Statistical criteria | $DE_{Tlast}$ | | $DE_{Tlast\_PK}$ | | $DE_{24}$ | | $DE_{168}$ | | $DE_{max}$ | |
|---|---|---|---|---|---|---|---|---|---|---|
| | Full | Best | Full | Best | Full | Best | Full | Best | Full | Best |
| **Gold nanomaterials** | | | | | | | | | | |
| $R^2$ | 0.31 | 0.28 | 0.32 | 0.32 | 0.33 | 0.32 | 0.33 | 0.33 | 0.36 | 0.31 |
| Adj-$R^2$ | 0 | 0 | 0.004 | 0.03 | 0.005 | 0.02 | 0.02 | 0.04 | 0.06 | 0.14 |
| *P*-value | 0.533 | 0.49 | 0.468 | 0.389 | 0.464 | 0.412 | 0.427 | 0.365 | 0.309 | 0.076 |
| AIC | 131 | 129 | 132 | 130 | 132 | 130 | 130 | 129 | 124 | 115 |
| BIC | 172 | 166 | 173 | 169 | 172 | 169 | 171 | 167 | 165 | 141 |
| **Inorganic nanomaterials** | | | | | | | | | | |
| $R^2$ | 0.44 | 0.42 | 0.45 | 0.43 | 0.43 | 0.43 | 0.49 | 0.46 | 0.46 | 0.45 |
| Adj-$R^2$ | 0.24 | 0.24 | 0.26 | 0.26 | 0.23 | 0.23 | 0.30 | 0.30 | 0.26 | 0.28 |
| *P*-value | **0.005** | **0.003** | **0.003** | **0.002** | **0.007** | **0.002** | **<0.001** | **<0.001** | **0.003** | **<0.001** |
| AIC | 184 | 182 | 188 | 186 | 180 | 176 | 182 | 181 | 174 | 170 |
| BIC | 253 | 243 | 258 | 247 | 249 | 237 | 252 | 243 | 244 | 232 |
| **Organic nanomaterials** | | | | | | | | | | |
| $R^2$ | 0.28 | 0.28 | 0.28 | 0.28 | 0.29 | 0.29 | 0.33 | 0.32 | 0.29 | 0.29 |
| Adj-$R^2$ | 0.19 | 0.19 | 0.19 | 0.20 | 0.20 | 0.20 | 0.25 | 0.25 | 0.21 | 0.21 |
| *P*-value | **<0.001** | **<0.001** | **<0.001** | **<0.001** | **<0.001** | **<0.001** | **<0.001** | **<0.001** | **<0.001** | **<0.001** |
| AIC | 463 | 463 | 458 | 457 | 454 | 454 | 478 | 476 | 449 | 448 |
| BIC | 560 | 560 | 555 | 550 | 551 | 551 | 575 | 566 | 546 | 541 |
| **All nanomaterials** | | | | | | | | | | |
| $R^2$ | 0.27 | 0.26 | 0.26 | 0.26 | 0.27 | 0.27 | 0.33 | 0.33 | 0.28 | 0.27 |
| Adj-$R^2$ | 0.19 | 0.19 | 0.18 | 0.18 | 0.19 | 0.19 | 0.25 | 0.25 | 0.21 | 0.20 |
| *P*-value | **<0.001** | **<0.001** | **<0.001** | **<0.001** | **<0.001** | **<0.001** | **<0.001** | **<0.001** | **<0.001** | **<0.001** |
| AIC | 655 | 652 | 658 | 656 | 641 | 639 | 669 | 667 | 633 | 627 |
| BIC | 792 | 782 | 795 | 789 | 778 | 773 | 806 | 800 | 770 | 741 |

$R^2$, coefficient of determination; Adj-$R^2$, adjusted $R^2$; AIC, Akaike information criterion; BIC, Bayesian information criterion; $DE_{Tlast}$ and $DE_{Tlast\_PK}$ are tumor delivery efficiency estimated at the last sampling time point according to original literature using PBPK modeling approach and non-physiologically based trapezoidal integration method, respectively; $DE_{24}$ and $DE_{168}$ represent tumor delivery efficiency estimated at 24 h and 168 h, respectively; $DE_{max}$ is the maximum tumor delivery efficiency; Full and Best represent full and best regression models for different sets of log-transformed tumor delivery efficiency.

**Table S9.** Multivariable linear regression results of selected models for the log-transformed tumor delivery efficiencies based on the 313 confidently predicted datasets.

| Statistical criteria | $DE_{Tlast\_PK}$ | | $DE_{24}$ | | $DE_{168}$ | | $DE_{max}$ | |
|---|---|---|---|---|---|---|---|---|
| | Full conf. | Best conf. | Full conf. | Best conf. | Full conf. | Best conf. | Full conf. | Best conf. |
| **Gold nanomaterials** | | | | | | | | |
| $R^2$ | 0.65 | 0.61 | 0.61 | 0.59 | 0.62 | 0.61 | 0.61 | 0.60 |
| Adj-$R^2$ | 0.47 | 0.49 | 0.41 | 0.46 | 0.42 | 0.48 | 0.41 | 0.47 |
| *P*-value | **<0.001** | **<0.001** | **0.004** | **<0.001** | **0.003** | **<0.001** | **0.004** | **<0.001** |
| AIC | 83 | 79 | 87 | 81 | 85 | 77 | 84 | 76 |
| BIC | 119 | 105 | 124 | 107 | 122 | 104 | 120 | 103 |
| **Inorganic nanomaterials** | | | | | | | | |
| $R^2$ | 0.51 | 0.46 | 0.53 | 0.53 | 0.57 | 0.53 | 0.52 | 0.51 |
| Adj-$R^2$ | 0.33 | 0.33 | 0.36 | 0.38 | 0.41 | 0.42 | 0.34 | 0.36 |
| *P*-value | **<0.001** | **<0.001** | **<0.001** | **<0.001** | **<0.001** | **<0.001** | **<0.001** | **<0.001** |
| AIC | 155 | 150 | 141 | 136 | 147 | 142 | 144 | 140 |
| BIC | 216 | 194 | 203 | 190 | 208 | 188 | 205 | 194 |
| **Organic nanomaterials** | | | | | | | | |
| $R^2$ | 0.43 | 0.43 | 0.42 | 0.42 | 0.46 | 0.46 | 0.44 | 0.44 |
| Adj-$R^2$ | 0.34 | 0.34 | 0.33 | 0.33 | 0.37 | 0.37 | 0.34 | 0.34 |
| *P*-value | **<0.001** | **<0.001** | **<0.001** | **<0.001** | **<0.001** | **<0.001** | **<0.001** | **<0.001** |
| AIC | 303 | 303 | 298 | 298 | 335 | 335 | 303 | 303 |
| BIC | 393 | 393 | 388 | 388 | 426 | 426 | 393 | 393 |
| **All nanomaterials** | | | | | | | | |
| $R^2$ | 0.35 | 0.35 | 0.36 | 0.36 | 0.40 | 0.40 | 0.37 | 0.37 |
| Adj-$R^2$ | 0.26 | 0.26 | 0.27 | 0.27 | 0.32 | 0.32 | 0.28 | 0.28 |
| *P*-value | **<0.001** | **<0.001** | **<0.001** | **<0.001** | **<0.001** | **<0.001** | **<0.001** | **<0.001** |
| AIC | 486 | 484 | 469 | 467 | 511 | 509 | 471 | 469 |
| BIC | 616 | 611 | 599 | 593 | 641 | 635 | 601 | 596 |

$R^2$, coefficient of determination; Adj-$R^2$, adjusted $R^2$; AIC, Akaike information criterion; BIC, Bayesian information criterion; $DE_{Tlast\_PK}$ is the tumor delivery efficiency estimated at the last sampling time point according to the original pharmacokinetic study; $DE_{24}$ and $DE_{168}$ represent tumor delivery efficiency at 24 h and 168 h; $DE_{max}$ is the maximum tumor delivery efficiency; Full conf. and Best conf. represent regression models based upon confidently estimated tumor delivery efficiency from 313 datasets.

**References**


(1) Zhong, J.; Wen, L.; Yang, S.; Xiang, L.; Chen, Q.; Xing, D. Imaging-Guided High-Efficient Photoacoustic Tumor Therapy with Targeting Gold Nanorods. *Nanomedicine (N. Y., NY, U. S.)* **2015**, *11*, 1499–1509.

(2) Goodrich, G. P.; Bao, L.; Gill-Sharp, K.; Sang, K. L.; Wang, J.; Payne, J. D. Photothermal Therapy in a Murine Colon Cancer Model Using Near-Infrared Absorbing Gold Nanorods. *J. Biomed. Opt.* **2010**, *15*, 018001.

(3) Meyers, J. D.; Cheng, Y.; Broome, A. M.; Agnes, R. S.; Schluchter, M. D.; Margevicius, S.; Wang, X.; Kenney, M. E.; Burda, C.; Basilion, J. P. Peptide-Targeted Gold Nanoparticles for Photodynamic Therapy of Brain Cancer. *Part. Part. Syst. Charact.* **2015**, *32*, 448–457.

(4) Dam, D. H. M.; Culver, K. S. B.; Kandela, I.; Lee, R. C.; Chandra, K.; Lee, H.; Mantis, C.; Ugolkov, A.; Mazar, A. P.; Odom, T. W. Biodistribution and *In Vivo* Toxicity of Aptamer-Loaded Gold Nanostars. *Nanomedicine (N. Y., NY, U. S.)* **2015**, *11*, 671–679.

(5) Sykes, E. A.; Chen, J.; Zheng, G.; Chan, W. C. W. Investigating the Impact of Nanoparticle Size on Active and Passive Tumor Targeting Efficiency. *ACS Nano* **2014**, *8*, 5696–5706.

(6) Hu, H.; Huang, P.; Weiss, O. J.; Yan, X.; Yue, X.; Zhang, M. G.; Tang, Y.; Nie, L.; Ma, Y.; Niu, G.; Wu, K.; Chen, X. PET and NIR Optical Imaging Using Self-Illuminating $^{64}$Cu-Doped Chelator-Free Gold Nanoclusters. *Biomaterials* **2014**, *35*, 9868–9876.

(7) Razzak, R.; Zhou, J.; Yang, X. H.; Pervez, N.; Bédard, E. L. R.; Moore, R. B.; Shaw, A.; Amanie, J.; Roa, W. H. The Biodistribution and Pharmacokinetic Evaluation of Choline-Bound Gold Nanoparticles in a Human Prostate Tumor Xenograft Model. *Clin. Investig. Med.* **2013**, *36*, E133–E142.

(8) Liu, X.; Li, H.; Chen, Y.; Jin, Q.; Ren, K.; Ji, J. Mixed-Charge Nanoparticles for Long Circulation, Low Reticuloendothelial System Clearance, and High Tumor Accumulation. *Adv. Healthcare Mater.* **2014**, *3*, 1439–1447.

(9) Cheng, K.; Kothapalli, S. R.; Liu, H.; Koh, A. L.; Jokerst, J. V.; Jiang, H.; Yang, M.; Li, J.; Levi, J.; Wu, J. C.; Gambhir, S. S.; Cheng, Z. Construction and Validation of Nano Gold Tripods for Molecular Imaging of Living Subjects. *J. Am. Chem. Soc.* **2014**, *136*, 3560–3571.

(10) Zhang, C.; Li, C.; Liu, Y.; Zhang, J.; Bao, C.; Liang, S.; Wang, Q.; Yang, Y.; Fu, H.; Wang, K.; Cui, D. Gold Nanoclusters-Based Nanoprobes for Simultaneous Fluorescence Imaging and Targeted Photodynamic Therapy with Superior Penetration and Retention Behavior in Tumors. *Adv. Funct. Mater.* **2015**, *25*, 1314–1325.

(11) Black, K. C. L.; Wang, Y.; Luehmann, H. P.; Cai, X.; Xing, W.; Pang, B.; Zhao, Y.; Cutler, C. S.; Wang, L. V.; Liu, Y.; Xia, Y. Radioactive $^{198}$Au-Doped Nanostructures with Different Shapes for *In Vivo* Analyses of Their Biodistribution, Tumor Uptake, and Intratumoral Distribution. *ACS Nano* **2014**, *8*, 4385–4394.

(12) Liu, J.; Yu, M.; Ning, X.; Zhou, C.; Yang, S.; Zheng, J. PEGylation and Zwitterionization: Pros and Cons in the Renal Clearance and Tumor Targeting of Near-IR-Emitting Gold Nanoparticles. *Angew. Chem. Int. Ed.* **2013**, *52*, 12572–12576.

(13) Karmani, L.; Labar, D.; Valembois, V.; Bouchat, V.; Nagaswaran, P. G.; Bol, A.; Gillart, J.; Levêque, P.; Bouzin, C.; Bonifazi, D.; Michiels, C.; Feron, O.; Grégoire, V.; Lucas, S.; Borght, T. Vander; Gallez, B. Antibody-Functionalized Nanoparticles for Imaging Cancer: Influence of Conjugation to Gold Nanoparticles on the Biodistribution of $^{89}$Zr-Labeled Cetuximab in Mice. *Contrast Media Mol. Imaging* **2013**, *8*, 402–408.

(14) Wang, Y.; Liu, Y.; Luehmann, H.; Xia, X.; Brown, P.; Jarreau, C.; Welch, M.; Xia, Y. Evaluating the Pharmacokinetics and *In Vivo* Cancer Targeting Capability of Au Nanocages by Positron Emission Tomography Imaging. *ACS Nano* **2012**, *6*, 5880–5888.

(15) Shah, N. B.; Vercellotti, G. M.; White, J. G.; Fegan, A.; Wagner, C. R.; Bischof, J. C. Blood-Nanoparticle Interactions and *In Vivo* Biodistribution: Impact of Surface PEG and Ligand

Properties. *Mol. Pharmaceutics* **2012**, *9*, 2146–2155.

(16) Kennedy, L. C.; Bear, A. S.; Young, J. K.; Lewinski, N. A.; Kim, J.; Foster, A. E.; Drezek, R. A. T Cells Enhance Gold Nanoparticle Delivery to Tumors *In Vivo*. *Nanoscale Res. Lett.* **2011**, *6*, 283.

(17) Gormley, A. J.; Malugin, A.; Ray, A.; Robinson, R.; Ghandehari, H. Biological Evaluation of RGDfK-Gold Nanorod Conjugates for Prostate Cancer Treatment. *J. Drug Targeting* **2011**, *19*, 915–924.

(18) Arnida; Janát-Amsbury, M. M.; Ray, A.; Peterson, C. M.; Ghandehari, H. Geometry and Surface Characteristics of Gold Nanoparticles Influence Their Biodistribution and Uptake by Macrophages. *Eur. J. Pharm. Biopharm.* **2011**, *77*, 417–423.

(19) Perrault, S. D.; Walkey, C.; Jennings, T.; Fischer, H. C.; Chan, W. C. W. Mediating Tumor Targeting Efficiency of Nanoparticles through Design. *Nano Lett.* **2009**, *9*, 1909–1915.

(20) Wang, J.; Bai, R.; Yang, R.; Liu, J.; Tang, J.; Liu, Y.; Li, J.; Chai, Z.; Chen, C. Size- and Surface Chemistry-Dependent Pharmacokinetics and Tumor Accumulation of Engineered Gold Nanoparticles after Intravenous Administration. *Metallomics* **2015**, *7*, 516–524.

(21) Chen, Q.; Wang, H.; Liu, H.; Wen, S.; Peng, C.; Shen, M.; Zhang, G.; Shi, X. Multifunctional Dendrimer-Entrapped Gold Nanoparticles Modified with RGD Peptide for Targeted Computed Tomography/Magnetic Resonance Dual-Modal Imaging of Tumors. *Anal. Chem.* **2015**, *87*, 3949–3956.

(22) Balogh, L.; Nigavekar, S. S.; Nair, B. M.; Lesniak, W.; Zhang, C.; Sung, L. Y.; Kariapper, M. S. T.; El-Jawahri, A.; Llanes, M.; Bolton, B.; Mamou, F.; Tan, W.; Hutson, A.; Minc, L.; Khan, M. K. Significant Effect of Size on the *In Vivo* Biodistribution of Gold Composite Nanodevices in Mouse Tumor Models. *Nanomedicine (N. Y., NY, U. S.)* **2007**, *3*, 281–296.

(23) Poon, W.; Zhang, X.; Bekah, D.; Teodoro, J. G.; Nadeau, J. L. Targeting B16 Tumors *In Vivo*

with Peptide-Conjugated Gold Nanoparticles. *Nanotechnology* **2015**, *26*, 285101.

(24) Chen, W. H.; Yang, C. X.; Qiu, W. X.; Luo, G. F.; Jia, H. Z.; Lei, Q.; Wang, X. Y.; Liu, G.; Zhuo, R. X.; Zhang, X. Z. Multifunctional Theranostic Nanoplatform for Cancer Combined Therapy Based on Gold Nanorods. *Adv. Healthcare Mater.* **2015**, *4*, 2247–2259.

(25) Elbialy, N. S.; Fathy, M. M.; Khalil, W. M. Doxorubicin Loaded Magnetic Gold Nanoparticles for *In Vivo* Targeted Drug Delivery. *Int. J. Pharm. (Amsterdam, Neth.)* **2015**, *490*, 190–199.

(26) Robinson, R.; Gerlach, W.; Ghandehari, H. Comparative Effect of Gold Nanorods and Nanocages for Prostate Tumor Hyperthermia. *J. Controlled Release* **2015**, *220*, 245–252.

(27) Camerin, M.; Moreno, M.; Marín, M. J.; Schofield, C. L.; Chambrier, I.; Cook, M. J.; Coppellotti, O.; Jori, G.; Russell, D. A. Delivery of a Hydrophobic Phthalocyanine Photosensitizer Using PEGylated Gold Nanoparticle Conjugates for the *In Vivo* Photodynamic Therapy of Amelanotic Melanoma. *Photochem. Photobiol. Sci.* **2016**, *15*, 618–625.

(28) Yang, M.; Cheng, K.; Qi, S.; Liu, H.; Jiang, Y.; Jiang, H.; Li, J.; Chen, K.; Zhang, H.; Cheng, Z. Affibody Modified and Radiolabeled Gold-Iron Oxide Hetero-Nanostructures for Tumor PET, Optical and MR Imaging. *Biomaterials* **2013**, *34*, 2796–2806.

(29) Zolata, H.; Abbasi Davani, F.; Afarideh, H. Synthesis, Characterization and Theranostic Evaluation of Indium-111 Labeled Multifunctional Superparamagnetic Iron Oxide Nanoparticles. *Nucl. Med. Biol.* **2015**, *42*, 164–170.

(30) Behnam Azad, B.; Banerjee, S. R.; Pullambhatla, M.; Lacerda, S.; Foss, C. A.; Wang, Y.; Ivkov, R.; Pomper, M. G. Evaluation of a PSMA-Targeted BNF Nanoparticle Construct. *Nanoscale* **2015**, *7*, 4432–4442.

(31) Yang, X.; Hong, H.; Grailer, J. J.; Rowland, I. J.; Javadi, A.; Hurley, S. A.; Xiao, Y.; Yang, Y.; Zhang, Y.; Nickles, R. J.; Cai, W.; Steeber, D. A.; Gong, S. CRGD-Functionalized, DOX-Conjugated, and $^{64}$Cu-Labeled Superparamagnetic Iron Oxide Nanoparticles for Targeted

Anticancer Drug Delivery and PET/MR Imaging. *Biomaterials* **2011**, *32*, 4151–4160.

(32) Quan, Q.; Xie, J.; Gao, H.; Yang, M.; Zhang, F.; Liu, G.; Lin, X.; Wang, A.; Eden, H. S.; Lee, S.; Zhang, G.; Chen, X. HSA Coated Iron Oxide Nanoparticles as Drug Delivery Vehicles for Cancer Therapy. *Mol. Pharmaceutics* **2011**, *8*, 1669–1676.

(33) DeNardo, S. J.; DeNardo, G. L.; Natarajan, A.; Miers, L. A.; Foreman, A. R.; Gruettner, C.; Adamson, G. N.; Ivkov, R. Thermal Dosimetry Predictive of Efficacy of 111In-ChL6 Nanoparticle AMF-Induced Thermoablative Therapy for Human Breast Cancer in Mice. *J. Nucl. Med.* **2007**, *48*, 437–444.

(34) Kanazaki, K.; Sano, K.; Makino, A.; Shimizu, Y.; Yamauchi, F.; Ogawa, S.; Ding, N.; Yano, T.; Temma, T.; Ono, M.; Saji, H. Development of Anti-HER2 Fragment Antibody Conjugated to Iron Oxide Nanoparticles for *In Vivo* HER2-Targeted Photoacoustic Tumor Imaging. *Nanomedicine (N. Y., NY, U. S.)* **2015**, *11*, 2051–2060.

(35) Chakravarty, R.; Goel, S.; Hong, H.; Chen, F.; Valdovinos, H. F.; Hernandez, R.; Barnhart, T. E.; Cai, W. Hollow Mesoporous Silica Nanoparticles for Tumor Vasculature Targeting and PET Image-Guided Drug Delivery. *Nanomedicine (London, U. K.)* **2015**, *10*, 1233–1246.

(36) Chen, M.; Fang, X.; Tang, S.; Zheng, N. Polypyrrole Nanoparticles for High-Performance *In Vivo* Near-Infrared Photothermal Cancer Therapy. *Chem. Commun. (Cambridge, U. K.)* **2012**, *48*, 8934–8936.

(37) Goel, S.; Chen, F.; Hong, H.; Valdovinos, H. F.; Hernandez, R.; Shi, S.; Barnhart, T. E.; Cai, W. $VEGF_{121}$-Conjugated Mesoporous Silica Nanoparticle: A Tumor Targeted Drug Delivery System. *ACS Appl. Mater. Interfaces* **2014**, *6*, 21677–21685.

(38) Chen, F.; Hong, H.; Shi, S.; Goel, S.; Valdovinos, H. F.; Hernandez, R.; Theuer, C. P.; Barnhart, T. E.; Cai, W. Engineering of Hollow Mesoporous Silica Nanoparticles for Remarkably Enhanced Tumor Active Targeting Efficacy. *Sci. Rep.* **2014**, *4*, 5080.

(39) Chen, F.; Nayak, T. R.; Goel, S.; Valdovinos, H. F.; Hong, H.; Theuer, C. P.; Barnhart, T. E.; Cai, W. *In Vivo* Tumor Vasculature Targeted PET/NIRF Imaging with TRC105(Fab)-Conjugated, Dual-Labeled Mesoporous Silica Nanoparticles. *Mol. Pharmaceutics* **2014**, *11*, 4007–4014.

(40) Benezra, M.; Penate-Medina, O.; Zanzonico, P. B.; Schaer, D.; Ow, H.; Burns, A.; DeStanchina, E.; Longo, V.; Herz, E.; Iyer, S.; Wolchok, J.; Larson, S. M.; Wiesner, U.; Bradbury, M. S. Multimodal Silica Nanoparticles Are Effective Cancer-Targeted Probes in a Model of Human Melanoma Find the Latest Version : Technical Advance Multimodal Silica Nanoparticles Are Effective Cancer-Targeted Probes in a Model of Human Melanoma. *J. Clin. Invest.* **2011**, *121*, 2768–2780.

(41) Chen, F.; Hong, H.; Zhang, Y.; Valdovinos, H. F.; Shi, S.; Kwon, G. S.; Theuer, C. P.; Barnhart, T. E.; Cai, W. *In Vivo* Tumor Targeting and Image-Guided Drug Delivery with Antibody-Conjugated, Radiolabeled Mesoporous Silica Nanoparticles. *ACS Nano* **2013**, *7*, 9027–9039.

(42) Huo, M.; Wang, L.; Chen, Y.; Shi, J. Tumor-Selective Catalytic Nanomedicine by Nanocatalyst Delivery. *Nat. Commun.* **2017**, *8*, 357.

(43) Xue, H.; Yu, Z.; Liu, Y.; Yuan, W.; Yang, T.; You, J.; He, X.; Lee, R. J.; Li, L.; Xu, C. Delivery of MiR-375 and Doxorubicin Hydrochloride by Lipid-Coated Hollow Mesoporous Silica Nanoparticles to Overcome Multiple Drug Resistance in Hepatocellular Carcinoma. *Int. J. Nanomed.* **2017**, *12*, 5271–5287.

(44) Kong, M.; Tang, J.; Qiao, Q.; Wu, T.; Qi, Y.; Tan, S.; Gao, X.; Zhang, Z. Biodegradable Hollow Mesoporous Silica Nanoparticles for Regulating Tumor Microenvironment and Enhancing Antitumor Efficiency. *Theranostics* **2017**, *7*, 3276–3292.

(45) Su, J.; Sun, H.; Meng, Q.; Zhang, P.; Yin, Q.; Li, Y. Enhanced Blood Suspensibility and Laser-Activated Tumor-Specific Drug Release of Theranostic Mesoporous Silica Nanoparticles by Functionalizing with Erythrocyte Membranes. *Theranostics* **2017**, *7*, 523–537.

(46) Hou, J.; Guo, C.; Shi, Y.; Liu, E.; Dong, W.; Yu, B.; Liu, S.; Gong, J. A Novel High Drug Loading Mussel-Inspired Polydopamine Hybrid Nanoparticle as a pH-Sensitive Vehicle for Drug Delivery. *Int. J. Pharm. (Amsterdam, Neth.)* **2017**, *533*, 73–83.

(47) Ansari, L.; Jaafari, M. R.; Bastami, T. R.; Malaekeh-Nikouei, B. Improved Anticancer Efficacy of Epirubicin by Magnetic Mesoporous Silica Nanoparticles: *In Vitro* and *In Vivo* Studies. *Artif. Cells, Nanomed., Biotechnol.* **2018**, *46*, 594–606.

(48) Wu, F.; Zhang, M.; Lu, H.; Liang, D.; Huang, Y.; Xia, Y.; Hu, Y.; Hu, S.; Wang, J.; Yi, X.; Zhang, J. Triple Stimuli-Responsive Magnetic Hollow Porous Carbon-Based Nanodrug Delivery System for Magnetic Resonance Imaging-Guided Synergistic Photothermal/Chemotherapy of Cancer. *ACS Appl. Mater. Interfaces* **2018**, *10*, 21939–21949.

(49) Cheng, X.; Li, D.; Lin, A.; Xu, J.; Wu, L.; Gu, H.; Huang, Z.; Liu, J.; Zhang, Y.; Yin, X. Fabrication of Multifunctional Triple-Responsive Platform Based on CuS-Capped Periodic Mesoporous Organosilica Nanoparticles for Chemo-Photothermal Therapy. *Int. J. Nanomed.* **2018**, *13*, 3661–3677.

(50) Hu, H.; Dai, A.; Sun, J.; Li, X.; Gao, F.; Wu, L.; Fang, Y.; Yang, H.; An, L.; Wu, H.; Yang, S. Aptamer-Conjugated $Mn_3O_4$@$SiO_2$ Core-Shell Nanoprobes for Targeted Magnetic Resonance Imaging. *Nanoscale* **2013**, *5*, 10447–10454.

(51) Lee, J.; Lee, T. S.; Ryu, J.; Hong, S.; Kang, M.; Im, K.; Kang, J. H.; Lim, S. M.; Park, S.; Song, R. RGD Peptide-Conjugated Multimodal NaGdF4:Yb3+/Er3+ Nanophosphors for Upconversion Luminescence, MR, and PET Imaging of Tumor Angiogenesis. *J. Nucl. Med.* **2013**, *54*, 96–103.

(52) Yu, J.; Yin, W.; Zheng, X.; Tian, G.; Zhang, X.; Bao, T.; Dong, X.; Wang, Z.; Gu, Z.; Ma, X.; Zhao, Y. Smart $MoS_2$/$Fe_3O_4$ Nanotheranostic for Magnetically Targeted Photothermal Therapy Guided by Magnetic Resonance/Photoacoustic Imaging. *Theranostics* **2015**, *5*, 931–945.

(53) Mi, P.; Kokuryo, D.; Cabral, H.; Kumagai, M.; Nomoto, T.; Aoki, I.; Terada, Y.; Kishimura, A.;

Nishiyama, N.; Kataoka, K. Hydrothermally Synthesized PEGylated Calcium Phosphate Nanoparticles Incorporating Gd-DTPA for Contrast Enhanced MRI Diagnosis of Solid Tumors. *J. Controlled Release* **2014**, *174*, 63–71.

(54) Huang, H.; Yue, T.; Xu, K.; Golzarian, J.; Yu, J.; Huang, J. Fabrication and Evaluation of Tumor-Targeted Positive MRI Contrast Agent Based on Ultrasmall MnO Nanoparticles. *Colloids Surf., B* **2015**, *131*, 148–154.

(55) Shi, S.; Fliss, B. C.; Gu, Z.; Zhu, Y.; Hong, H.; Valdovinos, H. F.; Hernandez, R.; Goel, S.; Luo, H.; Chen, F.; Barnhart, T. E.; Nickles, R. J.; Xu, Z. P.; Cai, W. Chelator-Free Labeling of Layered Double Hydroxide Nanoparticles for *In Vivo* PET Imaging. *Sci. Rep.* **2015**, *5*, 16930.

(56) Liu, L. X.; Li, B. X.; Wang, Q. Y.; Dong, Z. P.; Li, H. M.; Jin, Q. M.; Hong, H.; Zhang, J.; Wang, Y. An Integrative Folate-Based Metal Complex Nanotube as a Potent Antitumor Nanomedicine as well as an Efficient Tumor-Targeted Drug Carrier. *Bioconjugate Chem.* **2016**, *27*, 2863–2873.

(57) Shi, J.; Chen, Z.; Wang, L.; Wang, B.; Xu, L.; Hou, L.; Zhang, Z. A Tumor-Specific Cleavable Nanosystem of PEG-Modified C60@Au Hybrid Aggregates for Radio Frequency-Controlled Release, Hyperthermia, Photodynamic Therapy and X-Ray Imaging. *Acta Biomater.* **2016**, *29*, 282–297.

(58) Li, Z.; Hu, Y.; Howard, K. A. A.; Jiang, T.; Fan, X.; Miao, Z.; Sun, Y.; Besenbacher, F.; Yu, M. Multifunctional Bismuth Selenide Nanocomposites for Antitumor Thermo-Chemotherapy and Imaging. *ACS Nano* **2016**, *10*, 984–997.

(59) Dewi, N.; Mi, P.; Yanagie, H.; Sakurai, Y.; Morishita, Y.; Yanagawa, M.; Nakagawa, T.; Shinohara, A.; Matsukawa, T.; Yokoyama, K.; Cabral, H.; Suzuki, M.; Sakurai, Y.; Tanaka, H.; Ono, K.; Nishiyama, N.; Kataoka, K.; Takahashi, H. *In Vivo* Evaluation of Neutron Capture Therapy Effectivity Using Calcium Phosphate-Based Nanoparticles as Gd-DTPA Delivery Agent. *J. Cancer Res. Clin. Oncol.* **2016**, *142*, 767–775.

(60) Gao, Z.; Nakanishi, Y.; Noda, S.; Omachi, H.; Shinohara, H.; Kimura, H.; Nagasaki, Y. Development of $Gd_3N@C_{80}$ Encapsulated Redox Nanoparticles for High-Performance Magnetic Resonance Imaging. *J. Biomater. Sci., Polym. Ed.* **2017**, *28*, 1036–1050.

(61) Hou, L.; Shan, X.; Hao, L.; Feng, Q.; Zhang, Z. Copper Sulfide Nanoparticle-Based Localized Drug Delivery System as an Effective Cancer Synergistic Treatment and Theranostic Platform. *Acta Biomater.* **2017**, *54*, 307–320.

(62) Yu, H.; Tang, Z.; Zhang, D.; Song, W.; Zhang, Y.; Yang, Y.; Ahmad, Z.; Chen, X. Pharmacokinetics, Biodistribution and *In Vivo* Efficacy of Cisplatin Loaded Poly(L-Glutamic Acid)-*g*-Methoxy Poly(Ethylene Glycol) Complex Nanoparticles for Tumor Therapy. *J. Controlled Release* **2015**, *205*, 89–97.

(63) Guo, J.; Hong, H.; Chen, G.; Shi, S.; Zheng, Q.; Zhang, Y.; Theuer, C. P.; Barnhart, T. E.; Cai, W.; Gong, S. Image-Guided and Tumor-Targeted Drug Delivery with Radiolabeled Unimolecular Micelles. *Biomaterials* **2013**, *34*, 8323–8332.

(64) Shi, Y.; van der Meel, R.; Theek, B.; Oude Blenke, E.; Pieters, E. H. E.; Fens, M. H. A. M.; Ehling, J.; Schiffelers, R. M.; Storm, G.; van Nostrum, C. F.; Lammers, T.; Hennink, W. E. Complete Regression of Xenograft Tumors upon Targeted Delivery of Paclitaxel *via* ∏ - ∏ Stacking Stabilized Polymeric Micelles. *ACS Nano* **2015**, *9*, 3740–3752.

(65) Chen, Y.; Zhang, W.; Huang, Y.; Gao, F.; Sha, X.; Fang, X. Pluronic-Based Functional Polymeric Mixed Micelles for Co-Delivery of Doxorubicin and Paclitaxel to Multidrug Resistant Tumor. *Int. J. Pharm. (Amsterdam, Neth.)* **2015**, *488*, 44–58.

(66) Ding, M.; Song, N.; He, X.; Li, J.; Zhou, L.; Tan, H.; Fu, Q.; Gu, Q. Toward the Next-Generation Nanomedicines: Design of Multifunctional Multiblock Polyurethanes for Effective Cancer Treatment. *ACS Nano* **2013**, *7*, 1918–1928.

(67) Chu, K. S.; Hasan, W.; Rawal, S.; Walsh, M. D.; Enlow, E. M.; Luft, J. C.; Bridges, A. S.; Kuijer,

J. L.; Napier, M. E.; Zamboni, W. C.; DeSimone, J. M. Plasma, Tumor and Tissue Pharmacokinetics of Docetaxel Delivered *via* Nanoparticles of Different Sizes and Shapes in Mice Bearing SKOV-3 Human Ovarian Carcinoma Xenograft. *Nanomedicine (N. Y., NY, U. S.)* **2013**, *9*, 686–693.

(68) Chu, K. S.; Schorzman, A. N.; Finniss, M. C.; Bowerman, C. J.; Peng, L.; Luft, J. C.; Madden, A. J.; Wang, A. Z.; Zamboni, W. C.; DeSimone, J. M. Nanoparticle Drug Loading as a Design Parameter to Improve Docetaxel Pharmacokinetics and Efficacy. *Biomaterials* **2013**, *34*, 8424–8429.

(69) Ma, Y.; Sadoqi, M.; Shao, J. Biodistribution of Indocyanine Green-Loaded Nanoparticles with Surface Modifications of PEG and Folic Acid. *Int. J. Pharm. (Amsterdam, Neth.)* **2012**, *436*, 25–31.

(70) Cabral, H.; Matsumoto, Y.; Mizuno, K.; Chen, Q.; Murakami, M.; Kimura, M.; Terada, Y.; Kano, M. R.; Miyazono, K.; Uesaka, M.; Nishiyama, N.; Kataoka, K. Accumulation of Sub-100 nm Polymeric Micelles in Poorly Permeable Tumours Depends on Size. *Nat. Nanotechnol.* **2011**, *6*, 815–823.

(71) Guo, X.; Shi, C.; Wang, J.; Di, S.; Zhou, S. pH-Triggered Intracellular Release from Actively Targeting Polymer Micelles. *Biomaterials* **2013**, *34*, 4544–4554.

(72) Sumitani, S.; Oishi, M.; Nagasaki, Y. Carborane Confined Nanoparticles for Boron Neutron Capture Therapy: Improved Stability, Blood Circulation Time and Tumor Accumulation. *React. Funct. Polym.* **2011**, *71*, 684–693.

(73) Bae, Y.; Nishiyama, N.; Kataoka, K. *In Vivo* Antitumor Activity of the Folate-Conjugated pH-Sensitive Polymeric Micelle Selectively Releasing Adriamycin in the Intracellular Acidic Compartments. *Bioconjugate Chem.* **2007**, *18*, 1131–1139.

(74) Cabral, H.; Nishiyama, N.; Okazaki, S.; Koyama, H.; Kataoka, K. Preparation and Biological

Properties of Dichloro(1,2-Diaminocyclohexane) Platinum(II) (DACHPt)-Loaded Polymeric Micelles. *J. Controlled Release* **2005**, *101*, 223–232.

(75) Bibby, D. C.; Talmadge, J. E.; Dalal, M. K.; Kurz, S. G.; Chytil, K. M.; Barry, S. E.; Shand, D. G.; Steiert, M. Pharmacokinetics and Biodistribution of RGD-Targeted Doxorubicin-Loaded Nanoparticles in Tumor-Bearing Mice. *Int. J. Pharm. (Amsterdam, Neth.)* **2005**, *293*, 281–290.

(76) Bae, Y.; Nishiyama, N.; Fukushima, S.; Koyama, H.; Yasuhiro, M.; Kataoka, K. Preparation and Biological Characterization of Polymeric Micelle Drug Carriers with Intracellular pH-Triggered Drug Release Property: Tumor Permeability, Controlled Subcellular Drug Distribution, and Enhanced *In Vivo* Antitumor Efficacy. *Bioconjugate Chem.* **2005**, *16*, 122–130.

(77) Sasatsu, M.; Onishi, H.; Machida, Y. Preparation and Biodisposition of Methoxypolyethylene Glycol Amine-Poly($_{DL}$-Lactic Acid) Copolymer Nanoparticles Loaded with Pyrene-Ended Poly($_{DL}$-Lactic Acid). *Int. J. Pharm. (Amsterdam, Neth.)* **2008**, *358*, 271–277.

(78) Rossin, R.; Pan, D.; Qi, K.; Turner, J. L.; Sun, X.; Wooley, K. L.; Welch, M. J. Radiotherapy : Synthesis , Radiolabeling , and Biologic Evaluation. *Blood Vessels* **2005**, *46*, 1210–1218.

(79) Mondal, N.; Halder, K. K.; Kamila, M. M.; Debnath, M. C.; Pal, T. K.; Ghosal, S. K.; Sarkar, B. R.; Ganguly, S. Preparation, Characterization, and Biodistribution of Letrozole Loaded PLGA Nanoparticles in Ehrlich Ascites Tumor Bearing Mice. *Int. J. Pharm. (Amsterdam, Neth.)* **2010**, *397*, 194–200.

(80) He, C.; Hu, Y.; Yin, L.; Tang, C.; Yin, C. Effects of Particle Size and Surface Charge on Cellular Uptake and Biodistribution of Polymeric Nanoparticles. *Biomaterials* **2010**, *31*, 3657–3666.

(81) Cabral, H.; Nishiyama, N.; Kataoka, K. Optimization of (1,2-Diamino-Cyclohexane)Platinum(II)-Loaded Polymeric Micelles Directed to Improved Tumor Targeting and Enhanced Antitumor Activity. *J. Controlled Release* **2007**, *121*, 146–155.

(82) Pathak, A.; Kumar, P.; Chuttani, K.; Jain, S.; Mishra, A. K.; Vyas, S. P.; Gupta, K. C. Gene

Expression, Biodistribution, and Pharmacoscintigraphic Evaluation of Chondroitin Sulfate – PEI Nanoconstructs Mediated Tumor Gene Therapy. *ACS Nano* **2009**, *3*, 1493–1505.

(83) Shi, S.; Yang, K.; Hong, H.; Valdovinos, H. F.; Nayak, T. R.; Zhang, Y.; Theuer, C. P.; Barnhart, T. E.; Liu, Z.; Cai, W. Tumor Vasculature Targeting and Imaging in Living Mice with Reduced Graphene Oxide. *Biomaterials* **2013**, *34*, 3002–3009.

(84) Hong, H.; Yang, K.; Zhang, Y.; Engle, J. W.; Feng, L.; Yang, Y.; Nayak, T. R.; Goel, S.; Bean, J.; Theuer, C. P.; Barnhart, T. E.; Liu, Z.; Cai, W. *In Vivo* Targeting and Imaging of Tumor Vasculature with Radiolabeled, Antibody-Conjugated Nanographene. *ACS Nano* **2012**, *6*, 2361–2370.

(85) Xu, H.; Fan, M.; Elhissi, A. M. A.; Zhang, Z.; Wan, K. W.; Ahmed, W.; Phoenix, D. A.; Sun, X. PEGylated Graphene Oxide for Tumor-Targeted Delivery of Paclitaxel. *Nanomedicine (London, U. K.)* **2015**, *10*, 1247–1262.

(86) Shi, S.; Yang, K.; Hong, H.; Chen, F.; Valdovinos, H. F.; Goel, S.; Barnhart, T. E.; Liu, Z.; Cai, W. VEGFR Targeting Leads to Significantly Enhanced Tumor Uptake of Nanographene Oxide *In Vivo*. *Biomaterials* **2015**, *39*, 39–46.

(87) Hong, H.; Zhang, Y.; Engle, J. W.; Nayak, T. R.; Theuer, C. P.; Nickles, R. J.; Barnhart, T. E.; Cai, W. *In Vivo* Targeting and Positron Emission Tomography Imaging of Tumor Vasculature with $^{66}$Ga-Labeled Nano-Graphene. *Biomaterials* **2012**, *33*, 4147–4156.

(88) Liu, Z.; Cai, W.; He, L.; Nakayama, N.; Chen, K.; Sun, X.; Chen, X.; Dai, H. *In Vivo* Biodistribution and Highly Efficient Tumour Targeting of Carbon Nanotubes in Mice. *Nat. Nanotechnol.* **2007**, *2*, 47–52.

(89) Ekdawi, S. N.; Stewart, J. M. P.; Dunne, M.; Stapleton, S.; Mitsakakis, N.; Dou, Y. N.; Jaffray, D. A.; Allen, C. Spatial and Temporal Mapping of Heterogeneity in Liposome Uptake and Microvascular Distribution in an Orthotopic Tumor Xenograft Model. *J. Controlled Release* **2015**,

*207*, 101–111.

(90) Song, G.; Darr, D. B.; Santos, C. M.; Ross, M.; Valdivia, A.; Jordan, J. L.; Midkiff, B. R.; Cohen, S.; Nikolaishvili-Feinberg, N.; Miller, C. R.; Tarrant, T. K.; Rogers, A. B.; Dudley, A. C.; Perou, C. M.; Zamboni, W. C. Effects of Tumor Microenvironment Heterogeneity on Nanoparticle Disposition and Efficacy in Breast Cancer Tumor Models. *Clin. Cancer Res.* **2014**, *20*, 6083–6095.

(91) Negi, L. M.; Talegaonkar, S.; Jaggi, M.; Verma, A. K.; Verma, R.; Dobhal, S.; Kumar, V. Surface Engineered Nanostructured Lipid Carriers for Targeting MDR Tumor: Part II. *In Vivo* Biodistribution, Pharmacodynamic and Hematological Toxicity Studies. *Colloids Surf., B* **2014**, *123*, 610–615.

(92) Wong, A. W.; Ormsby, E.; Zhang, H.; Seo, J. W.; Mahakian, L. M.; Caskey, C. F.; Ferrara, K. W. A Comparison of Image Contrast with $^{64}$Cu-Labeled Long Circulating Liposomes and $^{18}$F-FDG in a Murine Model of Mammary Carcinoma. *Am. J. Nucl. Med. Mol. Imaging* **2013**, *3*, 32–43.

(93) Hirsjärvi, S.; Sancey, L.; Dufort, S.; Belloche, C.; Vanpouille-Box, C.; Garcion, E.; Coll, J. L.; Hindré, F.; Benoît, J. P. Effect of Particle Size on the Biodistribution of Lipid Nanocapsules: Comparison between Nuclear and Fluorescence Imaging and Counting. *Int. J. Pharm. (Amsterdam, Neth.)* **2013**, *453*, 594–600.

(94) Miyajima, Y.; Nakamura, H.; Kuwata, Y.; Lee, J.-D.; Masunaga, S.; Ono, K.; Maruyama, K. Transferrin-Loaded Nido-Carborane Liposomes: Tumor-Targeting Boron Delivery System for Neutron Capture Therapy. *Bioconjugate Chem.* **2006**, *17*, 1314–1320.

(95) Khalid, M. N.; Simard, P.; Hoarau, D.; Dragomir, A.; Leroux, J. C. Long Circulating Poly(Ethylene Glycol)-Decorated Lipid Nanocapsules Deliver Docetaxel to Solid Tumors. *Pharm. Res.* **2006**, *23*, 752–758.

(96) Paolino, D.; Cosco, D.; Racanicchi, L.; Trapasso, E.; Celia, C.; Iannone, M.; Puxeddu, E.;

Costante, G.; Filetti, S.; Russo, D.; Fresta, M. Gemcitabine-Loaded PEGylated Unilamellar Liposomes *vs* GEMZAR®: Biodistribution, Pharmacokinetic Features and *In Vivo* Antitumor Activity. *J. Controlled Release* **2010**, *144*, 144–150.

(97) Zamboni, W. C.; Strychor, S.; Joseph, E.; Walsh, D. R.; Zamboni, B. A.; Parise, R. A.; Tonda, M. E.; Yu, N. Y.; Engbers, C.; Eiseman, J. L. Plasma, Tumor, and Tissue Disposition of STEALTH Liposomal CKD-602 (S-CKD602) and Nonliposomal CKD-602 in Mice Bearing A375 Human Melanoma Xenografts. *Clin. Cancer Res.* **2007**, *13*, 7217–7223.

(98) Han, X.; Li, Z.; Sun, J.; Luo, C.; Li, L.; Liu, Y.; Du, Y.; Qiu, S.; Ai, X.; Wu, C.; Lian, H.; He, Z. Stealth CD44-Targeted Hyaluronic Acid Supramolecular Nanoassemblies for Doxorubicin Delivery: Probing the Effect of Uncovalent Pegylation Degree on Cellular Uptake and Blood Long Circulation. *J. Controlled Release* **2015**, *197*, 29–40.

(99) Yang, C.; Wang, X.; Yao, X.; Zhang, Y.; Wu, W.; Jiang, X. Hyaluronic Acid Nanogels with Enzyme-Sensitive Cross-Linking Group for Drug Delivery. *J. Controlled Release* **2015**, *205*, 206–217.

(100) Wu, W.; Yao, W.; Wang, X.; Xie, C.; Zhang, J.; Jiang, X. Bioreducible Heparin-Based Nanogel Drug Delivery System. *Biomaterials* **2015**, *39*, 260–268.

(101) Wang, X.; Yang, C.; Zhang, Y.; Zhen, X.; Wu, W.; Jiang, X. Delivery of Platinum(IV) Drug to Subcutaneous Tumor and Lung Metastasis Using Bradykinin-Potentiating Peptide-Decorated Chitosan Nanoparticles. *Biomaterials* **2014**, *35*, 6439–6453.

(102) Ganesh, S.; Iyer, A. K.; Gattacceca, F.; Morrissey, D. V.; Amiji, M. M. *In Vivo* Biodistribution of siRNA and Cisplatin Administered Using CD44-Targeted Hyaluronic Acid Nanoparticles. *J. Controlled Release* **2013**, *172*, 699–706.

(103) Xu, J.; Gattacceca, F.; Amiji, M. Biodistribution and Pharmacokinetics of EGFR-Targeted Thiolated Gelatin Nanoparticles Following Systemic Administration in Pancreatic Tumor-

Bearing Mice. *Mol. Pharmaceutics* **2013**, *10*, 2031–2044.

(104) Cheng, Y.; Yu, S.; Zhen, X.; Wang, X.; Wu, W.; Jiang, X. Alginic Acid Nanoparticles Prepared through Counterion Complexation Method as a Drug Delivery System. *ACS Appl. Mater. Interfaces* **2012**, *4*, 5325–5332.

(105) Qian, H.; Wang, X.; Yuan, K.; Xie, C.; Wu, W.; Jiang, X.; Hu, L. Delivery of Doxorubicin *In Vitro* and *In Vivo* Using Bio-Reductive Cellulose Nanogels. *Biomater. Sci.* **2014**, *2*, 220–232.

(106) Sadekar, S.; Ray, A.; Janàt-Amsbury, M.; Peterson, C. M.; Ghandehari, H. Comparative Biodistribution of PAMAM Dendrimers and HPMA Copolymers in Ovarian-Tumor-Bearing Mice. *Biomacromolecules* **2011**, *12*, 88–96.

(107) Okuda, T.; Kawakami, S.; Akimoto, N.; Niidome, T.; Yamashita, F.; Hashida, M. PEGylated Lysine Dendrimers for Tumor-Selective Targeting after Intravenous Injection in Tumor-Bearing Mice. *J. Controlled Release* **2006**, *116*, 330–336.

(108) Kukowska-Latallo, J. F.; Candido, K. A.; Cao, Z.; Nigavekar, S. S.; Majoros, I. J.; Thomas, T. P.; Balogh, L. P.; Khan, M. K.; Baker, J. R. Nanoparticle Targeting of Anticancer Drug Improves Therapeutic Response in Animal Model of Human Epithelial Cancer. *Cancer Res.* **2005**, *65*, 5317–5324.

(109) Sadekar, S.; Linares, O.; Noh, G. J.; Hubbard, D.; Ray, A.; Janát-Amsbury, M.; Peterson, C. M.; Facelli, J.; Ghandehari, H. Comparative Pharmacokinetics of PAMAM-OH Dendrimers and HPMA Copolymers in Ovarian Tumor-Bearing Mice. *Drug Delivery Transl. Res.* **2013**, *3*, 260–271.

(110) Wu, M.; Shi, J.; Fan, D.; Zhou, Q.; Wang, F.; Niu, Z.; Huang, Y. Biobehavior in Normal and Tumor-Bearing Mice of Tobacco Mosaic Virus. *Biomacromolecules* **2013**, *14*, 4032–4037.

(111) Tian, B.; Zhang, X.; Yu, C.; Zhou, M.; Zhang, X. The Aspect Ratio Effect of Drug Nanocrystals on Cellular Internalization Efficiency, Uptake Mechanisms, and *In Vitro* and *In Vivo* Anticancer

Efficiencies. *Nanoscale* **2015**, *7*, 3588–3593.

(112) Kim, J. H.; Kim, Y.; Bae, K. H.; Park, T. G.; Lee, J. H.; Park, K. Tumor-Targeted Delivery of Paclitaxel Using Low Density Lipoprotein-Mimetic Solid Lipid Nanoparticles. *Mol. Pharmaceutics* **2015**, *12*, 1230–1241.

(113) Harivardhan Reddy, L.; Sharma, R. K.; Chuttani, K.; Mishra, A. K.; Murthy, R. S. R. Influence of Administration Route on Tumor Uptake and Biodistribution of Etoposide Loaded Solid Lipid Nanoparticles in Dalton's Lymphoma Tumor Bearing Mice. *J. Controlled Release* **2005**, *105*, 185–198.

(114) Agrawal, U.; Chashoo, G.; Sharma, P. R.; Kumar, A.; Saxena, A. K.; Vyas, S. P. Tailored Polymer-Lipid Hybrid Nanoparticles for the Delivery of Drug Conjugate: Dual Strategy for Brain Targeting. *Colloids Surf., B* **2015**, *126*, 414–425.

(115) Alibolandi, M.; Sadeghi, F.; Abnous, K.; Atyabi, F.; Ramezani, M.; Hadizadeh, F. The Chemotherapeutic Potential of Doxorubicin-Loaded PEG-*b*-PLGA Nanopolymersomes in Mouse Breast Cancer Model. *Eur. J. Pharm. Biopharm.* **2015**, *94*, 521–531.

(116) Dalela, M.; Shrivastav, T. G.; Kharbanda, S.; Singh, H. pH-Sensitive Biocompatible Nanoparticles of Paclitaxel-Conjugated Poly(Styrene-*Co*-Maleic Acid) for Anticancer Drug Delivery in Solid Tumors of Syngeneic Mice. *ACS Appl. Mater. Interfaces* **2015**, *7*, 26530–26548.

(117) Du, X. J.; Wang, J. L.; Liu, W. W.; Yang, J. X.; Sun, C. Y.; Sun, R.; Li, H. J.; Shen, S.; Luo, Y. L.; Ye, X. D.; Zhu, Y. H.; Yang, X. Z.; Wang, J. Regulating the Surface Poly(Ethylene Glycol) Density of Polymeric Nanoparticles and Evaluating Its Role in Drug Delivery *In Vivo*. *Biomaterials* **2015**, *69*, 1–11.

(118) He, Z.; Huang, J.; Xu, Y.; Zhang, X.; Teng, Y.; Huang, C.; Wu, Y.; Zhang, X.; Zhang, H.; Sun, W. Co-Delivery of Cisplatin and Paclitaxel by Folic Acid Conjugated Amphiphilic PEG-PLGA Copolymer Nanoparticles for the Treatment of Non-Small Lung Cancer. *Oncotarget* **2015**, *6*,

42150–42168.

(119) He, C.; Liu, D.; Lin, W. Self-Assembled Core-Shell Nanoparticles for Combined Chemotherapy and Photodynamic Therapy of Resistant Head and Neck Cancers. *ACS Nano* **2015**, *9*, 991–1003.

(120) Kudo, S.; Nagasaki, Y. A Novel Nitric Oxide-Based Anticancer Therapeutics by Macrophage-Targeted Poly(L-Arginine)-Based Nanoparticles. *J. Controlled Release* **2015**, *217*, 256–262.

(121) Li, M.; Tang, Z.; Zhang, Y.; Lv, S.; Li, Q.; Chen, X. Targeted Delivery of Cisplatin by LHRH-Peptide Conjugated Dextran Nanoparticles Suppresses Breast Cancer Growth and Metastasis. *Acta Biomater.* **2015**, *18*, 132–143.

(122) Mastria, E. M.; Chen, M.; McDaniel, J. R.; Li, X.; Hyun, J.; Dewhirst, M. W.; Chilkoti, A. Doxorubicin-Conjugated Polypeptide Nanoparticles Inhibit Metastasis in Two Murine Models of Carcinoma. *J. Controlled Release* **2015**, *208*, 52–58.

(123) Poon, C.; He, C.; Liu, D.; Lu, K.; Lin, W. Self-Assembled Nanoscale Coordination Polymers Carrying Oxaliplatin and Gemcitabine for Synergistic Combination Therapy of Pancreatic Cancer. *J. Controlled Release* **2015**, *201*, 90–99.

(124) Yao, X.; Xie, C.; Chen, W.; Yang, C.; Wu, W.; Jiang, X. Platinum-Incorporating Poly(*N*-Vinylpyrrolidone)-Poly(Aspartic Acid) Pseudoblock Copolymer Nanoparticles for Drug Delivery. *Biomacromolecules* **2015**, *16*, 2059–2071.

(125) Wang, J.; Mao, W.; Lock, L. L.; Tang, J.; Sui, M.; Sun, W.; Cui, H.; Xu, D.; Shen, Y. The Role of Micelle Size in Tumor Accumulation, Penetration, and Treatment. *ACS Nano* **2015**, *9*, 7195–7206.

(126) Xiong, H.; Zhou, D.; Qi, Y.; Zhang, Z.; Xie, Z.; Chen, X.; Jing, X.; Meng, F.; Huang, Y. Doxorubicin-Loaded Carborane-Conjugated Polymeric Nanoparticles as Delivery System for Combination Cancer Therapy. *Biomacromolecules* **2015**, *16*, 3980–3988.

(127) Starmans, L. W. E.; Hummelink, M. A. P. M.; Rossin, R.; Kneepkens, E. C. M.; Lamerichs, R.;

Donato, K.; Nicolay, K.; Grüll, H. $^{89}$Zr- and Fe-Labeled Polymeric Micelles for Dual Modality PET and $T_1$-Weighted MR Imaging. *Adv. Healthcare Mater.* **2015**, *4*, 2137–2145.

(128) Xu, P.; Meng, Q.; Sun, H.; Yin, Q.; Yu, H.; Zhang, Z.; Cao, M.; Zhang, Y.; Li, Y. Shrapnel Nanoparticles Loading Docetaxel Inhibit Metastasis and Growth of Breast Cancer. *Biomaterials* **2015**, *64*, 10–20.

(129) Zhang, L.; Liu, F.; Li, G.; Zhou, Y.; Yang, Y. Twin-Arginine Translocation Peptide Conjugated Epirubicin-Loaded Nanoparticles for Enhanced Tumor Penetrating and Targeting. *J. Pharm. Sci. (Philadelphia, PA, U. S.)* **2015**, *104*, 4185–4196.

(130) Wei, H.; Xu, L.; Sun, Y.; Li, G.; Cui, Z.; Yan, G.; Chen, Q.; Yin, H.; Ma, C. Preliminary Pharmacokinetics of PEGylated Oxaliplatin Polylactic Acid Nanoparticles in Rabbits and Tumor-Bearing Mice. *Artif. Cells, Nanomed., Biotechnol.* **2015**, *43*, 258–262.

(131) Zhang, W.; Sun, J.; Fang, W.; Ai, X.; Cai, C.; Tang, Y.; Su, X.; Feng, Z.; Liu, Y.; Tao, M.; Yan, X.; Chen, G.; He, Z. Nanomicelles Based on X-Shaped Four-Armed Peglyated Distearylglycerol as Long Circulating System for Doxorubicin Delivery. *Eur. J. Pharm. Sci.* **2015**, *66*, 96–106.

(132) Dai, Y.; Xing, H.; Song, F.; Yang, Y.; Qiu, Z.; Lu, X.; Liu, Q.; Ren, S.; Chen, X.; Li, N. Biotin-Conjugated Multilayer Poly [D,L-Lactide-Co-Glycolide]-Lecithin-Polyethylene Glycol Nanoparticles for Targeted Delivery of Doxorubicin. *J. Pharm. Sci. (Philadelphia, PA, U. S.)* **2016**, *105*, 2949–2958.

(133) He, C.; Poon, C.; Chan, C.; Yamada, S. D.; Lin, W. Nanoscale Coordination Polymers Codeliver Chemotherapeutics and Sirnas to Eradicate Tumors of Cisplatin-Resistant Ovarian Cancer. *J. Am. Chem. Soc.* **2016**, *138*, 6010–6019.

(134) Huang, P.; Liu, J.; Wang, W.; Zhang, Y.; Zhao, F.; Kong, D.; Liu, J.; Dong, A. Zwitterionic Nanoparticles Constructed from Bioreducible RAFT–ROP Double Head Agent for Shell Shedding Triggered Intracellular Drug Delivery. *Acta Biomater.* **2016**, *40*, 263–272.

(135) Nascimento, A. V.; Gattacceca, F.; Singh, A.; Bousbaa, H.; Ferreira, D.; Sarmento, B.; Amiji, M. M. Biodistribution and Pharmacokinetics of Mad2 siRNA-Loaded EGFR-Targeted Chitosan Nanoparticles in Cisplatin Sensitive and Resistant Lung Cancer Models. *Nanomedicine (London, U. K.)* **2016**, *11*, 767–781.

(136) Chen, Y.; Xia, R.; Huang, Y.; Zhao, W.; Li, J.; Zhang, X.; Wang, P.; Venkataramanan, R.; Fan, J.; Xie, W.; Ma, X.; Lu, B.; Li, S. An Immunostimulatory Dual-Functional Nanocarrier That Improves Cancer Immunochemotherapy. *Nat. Commun.* **2016**, *7*, 13443.

(137) Tang, Z.; Zhang, L.; Wang, Y.; Li, D.; Zhong, Z.; Zhou, S. Redox-Responsive Star-Shaped Magnetic Micelles with Active-Targeted and Magnetic-Guided Functions for Cancer Therapy. *Acta Biomater.* **2016**, *42*, 232–246.

(138) Liu, H.; Gao, M.; Xu, H.; Guan, X.; Lv, L.; Deng, S.; Zhang, C.; Tian, Y. A Promising Emodin-Loaded Poly (Lactic-*Co*-Glycolic Acid)-*d*-*α*-Tocopheryl Polyethylene Glycol 1000 Succinate Nanoparticles for Liver Cancer Therapy. *Pharm. Res.* **2016**, *33*, 217–236.

(139) Qu, Q.; Wang, Y.; Zhang, L.; Zhang, X.; Zhou, S. A Nanoplatform with Precise Control over Release of Cargo for Enhanced Cancer Therapy. *Small* **2016**, *12*, 1378–1390.

(140) Tomalova, B.; Sirova, M.; Rossmann, P.; Pola, R.; Strohalm, J.; Chytil, P.; Cerny, V.; Tomala, J.; Kabesova, M.; Rihova, B.; Ulbrich, K.; Etrych, T.; Kovar, M. The Structure-Dependent Toxicity, Pharmacokinetics and Anti-Tumour Activity of HPMA Copolymer Conjugates in the Treatment of Solid Tumours and Leukaemia. *J. Controlled Release* **2016**, *223*, 1–10.

(141) Ghanghoria, R.; Tekade, R. K.; Mishra, A. K.; Chuttani, K.; Jain, N. K. Luteinizing Hormone-Releasing Hormone Peptide Tethered Nanoparticulate System for Enhanced Antitumoral Efficacy of Paclitaxel. *Nanomedicine (London, U. K.)* **2016**, *11*, 797–816.

(142) Zhang, L.; Li, G.; Gao, M.; Liu, X.; Ji, B.; Hua, R.; Zhou, Y.; Yang, Y. RGD-Peptide Conjugated Inulin-Ibuprofen Nanoparticles for Targeted Delivery of Epirubicin. *Colloids Surf., B* **2016**, *144*,

81–89.

(143) Mei, L.; Liu, Y.; Zhang, H. J.; Zhang, Z.; Gao, H.; He, Q. Antitumor and Antimetastasis Activities of Heparin-Based Micelle Served as Both Carrier and Drug. *ACS Appl. Mater. Interfaces* **2016**, *8*, 9577–9589.

(144) Svenson, S.; Case, R. I.; Cole, R. O.; Hwang, J.; Kabir, S. R.; Lazarus, D.; Lim Soo, P.; Ng, P. S.; Peters, C.; Shum, P.; Sweryda-Krawiec, B.; Tripathi, S.; van der Poll, D.; Eliasof, S. Tumor Selective Silencing Using an RNAi-Conjugated Polymeric Nanopharmaceutical. *Mol. Pharmaceutics* **2016**, *13*, 737–747.

(145) Zou, Y.; Fang, Y.; Meng, H.; Meng, F.; Deng, C.; Zhang, J.; Zhong, Z. Self-Crosslinkable and Intracellularly Decrosslinkable Biodegradable Micellar Nanoparticles: A Robust, Simple and Multifunctional Nanoplatform for High-Efficiency Targeted Cancer Chemotherapy. *J. Controlled Release* **2016**, *244*, 326–335.

(146) He, R.; Yin, C. Trimethyl Chitosan Based Conjugates for Oral and Intravenous Delivery of Paclitaxel. *Acta Biomater.* **2017**, *53*, 355–366.

(147) Roy, A.; Zhao, Y.; Yang, Y.; Szeitz, A.; Klassen, T.; Li, S. D. Selective Targeting and Therapy of Metastatic and Multidrug Resistant Tumors Using a Long Circulating Podophyllotoxin Nanoparticle. *Biomaterials* **2017**, *137*, 11–22.

(148) Yan, G.; Wang, J.; Hu, L.; Wang, X.; Yang, G.; Fu, S.; Cheng, X.; Zhang, P.; Tang, R. Stepwise Targeted Drug Delivery to Liver Cancer Cells for Enhanced Therapeutic Efficacy by Galactose-Grafted, Ultra-pH-Sensitive Micelles. *Acta Biomater.* **2017**, *51*, 363–373.

(149) Yan, G.; Wang, J.; Qin, J.; Hu, L.; Zhang, P.; Wang, X.; Tang, R. Well-Defined Poly(Ortho Ester Amides) for Potential Drug Carriers: Probing the Effect of Extra- and Intracellular Drug Release on Chemotherapeutic Efficacy. *Macromol. Biosci.* **2017**, *17*, 1600503.

(150) Wang, F.; Wang, Y.; Ma, Q.; Cao, Y.; Yu, B. Development and Characterization of Folic Acid-

Conjugated Chitosan Nanoparticles for Targeted and Controlled Delivery of Gemcitabinein Lung Cancer Therapeutics. *Artif. Cells, Nanomed., Biotechnol.* **2017**, *45*, 1530–1538.

(151) Deng, H.; Zhao, X.; Deng, L.; Liu, J.; Dong, A. Reactive Oxygen Species Activated Nanoparticles with Tumor Acidity Internalization for Precise Anticancer Therapy. *J. Controlled Release* **2017**, *255*, 142–153.

(152) Wu, J.; Tang, C.; Yin, C. Co-Delivery of Doxorubicin and Interleukin-2 *via* Chitosan Based Nanoparticles for Enhanced Antitumor Efficacy. *Acta Biomater.* **2017**, *47*, 81–90.

(153) Gou, J.; Liang, Y.; Miao, L.; Guo, W.; Chao, Y.; He, H.; Zhang, Y.; Yang, J.; Wu, C.; Yin, T.; Wang, Y.; Tang, X. Improved Tumor Tissue Penetration and Tumor Cell Uptake Achieved by Delayed Charge Reversal Nanoparticles. *Acta Biomater.* **2017**, *62*, 157–166.

(154) Logie, J.; Ganesh, A. N.; Aman, A. M.; Al-Awar, R. S.; Shoichet, M. S. Preclinical Evaluation of Taxane-Binding Peptide-Modified Polymeric Micelles Loaded with Docetaxel in an Orthotopic Breast Cancer Mouse Model. *Biomaterials* **2017**, *123*, 39–47.

(155) Hoang, B.; Ernsting, M. J.; Tang, W. H. S.; Bteich, J.; Undzys, E.; Kiyota, T.; Li, S. D. Cabazitaxel-Conjugated Nanoparticles for Docetaxel-Resistant and Bone Metastatic Prostate Cancer. *Cancer Lett. (N. Y., NY, U. S.)* **2017**, *410*, 169–179.

(156) Wang, J.; Lee, G. Y.; Lu, Q.; Peng, X.; Wu, J.; Wu, S.; Kairdolf, B. A.; Nie, S.; Wang, Y.; Lane, L. A. Quantitative Examination of the Active Targeting Effect: The Key Factor for Maximal Tumor Accumulation and Retention of Short-Circulated Biopolymeric Nanocarriers. *Bioconjugate Chem.* **2017**, *28*, 1351–1355.

(157) Boissenot, T.; Bordat, A.; Larrat, B.; Varna, M.; Chacun, H.; Paci, A.; Poinsignon, V.; Fattal, E.; Tsapis, N. Ultrasound-Induced Mild Hyperthermia Improves the Anticancer Efficacy of Both Taxol® and Paclitaxel-Loaded Nanocapsules. *J. Controlled Release* **2017**, *264*, 219–227.

(158) Wang, L.; Li, D.; Hao, Y.; Niu, M.; Hu, Y.; Zhao, H.; Chang, J.; Zhang, Z.; Zhang, Y. Gold

Nanorod-Based Poly(Lactic-*Co*-Glycolic Acid) with Manganese Dioxide Core-Shell Structured Multifunctional Nanoplatform for Cancer Theranostic Applications. *Int. J. Nanomed.* **2017**, *12*, 3059–3075.

(159) Li, C.; Ge, X.; Wang, L. Construction and Comparison of Different Nanocarriers for Co-Delivery of Cisplatin and Curcumin: A Synergistic Combination Nanotherapy for Cervical Cancer. *Biomed. Pharmacother.* **2017**, *86*, 628–636.

(160) Zhang, R. X.; Cai, P.; Zhang, T.; Chen, K.; Li, J.; Cheng, J.; Pang, K. S.; Adissu, H. A.; Rauth, A. M.; Wu, X. Y. Polymer-Lipid Hybrid Nanoparticles Synchronize Pharmacokinetics of Co-Encapsulated Doxorubicin-Mitomycin C and Enable Their Spatiotemporal Co-Delivery and Local Bioavailability in Breast Tumor. *Nanomedicine (N. Y., NY, U. S.)* **2016**, *12*, 1279–1290.

(161) Shalgunov, V.; Zaytseva-Zotova, D.; Zintchenko, A.; Levada, T.; Shilov, Y.; Andreyev, D.; Dzhumashev, D.; Metelkin, E.; Urusova, A.; Demin, O.; McDonnell, K.; Troiano, G.; Zale, S.; Safarova, E. Comprehensive Study of the Drug Delivery Properties of Poly(L-Lactide)-Poly(Ethylene Glycol) Nanoparticles in Rats and Tumor-Bearing Mice. *J. Controlled Release* **2017**, *261*, 31–42.

(162) Liu, H.; Lu, H.; Liao, L.; Zhang, X.; Gong, T.; Zhang, Z. Lipid Nanoparticles Loaded with 7-Ethyl-10-Hydroxycamptothecin-Phospholipid Complex: *In Vitro* and *In Vivo* Studies. *Drug Delivery* **2015**, *22*, 701–709.

(163) Nikpoor, A. R.; Tavakkol-Afshari, J.; Gholizadeh, Z.; Sadri, K.; Babaei, M. H.; Chamani, J.; Badiee, A.; Jalali, S. A.; Jaafari, M. R. Nanoliposome-Mediated Targeting of Antibodies to Tumors: IVIG Antibodies as a Model. *Int. J. Pharm. (Amsterdam, Neth.)* **2015**, *495*, 162–170.

(164) Mussi, S. V.; Parekh, G.; Pattekari, P.; Levchenko, T.; Lvov, Y.; Ferreira, L. A. M.; Torchilin, V. P. Improved Pharmacokinetics and Enhanced Tumor Growth Inhibition Using a Nanostructured Lipid Carrier Loaded with Doxorubicin and Modified with a Layer-by-Layer Polyelectrolyte

Coating. *Int. J. Pharm. (Amsterdam, Neth.)* **2015**, *495*, 186–193.

(165) Yeh, C. Y.; Hsiao, J. K.; Wang, Y. P.; Lan, C. H.; Wu, H. C. Peptide-Conjugated Nanoparticles for Targeted Imaging and Therapy of Prostate Cancer. *Biomaterials* **2016**, *99*, 1–15.

(166) Wang, M.; Li, J.; Li, X.; Mu, H.; Zhang, X.; Shi, Y.; Chu, Y.; Wang, A.; Wu, Z.; Sun, K. Magnetically and pH Dual Responsive Dendrosomes for Tumor Accumulation Enhanced Folate-Targeted Hybrid Drug Delivery. *J. Controlled Release* **2016**, *232*, 161–174.

(167) Lin, L.; Wang, X.; Li, X.; Yang, Y.; Yue, X.; Zhang, Q.; Dai, Z. Modulating Drug Release Rate from Partially Silica-Coated Bicellar Nanodisc by Incorporating PEGylated Phospholipid. *Bioconjugate Chem.* **2017**, *28*, 53–63.

(168) Zhu, B.; Yu, L.; Yue, Q. C. Co-Delivery of Vincristine and Quercetin by Nanocarriers for Lymphoma Combination Chemotherapy. *Biomed. Pharmacother.* **2017**, *91*, 287–294.

(169) Ni, S.; Qiu, L.; Zhang, G.; Zhou, H.; Han, Y. Lymph Cancer Chemotherapy: Delivery of Doxorubicin-Gemcitabine Prodrug and Vincristine by Nanostructured Lipid Carriers. *Int. J. Nanomed.* **2017**, *12*, 1565–1576.

(170) Kim, J. E.; Park, Y. J. Paclitaxel-Loaded Hyaluronan Solid Nanoemulsions for Enhanced Treatment Efficacy in Ovarian Cancer. *Int. J. Nanomed.* **2017**, *12*, 645–658.

(171) Chen, L.; Chen, B.; Deng, L.; Gao, B.; Zhang, Y.; Wu, C.; Yu, N.; Zhou, Q.; Yao, J.; Chen, J. An Optimized Two-Vial Formulation Lipid Nanoemulsion of Paclitaxel for Targeted Delivery to Tumor. *Int. J. Pharm. (Amsterdam, Neth.)* **2017**, *534*, 308–315.

(172) Kesharwani, P.; Tekade, R. K.; Jain, N. K. Generation Dependent Safety and Efficacy of Folic Acid Conjugated Dendrimer Based Anticancer Drug Formulations. *Pharm. Res.* **2015**, *32*, 1438–1450.

(173) Yan, C.; Gu, J.; Hou, D.; Jing, H.; Wang, J.; Guo, Y.; Katsumi, H.; Sakane, T.; Yamamoto, A. Improved Tumor Targetability of Tat-Conjugated PAMAM Dendrimers as a Novel Nanosized

Anti-Tumor Drug Carrier. *Drug Dev. Ind. Pharm.* **2015**, *41*, 617–622.

(174) Ohyama, A.; Higashi, T.; Motoyama, K.; Arima, H. *In Vitro* and *In Vivo* Tumor-Targeting siRNA Delivery Using Folate-PEG-Appended Dendrimer (G4)/*α*-Cyclodextrin Conjugates. *Bioconjugate Chem.* **2016**, *27*, 521–532.

(175) Narmani, A.; Yavari, K.; Mohammadnejad, J. Imaging, Biodistribution and *In Vitro* Study of Smart $^{99m}$Tc-PAMAM G4 Dendrimer as Novel Nano-Complex. *Colloids Surf., B* **2017**, *159*, 232–240.

(176) Battogtokh, G.; Kang, J. H.; Ko, Y. T. Long-Circulating Self-Assembled Cholesteryl Albumin Nanoparticles Enhance Tumor Accumulation of Hydrophobic Anticancer Drug. *Eur. J. Pharm. Biopharm.* **2015**, *96*, 96–105.

(177) Wan, X.; Zheng, X.; Pang, X.; Zhang, Z.; Jing, T.; Xu, W.; Zhang, Q. The Potential Use of Lapatinib-Loaded Human Serum Albumin Nanoparticles in the Treatment of Triple-Negative Breast Cancer. *Int. J. Pharm. (Amsterdam, Neth.)* **2002**, *8*, 131–138.

(178) Li, F.; Zheng, C.; Xin, J.; Chen, F.; Ling, H.; Sun, L.; Webster, T. J.; Ming, X.; Liu, J. Enhanced Tumor Delivery and Antitumor Response of Doxorubicin-Loaded Albumin Nanoparticles Formulated Based on a Schiff Base. *Int. J. Nanomed.* **2016**, *11*, 3875–3890.

(179) Qu, N.; Lee, R. J.; Sun, Y.; Cai, G.; Wang, J.; Wang, M.; Lu, J.; Meng, Q.; Teng, L.; Wang, D.; Teng, L. Cabazitaxel-Loaded Human Serum Albumin Nanoparticles as a Therapeutic Agent against Prostate Cancer. *Int. J. Nanomed.* **2016**, *11*, 3451–3459.

(180) Yin, T.; Cai, H.; Liu, J.; Cui, B.; Wang, L.; Yin, L.; Zhou, J.; Huo, M. Biological Evaluation of PEG Modified Nanosuspensions Based on Human Serum Albumin for Tumor Targeted Delivery of Paclitaxel. *Eur. J. Pharm. Sci.* **2016**, *83*, 79–87.

(181) Zhang, Z.; Wan, J.; Sun, L.; Li, Y.; Guo, J.; Wang, C. Zinc Finger-Inspired Nanohydrogels with Glutathione/pH Triggered Degradation Based on Coordination Substitution for Highly Efficient

Delivery of Anti-Cancer Drugs. *J. Controlled Release* **2016**, *225*, 96–108.

(182) Yang, C.; Li, C.; Zhang, P.; Wu, W.; Jiang, X. Redox Responsive Hyaluronic Acid Nanogels for Treating RHAMM (CD168) Over-Expressive Cancer, Both Primary and Metastatic Tumors. *Theranostics* **2017**, *7*, 1719–1734.

(183) Yang, G.; Wang, X.; Fu, S.; Tang, R.; Wang, J. pH-Triggered Chitosan Nanogels *via* an Ortho Ester-Based Linkage for Efficient Chemotherapy. *Acta Biomater.* **2017**, *60*, 232–243.

(184) Mehra, N. K.; Jain, N. K. One Platform Comparison of Estrone and Folic Acid Anchored Surface Engineered MWCNTs for Doxorubicin Delivery. *Mol. Pharmaceutics* **2015**, *12*, 630–643.

(185) Oh, Y.; Swierczewska, M.; Kim, T. H.; Lim, S. M.; Eom, H. N.; Park, J. H.; Na, D. H.; Kim, K.; Lee, K. C.; Pomper, M. G.; Lee, S. Delivery of Tumor-Homing TRAIL Sensitizer with Long-Acting TRAIL as a Therapy for TRAIL-Resistant Tumors. *J. Controlled Release* **2015**, *220*, 671–681.

(186) Yang, L.; Jiang, J.; Hong, J.; Di, J.; Liao, Y.; Kuang, H.; Wang, X. High Drug Payload 10-Hydroxycamptothecin Nanosuspensions Stabilized by Cholesterol-PEG: *In Vitro* and *In Vivo* Investigation. *J. Biomed. Nanotechnol.* **2015**, *11*, 711–721.

(187) Zhang, X.; Zhang, T.; Ye, Y.; Chen, H.; Sun, H.; Zhou, X.; Ma, Z.; Wu, B. Phospholipid-Stabilized Mesoporous Carbon Nanospheres as Versatile Carriers for Systemic Delivery of Amphiphobic SNX-2112 (a Hsp90 Inhibitor) with Enhanced Antitumor Effect. *Eur. J. Pharm. Biopharm.* **2015**, *94*, 30–41.

(188) Li, W.; Yi, X.; Liu, X.; Zhang, Z.; Fu, Y.; Gong, T. Hyaluronic Acid Ion-Pairing Nanoparticles for Targeted Tumor Therapy. *J. Controlled Release* **2016**, *225*, 170–182.

(189) Du, L.; Zhang, B.; Lei, Y.; Wang, S.; Jin, Y. Long-Circulating and Liver-Targeted Nanoassemblies of Cyclic Phosphoryl *N*-Dodecanoyl Gemcitabine for the Treatment of Hepatocellular Carcinoma. *Biomed. Pharmacother.* **2016**, *79*, 208–214.

(190) Jiang, Y.; Yang, N.; Zhang, H.; Sun, B.; Hou, C.; Ji, C.; Zheng, J.; Liu, Y.; Zuo, P. Enhanced *In Vivo* Antitumor Efficacy of Dual-Functional Peptide-Modified Docetaxel Nanoparticles through Tumor Targeting and Hsp90 Inhibition. *J. Controlled Release* **2016**, *221*, 26–36.

(191) Yang, X.; Liu, Y.; Zhao, Y.; Han, M.; Guo, Y.; Kuang, H.; Wang, X. A Stabilizer-Free and Organic Solvent-Free Method to Prepare 10-Hydroxycamptothecin Nanocrystals: *In Vitro* and *In Vivo* Evaluation. *Int. J. Nanomed.* **2016**, *11*, 2979–2994.

(192) Shi, J.; Wang, B.; Chen, Z.; Liu, W.; Pan, J.; Hou, L.; Zhang, Z. A Multi-Functional Tumor Theranostic Nanoplatform for MRI Guided Photothermal-Chemotherapy. *Pharm. Res.* **2016**, *33*, 1472–1485.

(193) Cheng, X.; Wang, X.; Cao, Z.; Yao, W.; Wang, J.; Tang, R. Folic Acid-Modified Soy Protein Nanoparticles for Enhanced Targeting and Inhibitory. *Mater. Sci. Eng., C* **2017**, *71*, 298–307.

(194) Hong, J.; Liu, Y.; Xiao, Y.; Yang, X.; Su, W.; Zhang, M.; Liao, Y.; Kuang, H.; Wang, X. High Drug Payload Curcumin Nanosuspensions Stabilized by MPEG-DSPE and SPC: *In Vitro* and *In Vivo* Evaluation. *Drug Delivery* **2017**, *24*, 109–120.

(195) Cui, T.; Zhang, S.; Sun, H. Co-Delivery of Doxorubicin and pH-Sensitive Curcumin Prodrug by Transferrin-Targeted Nanoparticles for Breast Cancer Treatment. *Oncol. Rep.* **2017**, *37*, 1253–1260.

(196) Guo, Y.; Zhao, Y.; Wang, T.; Li, R.; Han, M.; Dong, Z.; Zhu, C.; Wang, X. Hydroxycamptothecin Nanorods Prepared by Fluorescently Labeled Oligoethylene Glycols (OEG) Codendrimer: Antitumor Efficacy *In Vitro* and *In Vivo*. *Bioconjugate Chem.* **2017**, *28*, 390–399.

(197) Liu, G.; Tsai, H.-I.; Zeng, X.; Zuo, Y.; Tao, W.; Han, J.; Mei, L. Phosphorylcholine-Based Stealthy Nanocapsules Enabling Tumor Microenvironment-Responsive Doxorubicin Release for Tumor Suppression. *Theranostics* **2017**, *7*, 1192–1203.

(198) Xu, S.; Zhu, X.; Huang, W.; Zhou, Y.; Yan, D. Supramolecular Cisplatin-Vorinostat Nanodrug

for Overcoming Drug Resistance in Cancer Synergistic Therapy. *J. Controlled Release* **2017**, *266*, 36–46.

(199) Dai, L.; Zhu, W.; Si, C.; Lei, J. "Nano-Ginseng" for Enhanced Cytotoxicity AGAINST Cancer Cells. *Int. J. Mol. Sci.* **2018**, *19*, 627.

(200) Park, J.; Park, J. E.; Hedrick, V. E.; Wood, K. V.; Bonham, C.; Lee, W.; Yeo, Y. A Comparative *In Vivo* Study of Albumin-Coated Paclitaxel Nanocrystals and Abraxane. *Small* **2018**, *14*, 1703670.

(201) Sykes, E. A.; Dai, Q.; Sarsons, C. D.; Chen, J.; Rocheleau, J. V.; Hwang, D. M.; Zheng, G.; Cramb, D. T.; Rinker, K. D.; Chan, W. C. W. Tailoring Nanoparticle Designs to Target Cancer Based on Tumor Pathophysiology. *Proc. Natl. Acad. Sci. U. S. A.* **2016**, *113*, E1142–E1151.

(202) Chiou, W. L. Critical Evaluation of the Potential Error in Pharmacokinetic Studies of Using the Linear Trapezoidal Rule Method for the Calculation of the Area under the Plasma Level-Time Curve. *J. Pharmacokinet. Biopharm.* **1978**, *6*, 539–546.

(203) Wilhelm, S.; Tavares, A. J.; Dai, Q.; Ohta, S.; Audet, J.; Dvorak, H. F.; Chan, W. C. W. Analysis of Nanoparticle Delivery to Tumours. *Nat. Rev. Mater.* **2016**, *1*, 16014.

**Berkeley Madonna example code for PBPK modeling in tumor-bearing mice (Karmani *et al.*, 2013)**

```
METHOD RK4

STARTTIME = 0
STOPTIME = 168
DT = 0.00015625
DTOUT = 0.1

{Physiological parameters}
; Blood flow rate (Fraction of cardiac output, unitless)
QCC = 16.5                      ; Cardiac output (L/h/kg^0.75) (Brown et al.,1997)
QLuC = 1                        ; Fraction of blood flow to lung (Brown et al., 1997)
QLC = 0.02                      ; Fraction of artery blood flow to liver (Brown et al., 1997, Table 23)
QBRC = 0.033                    ; Fraction of blood flow to brain (Brown et al., 1997, Table 23)
QKC = 0.091                     ; Fraction of blood flow to kidneys (Brown et al., 1997, Table 23)
QSC = 0.011                     ; Fraction of blood flow to spleen (Lin et al., 2008; Davies and Morris, 1993)
QMC = 0.159                     ; Fraction of blood flow to muscle (Brown et al., 1997, Tables 23 & 24)
QTC = 0.01                      ; Fraction of blood flow to tumor (fitted)
QRC = 1-(QLC+QSC+QKC+QBRC+QMC+QTC)          ; Fraction of blood flow to rest of body (Calculated)

; Tissue volumes (Fraction of body weight, unitless)
BW = 0.0345                     ; Body weight (kg) (Cho et al., 2009; 2010)
VLC = 0.055                     ; Liver (Brown et al., 1997, Table 21)
VBRC = 0.017                    ; Brain (Brown et al., 1997, Table 21)
VKC = 0.017                     ; Kidneys (Brown et al., 1997, Table 21)
VSC = 0.005                     ; Spleen (Lin et al., 2008; Davies and Morris, 1993)
VLuC = 0.007                    ; Lungs (Brown et al., 1997, Table 21)
VBloodC = 0.06                  ; Blood (Chen et al., 2015)
VPlasmaC = 0.0355               ; Plasma (Davies and Morris, 1993 with hematocrit of 0.41 for red blood cells)
VMC = 0.384                     ; Muscle (Brown et al., 1997, Table 21)
VTC = 0.021                     ; Tumor (Sykes et al., 2014; Wilhelm et al., 2016)
VRC = 1-(VLC+VSC+VKC+VLuC+VBRC+VMC+VPlasmaC+VTC)          ; Rest of body (Calculated)

; Blood volume fraction in organs and tissues (percentage of organs/tissues, unitless)
BVL = 0.31                      ; Liver (Brown et al., 1997; Table 30)
BVBR = 0.03                     ; Brain (Brown et al., 1997, Table 30)
BVK = 0.24                      ; Kidneys (Brown et al., 1997, Table 30)
BVS = 0.17                      ; Spleen (Brown et al., 1997, Table 30)
BVLu = 0.5                      ; Lungs (Brown et al., 1997, Table 30)
BVM = 0.04                      ; Muscle (Brown et al., 1997, Table 30)
BVR = 0.04                      ; Rest of body (Brown et al., 1997, Table 30, assume equal to the muscle)
BVT = 0.01                      ; Tumor (fitted)

; Tissue:plasma distribution coefficients (PCs), unitless; these values were from our published mouse PBPK
model (Lin et al., 2016) or fitted by calibrating with healthy mouse pharmacokinetic data for gold nanoparticles
from (Cho et al., 2010)
PL = 0.08                       ; Liver
PBR = 0.15                      ; Brain
PK = 0.15                       ; Kidneys
PS = 0.15                       ; Spleen
PLu = 0.15                      ; Lungs
PM = 0.15                       ; Muscle
PR = 0.15                       ; Rest of body
PT = 0.065                      ; Tumor (fitted)
```

; Membrane-limited permeability coefficient constants, unitless; these values were from our published mouse PBPK model (Lin *et al.*, 2016) or fitted by calibrating with healthy mouse pharmacokinetic data for gold nanoparticles from (Cho *et al.*, 2010)

```
PALC = 0.001            ; Liver
PABRC = 0.000001        ; Brain
PAKC = 0.01             ; Kidneys
PASC =0.15              ; Spleen
PALuC = 0.001           ; Lungs
PAMC = 0.00005          ; Muscle
PARC = 0.00005          ; Rest of body
PATC = 0.03             ; Tumor (fitted)

; Endocytic parameters; RES represent endocytic/phagocytic cells; L, S, K, Lu, M, R, and T represent liver, spleen, kidneys, lungs, muscle, rest of body, and tumor, respectively.
KLRESrelease = 0.0015   ; Release rate constant of phagocytic cells, (h-1)
KLRESmax = 0.3          ; Maximum uptake rate constant of phagocytic cells, (h-1)
KLRES50 = 48            ; Time reaching half maximum uptake rate, (h)
KLRESn = 5              ; Hill coefficient, (unitless)

KSRESrelease = 0.001    ; Release rate constant of phagocytic cells, (h-1)
KSRESmax = 5            ; Maximum uptake rate constant of phagocytic cells, (h-1)
KSRES50 = 36            ; Time reaching half maximum uptake rate, (h)
KSRESn = 5              ; Hill coefficient, (unitless)

KKRESrelease = 0.001    ; Release rate constant of phagocytic cells, (h-1)
KKRESmax = 0.12         ; Maximum uptake rate constant of phagocytic cells, (h-1)
KKRES50 = 48            ; Time reaching half maximum uptake rate, (h)
KKRESn = 5              ; Hill coefficient, (unitless)

KLuRESrelease = 0.003   ; Release rate constant of phagocytic cells, (h-1)
KLuRESmax = 0.085       ; Maximum uptake rate constant of phagocytic cells, (h-1)
KLuRES50 = 48           ; Time reaching half maximum uptake rate, (h)
KLuRESn = 5             ; Hill coefficient, (unitless)

KMRESrelease = 0.005    ; Release rate constant of phagocytic cells, (h-1)
KMRESmax = 0.4          ; Maximum uptake rate constant of phagocytic cells, (h-1)
KMRES50 = 48            ; Time reaching half maximum uptake rate, (h)
KMRESn = 5              ; Hill coefficient, (unitless)

KRRESrelease = 0.005    ; Release rate constant of phagocytic cells, (h-1)
KRRESmax = 0.4          ; Maximum uptake rate constant of phagocytic cells, (h-1)
KRRES50 = 48            ; Time reaching half maximum uptake rate, (h)
KRRESn = 5              ; Hill coefficient, (unitless)

KTRESrelease = 0.0009   ; Release rate constant of phagocytic cells, (h-1)
KTRESmax = 0.065        ; Maximum uptake rate constant of phagocytic cells, (h-1)
KTRES50 = 4.2           ; Time reaching half maximum uptake rate, (h)
KTRESn = 5              ; Hill coefficient, (unitless)

; Biliary excretion
KbileC = 0.00003        ; Biliary clearance (L/hr/kg^0.75)
                        ; L/hr/kg changed to L/h/kg^0.75 for interspecies extrapolation

; Urine excretion
KurineC = 0.000003      ; Urine clearance (L/hr/kg^0.75)
                        ; L/hr changed to L/h/kg^0.75 for interspecies extrapolation
```

```
; Scaled parameters
; Cardiac output and regional blood blow (L/h)
QC = QCC*BW**0.75                          ; Cardiac output
QL = QC*QLC                                ; Blood flow to liver
QBR = QC*QBRC                              ; Blood flow to brain
QK = QC*QKC                                ; Blood flow to kidneys
QS = QC*QSC                                ; Blood flow to spleen
QM = QC*QMC                                ; Blood flow to muscle
QR = QC*QRC                                ; Blood flow to rest of body
QT = QC*QTC                                ; Blood flow to tumor
Qbal = QC-QL-QBR-QK-QS-QM-QR-QT            ; Blood flow balance equation

; Tissue volumes (L)
VL = BW*VLC                                ; Liver
VBR = BW*VBRC                              ; Brain
VK = BW*VKC                                ; Kidneys
VS = BW*VSC                                ; Spleen
VLu = BW*VLuC                              ; Lungs
VBlood = BW*VBloodC                        ; Blood
VPlasma = BW*VPlasmaC                      ; Plasma
VM = BW*VMC                                ; Muscle
VR = BW*VRC                                ; Rest of body
VT = BW*VTC                                ; Tumor
Vbal = BW-VL-VBR-VK-VS-VLu-VPlasma-VM-VR-VT          ; Tissue volume balance equation

VLb = VL*BVL                               ; Weight/volume of capillary blood in liver compartment
VLt = VL-VLb                               ; Weight/volume of tissue in liver compartment
VBRb = VBR*BVBR                            ; Weight/volume of capillary blood in brain compartment
VBRt = VBR-VBRb                            ; Weight/volume of tissue in brain compartment
VKb = VK*BVK                               ; Weight/volume of capillary blood in kidney compartment
VKt = VK-VKb                               ; Weight/volume of tissue in kidney compartment
VSb = VS*BVS                               ; Weight/volume of capillary blood in spleen compartment
VSt = VS-VSb                               ; Weight/volume of tissue in spleen compartment
VLub = VLu*BVLu                            ; Weight/volume of capillary blood in lung compartment
VLut = VLu-VLub                            ; Weight/volume of tissue in lung compartment
VMb = VM*BVM                               ; Weight/volume of capillary blood in muscle compartment
VMt = VM-VMb                               ; Weight/volume of tissue in muscle compartment
VRb = VR*BVR                               ; Weight/volume of capillary blood in rest of body compartment
VRt = VR-VRb                               ; Weight/volume of tissue in rest of body compartment
VTb = VT*BVT                               ; Weight/volume of capillary blood in tumor compartment
VTt = VT-VTb                               ; Weight/volume of tissue in tumor compartment

; Permeability coefficient-surface area cross-product (L/h)
PAL = PALC*QL                              ; Liver
PABR = PABRC*QBR                           ; Brain
PAK = PAKC*QK                              ; Kidneys
PAS = PASC*QS                              ; Spleen
PALu = PALuC*QC                            ; Lungs
PAM = PAMC*QM                              ; Muscle
PAR = PARC*QR                              ; Rest of body
PAT = PATC*QT                              ; Tumor

; Endocytosis rate (h-1)
KLRESUP = (KLRESmax*TIME^KLRESn)/(KLRES50^KLRESn+TIME^KLRESn)          ; Liver
KSRESUP = (KSRESmax*TIME^KSRESn)/(KSRES50^KSRESn+TIME^KSRESn)          ; Spleen
KKRESUP = (KKRESmax*TIME^KKRESn)/(KKRES50^KKRESn+TIME^KKRESn)          ; Kidneys
KLuRESUP = (KLuRESmax*TIME^KLuRESn)/(KLuRES50^KLuRESn+TIME^KLuRESn)    ; Lungs
KMRESUP = (KMRESmax*TIME^KMRESn)/(KMRES50^KMRESn+TIME^KMRESn)          ; Muscle
```

```
KRRESUP = (KRRESmax*TIME^KRRESn)/(KRRES50^KRRESn+TIME^KRRESn)        ; Rest of body
KTRESUP = (KTRESmax*TIME^KTRESn)/(KTRES50^KTRESn+TIME^KTRESn)        ; Tumor


; IV Dosing
Timeiv = 0.005 ; IV infusion time (h), set, approximately 15-20 seconds, on average 18 sec
PDOSEiv = 8.17 ; mg/kg (Karmani et al. (2013); mice, IV route)

DOSEiv = PDOSEiv*BW                ; mg
IVR = DOSEiv/Timeiv                ; mg/h
RIV = IVR*(1.-step(1,Timeiv))      ; mg/h
d/dt(AIV) = RIV
init AIV = 0

; Elimination
Kbile = KbileC*BW**0.75            ; L/h
Kurine = KurineC*BW**0.75          ; L/h

{Blood compartment}
; CA = Arterial blood concentration (mg/L or μg/ml)
RA = QC*CVLu - QC*CA
d/dt(AA) = RA
init AA = 0
CA = AA/(VPlasma*0.2)
d/dt(AUCCA) = CA
init AUCCA = 0

; CV = Venous blood concentration (mg/L or ug/ml)
RV = QL*CVL + QBR*CVBR + QK*CVK + QM*CVM + QR*CVR + QT*CVT + RIV - QC*CV
d/dt(AV) = RV
init AV = 0
CV = AV/(VPlasma*0.8)
d/dt(AUCCV) = CV
init AUCCV = 0
APlasma = AA+AV
CPlasma = APlasma/VPlasma

{Lung compartment (mg/kg or ug/g)}
; Membrane-limited model: AuNP in capillary blood of Lung
RLub = QC*(CV-CVLu) - PALu*CVLu + (PALu*CLut)/PLu
d/dt(ALub) = RLub
init ALub = 0
CVLu = ALub/VLub

; Membrane-limited model: AuNP in interstitial tissue of Lung
RLut = PALu*CVLu - (PALu*CLut)/PLu - KLuRESup*ALut + KLuRESrelease*ALuRES
d/dt(ALut) = RLut
init ALut = 0
CLut = ALut/VLut

; Phagocytosis: AuNP in phagocytic cells of Lung tissue
RLuRES = KLuRESUP*ALut-KLuRESrelease*ALuRES
d/dt(ALuRES) = RLuRES
init ALuRES = 0

; Total AuNP in Lung
ALung = ALub+ALut+ALuRES
CLung = (ALub+ALut+ALuRES)/VLu
```

```
ALungt = ALut+ALuRES
CLungt = (ALut+ALuRES)/VLut

{Brain compartment (mg/kg or ug/g)}
; Membrane-limited model: AuNP in capillary blood of Brain
RBRb = QBR*(CA-CVBR) - PABR*CVBR + (PABR*CBRt)/PBR
d/dt(ABRb) = RBRb
init ABRb = 0
CVBR = ABRb/VBRb

; Membrane-limited model: AuNP in interstitial tissue of Brain
RBRt = PABR*CVBR - (PABR*CBRt)/PBR
d/dt(ABRt) = RBRt
init ABRt = 0
CBRt = ABRt/VBRt

; Total AuNP in Brain
ABrain = ABRb+ABRt
CBrain = ABrain/VBR

{Muscle compartment (mg/kg or ug/g)}
; Membrane-limited model: AuNP in capillary blood of Muscle
RMb = QM*(CA-CVM) - PAM*CVM + (PAM*CMt)/PM
d/dt(AMb) = RMb
init AMb = 0
CVM = AMb/VMb

; Membrane-limited model: AuNP in interstitial tissue of Muscle
RMt = PAM*CVM - (PAM*CMt)/PM - KMRESUP*AMt + KMRESrelease*AMRES
d/dt(AMt) = RMt
init AMt = 0
CMt = AMt/VMt

; Phagocytosis: AuNP in phagocytic cells of Muscle
RMRES = KMRESUP*AMt-KMRESrelease*AMRES
d/dt(AMRES) = RMRES
init AMRES = 0

; Total AuNP in Muscle
AMuscle = AMb+AMt+AMRES
CMuscle = (AMb+AMt+AMRES)/VM
AMusclet = AMt+AMRES
CMusclet = (AMt+AMRES)/VMt

{Rest of body compartment (mg/kg or ug/g)}
; Membrane-limited model: AuNP in capillary blood of Rest of body
RRb = QR*(CA-CVR) - PAR*CVR + (PAR*CRt)/PR
d/dt(ARb) = RRb
init ARb = 0
CVR = ARb/VRb

; Membrane-limited model: AuNP in interstitial tissue of Rest of body
RRt = PAR*CVR - (PAR*CRt)/PR - KRRESUP*ARt + KRRESrelease*ARRES
d/dt(ARt) = RRt
init ARt = 0
CRt = ARt/VRt
```

```
; Phagocytosis: AuNP in phagocytic cells of Rest of body tissue
RRRES = KRRESUP*ARt-KRRESrelease*ARRES
d/dt(ARRES) = RRRES
init ARRES = 0

; Total AuNP in Rest of body
Arestall = ARb+ARt+ARRES
Crestall = (ARb+ARt+ARRES)/VR
Aresttissue = ARt+ARRES
Cresttissue = (ARt+ARRES)/VRt

{Kidney compartment (mg/kg or ug/g)}
; Membrane-limited model: AuNP in capillary blood of Kidney
RKb = QK*(CA-CVK) - PAK*CVK + (PAK*CKt)/PK - Rurine
d/dt(AKb) = RKb
init AKb = 0
CVK = AKb/VKb

; Membrane-limited model: AuNP in interstitial tissue of Kidney
RKt = PAK*CVK - (PAK*CKt)/PK - KKRESUP*AKt + KKRESrelease*AKRES
d/dt(AKt) = RKt
init AKt = 0
CKt = AKt/VKt

; Phagocytosis: AuNP in phagocytic cells of Kidney tissue
RKRES = KKRESUP*AKt-KKRESrelease*AKRES
d/dt(AKRES) = RKRES
init AKRES = 0

; Total AuNP in Kidney
AKidney = AKb+AKt+AKRES
CKidney = (AKb+AKt+AKRES)/VK
AKidneyt = AKt+AKRES
CKidneyt = (AKt+AKRES)/VKt

; Urinary excretion
Rurine = Kurine*CVK ;mg/h
d/dt(Aurine) = Rurine
init Aurine = 0

{Spleen compartment (mg/kg or ug/g)}
; Membrane-limited model: AuNP in capillary blood of Spleen
RSb = QS*(CA-CVS) - PAS*CVS + (PAS*CSt)/PS
d/dt(ASb) = RSb
init ASb = 0
CVS = ASb/VSb

; Membrane-limited model: AuNP in interstitial tissue of Spleen
RSt = PAS*CVS - (PAS*CSt)/PS - KSRESUP*ASt + KSRESrelease*ASRES
d/dt(ASt) = RSt
init ASt = 0
CSt = ASt/VSt

; Phagocytosis: AuNP in phagocytic cells of Spleen tissue
;RSRES = KSRESUP*AA-KSRESrelease*ASRES
RSRES = KSRESUP*ASt-KSRESrelease*ASRES
d/dt(ASRES) = RSRES
init ASRES = 0
```

```
; Total AuNP in Spleen
ASpleen = ASb+ASt+ASRES
CSpleen = (ASb+ASt+ASRES)/VS
ASpleent = ASt+ASRES
CSpleent = (ASt+ASRES)/VSt
d/dt(AUCCS) = CSpleen
init AUCCS = 0

{Liver compartment (mg/kg or ug/g)}
; Membrane-limited model: AuNP in capillary blood of Liver
RLb = QL*(CA-CVL) + QS*CVS - PAL*CVL + (PAL*CLt)/PL - KLRESUP*ALb + KLRESrelease*ALRES
d/dt(ALb) = RLb
init ALb = 0
CVL = ALb/VLb

; Membrane-limited model: AuNP in interstitial tissue of Liver
RLt = PAL*CVL - (PAL*CLt)/PL - Rbile
d/dt(ALt) = RLt
init ALt = 0
CLt = ALt/VLt

; Phagocytosis: AuNP in phagocytic cells attach to Liver capillary wall
;RLRES = KLRESUP*AA-KLRESrelease*ALRES
RLRES = KLRESUP*ALb-KLRESrelease*ALRES
d/dt(ALRES) = RLRES
init ALRES = 0

; Total AuNP in Liver
ALiver = ALb+ALt+ALRES
CLiver = (ALb+ALt+ALRES)/VL
ALivert = ALt+ALRES
CLivert = (ALt+ALRES)/VLt
d/dt(AUCCL) = CLiver
init AUCCL = 0

; Biliary excretion
Rbile = Kbile*CLt ; mg/h
d/dt(Abile) = Rbile
init Abile = 0

{Tumor compartment (mg/kg or ug/g)}
; Membrane-limited model: AuNP in capillary blood of Tumor
RTb = QT*(CA-CVT) - PAT*CVT + (PAT*CTt)/PT
d/dt(ATb) = RTb
init ATb = 0
CVT = ATb/VTb

; Membrane-limited model: AuNP in Tumor interstitium
RTt = PAT*CVT - (PAT*CTt)/PT - KTRESUP1*ATt + KTRESrelease*ATRES
d/dt(ATt) = RTt
init ATt = 0
CTt = ATt/VTt
```

```
; Phagocytosis: AuNP in tumor cells of Tumor interstitium
RTRES = KTRESUP*ATt-KTRESrelease*ATRES
RTRESUP = KTRESUP*ATt
RTRESrelease = KTRESrelease*ATRES
d/dt(ATRES) = RTRES
init ATRES = 0

; Total AuNP in Tumor
ATumor = ATb+ATt+ATRES
CTumor = (ATb+ATt+ATRES)/VT
ATumort = ATt+ATRES
CTumort = (ATt+ATRES)/VTt; mg/kg or ug/g tumor
d/dt(AUCCT) = 100*(ATumort/Doseiv)
init AUCCT = 0

Tumorperc = 100*(ATumort/Doseiv)/VTt/1000          ; %ID/g
TumorpercID = 100*(ATumort/Doseiv)                 ; %ID

; Mass balance
Tmass = AA+AV+ALiver+ABrain+AKidney+ALung+Arestall+AMuscle+ASpleen+Abile+Aurine+ATumor
Bal = AIV-Tmass
```